SECTION 6

FRACTOGRAPHY AND OTHER EXAMINATIONS

6.1 Introduction

Following the completion of burst testing, the left side of each of the burst opening fracture faces was examined by Scanning Electron Microscopy (SEM) and Energy Dispersive Spectrometry (EDS) in order to characterize the fracture morphology and surface chemistry. EDS results presented were normalized to 100% and are considered to be semi-quantitative in nature due to the obvious deficiencies in EDS analysis of surface deposits which exhibit variable thickness, distributions, and concentration gradients.

The specimens used for these examinations were limited to burst-related specimens.

<u>R10C39 HL</u>

- H02 Plate – Piece 3B2A
- H03 Plate – Piece 4B2A
- Freespan burst – Piece 3C2A

<u>R11C41 HL</u>

- Top of Tubesheet – Piece 2B2
- Burst above TTS – Piece 2B2A
- H02 Plate – Piece 3B2A
- H03 Plate – Piece 4B2A
- Freespan burst – Piece 5A2A

6.2 Examination Procedure

A section of tubing containing the burst opening was removed from each test piece by cutting with a Dremmel Moto wheel (#409) above and below the opening. The burst opening was split longitudinally to facilitate examination of the fracture face. After cutting, these were blown with a jet of dry oil-free air to remove any particulates from the fracture surfaces. Standard examination procedures were used for the SEM/EDS examinations. Fracture surfaces were examined in the as-burst condition. The fracture faces were ultrasonically cleaned in water after EDS analysis. The ASTM has not published specific procedures for fractography examinations. However, the growing body of experience with these techniques has led to a *de facto* recognition and acceptance of carefully conducted examinations. A useful compilation of fractographs is available to enhance the interpretation of this data from sources such as *The Metals Handbook, Volume 12, Fractography,* 9th Edition, American Society of Metals, 1985.

Fractographs were taken of the fracture surfaces at several magnifications. General features of the burst opening surfaces, as well as characterization of the OD surface in the area of the burst were discernible at relatively low magnification. For more detailed analyses of the SCC features and local depth of degradation, fractographs at higher magnification were obtained. If necessary, a montage of the crack surface was assembled. The extent and nature of the degradation was then characterized directly on each montage. From these measurements, and knowledge of the tube wall thickness, it was possible to calculate the depth (or percent through-wall) of the stress corrosion cracking.

Energy Dispersive Spectrometry (EDS) is useful in identifying potential surface or crack face contamination if such is present and can analyze for elements down to atomic number 11. Analyses were run on one or more regions of each of the samples for which fractography was performed. A tabular summary of the data, as well as images of several of the EDS spectra, is included in the discussion for each of the fracture surfaces.

6.3 Results of Fractography and EDS Analyses

The following table describes the location (azimuthal orientation) of the examinations performed.

Tube	Axial Location	Piece	Azimuthal Orientation of Burst
R10C39 HL	H02 Plate	3B2A	90°
	H03 Plate	4B2A	315°
	Freespan	3C2A	120°
R11C41 HL	TTS	2B2	n/a
	Freespan above TTS	2B2A	300°
	H02 Plate	3B2A	220°
	H03 Plate	4B2A	60°
	Freespan	5A2A	330°

R10C39 HL - Piece 3B2 – Section 3B2A (HO2 Plate)

The H02 plate intersection of the R10C39 HL tube was identified to contain an SAI by both field and laboratory eddy current inspections. Following completion of the leak and burst testing, the burst specimen from the H02 plate was sectioned to allow fractography of the burst opening, as well as the area adjacent to the burst. The azimuthal location of the burst opening was 90°. A 1.125-inch long piece containing the burst opening was cut from the burst specimen. A longitudinal section containing the burst fracture was removed to facilitate the examination of the burst plane. The burst face contained both intergranular and ductile fracture features. The length of the axial cracking was approximately 0.6 inch and did not extend outside of the tube to plate intersection. A montage showing the burst fracture face is shown in Figure 6-1 while the intergranular fracture profile is shown in Figure 6-2. Examination of the fracture profile confirmed the through-wall extent of the intergranular cracking at one location. This region is shown in Figure 6-3, while areas illustrating both ductile and intergranular fracture features are shown in Figure 6-4. The average depth of the intergranular cracking over the length of the indication was 30.6 mils or 66.5% through-wall based on an original wall thickness of 46 mils in the area of the indication. The original wall thickness was determined by averaging the thickness obtained at the ends of the burst specimen at or near the azimuthal orientation of the burst. Examination of the fracture face showed a number of ductile ligaments within the intergranular regions. The dimensions of these ductile ligaments are summarized in Table 6-3, while photomicrographs illustrating the general appearance of the ligaments are provided in Figure 6-5.

The fracture face contained a considerable amount of foreign debris. This is typical when a bladder, foil, and lubricant are required to perform the burst test. Nevertheless, the grain facets are defined, although somewhat rounded. This is typical of OD-initiated IGSCC. Examination of the OD surface adjacent to the burst showed no unusual features, although evidence of a shallow axial scratch was noted. The OD surface adjacent to the burst opening is shown in Figure 6-6. Based on the apparent lack of oxide deposit, the shallow scratch likely occurred during the tube removal process.

Results of EDS analyses of IGSCC, ductile, and OD surface areas are presented in Table 6-1 and Figure 6-7. Iron, nickel, and chromium, along with carbon and oxygen were identified on all surfaces. Aluminum, silicon, calcium, titanium, manganese, and copper were seen on the IGSCC areas, while the ductile fracture showed the additional presence of magnesium, aluminum, and silicon. Calcium, titanium, manganese, or copper were not detected on the ductile fracture face. In addition to the above noted species, phosphorus and sulfur were identified on the OD surface. It should be pointed out that the detection of species other than iron, nickel, and chromium is not unusual and that the species noted above are normally detected on the fracture face of ODSCC specimens.

R10C39 HL – Piece 3C – Section 3C2A (Freespan)

A section of tube above the H02 plate was burst tested to determine the non-degraded burst strength of the R10C39 tube material. The azimuthal location of the burst opening was 120°. A 2.0-inch long piece containing the burst opening was cut from the burst specimen. A longitudinal section containing the burst fracture was removed to facilitate the examination of the burst plane. The burst face exhibited 100% ductile fracture with evidence of intergranular fracture features. SEM photomicrographs of the ductile fracture features are shown in Figure 6-8, while EDS results are provided in Table 6-1. No abnormal species were noted on the fracture face or on the OD surface adjacent to the burst opening.

R10C39 HL - Piece 4B2 – Section 4B2A (H03 Plate)

Based on field and laboratory eddy current inspections, no indications were reported at the H03 plate intersection of the R10C39 HL tube. Nevertheless, a burst test was performed to support the Watts Bar Unit 1 Alternate Repair Criteria. Following completion of the leak and burst testing, the H03 plate intersection area was sectioned to allow fractography of the burst opening, as well as the area adjacent to the burst. The azimuthal location of the burst opening was 315°. A 1.6- inch long piece containing the burst opening was cut from the burst specimen. A longitudinal section containing the burst fracture was removed to facilitate the examination of the burst plane. The burst face contained both intergranular and ductile fracture features. No intergranular cracking was noted outside of the plate to tube intersection. A montage showing the burst fracture face is shown in Figure 6-9 while the intergranular fracture profile is shown in Figure 6-10. The overall length of the observed cracking was approximately 0.21 inch. The maximum depth of IGSCC was approximately 18 mils with an average depth of 9.4 mils. Based on an original wall thickness of 45.5 mils, the maximum through-wall depth was 39.6% with an average depth of 20.6%. The original wall thickness was determined by averaging the thickness obtained at the ends of the burst specimen at or near the azimuthal orientation of the burst.

As seen in Figure 6-10, the crack profile illustrates three (3) individual cracks separated by non-degraded ligaments. Based on the appearance of crack face and the presence of ligaments exhibiting ductile fracture, the intergranular fracture face contained multiple crack fronts. Figure 6-11 presents a fractograph of the partial throughwall IGSCC observed at the H03 plate, while Figure 6-12 illustrates the OD surface adjacent to the burst. The delineation between the intergranular fracture near the OD surface and the ductile fracture near the ID surface is easily seen. The fracture face near the OD has a "rock-candy" appearance which is typical of Alloy 600 intergranular cracking. The fracture face near the ID has a "dimpled" appearance which is characteristic of ductile tearing. The region of ductile tearing was the result of non-corroded metal being torn apart by hoop tensile stresses during the burst test. This surface appearance is typical of burst-tested non-degraded Alloy 600 steam generator tubing. The somewhat rounded appearance of the grain facets seen in Figure 6-11 suggests a thick surface oxide or deposit. This appearance is typical for OD-initiated stress corrosion cracking of mill annealed Alloy 600.

Examination of the fracture face showed a number of ductile ligaments within the intergranular regions. The dimensions of these ductile ligaments are summarized in Table 6-3, while a photomicrograph illustrating the general appearance of one of the ligaments is provided in Figure 6-13.

Results of EDS analyses of IGSCC, ductile, and OD surface areas are presented in Table 6-1 and Figure 6-14. Iron, nickel, and chromium, along with carbon and oxygen were identified on all surfaces. Aluminum, silicon, calcium, titanium, manganese, and copper were seen on the IGSCC areas, while the ductile fracture showed the additional presence of magnesium, aluminum, and silicon. Calcium, titanium, manganese, or copper were not detected on the ductile fracture face. In addition to the above noted species, phosphorus and sulfur were identified on the OD surface. It should be pointed out that the detection of species other than iron, nickel, and chromium is not unusual and that the species noted above are normally detected on the fracture face of ODSCC specimens.

<u>R11C41 HL – Piece 2B– Section 2B2A</u>

Piece 2B of R11C41 HL was identified with an SCI at the top of the tubesheet (TTS) by both field and laboratory eddy current examinations. As discussed in Section 5, this piece was identified for leak and burst testing. During the testing, an area of the tube above the TTS burst at 13,028 psi. No evidence of leakage at the SCI was noted. The TTS area containing the single circumferential indication "bulged" but did not burst. Visual examination of this area revealed multiple short circumferential cracks positioned around the circumference of the expansion transition and basically located at the same elevation. Figure 6-15 is a montage of the OD surface showing the indications observed following pressurization. As can be seen, the cracks are relatively short in circumferential extent and separated by non-degraded material. In order to further examine the area of the indication, a tensile load was applied to the SCI region resulting in a transverse fracture through the plane of the indication. The failure load was 2100 lbs.

The SEM examination revealed the degradation to be intergranular stress corrosion cracking that initiated at the OD surface of the tube. Multiple crack planes were seen with evidence of ductile ligaments connecting the crack planes. The crack planes did not appear to extend outside the expansion transition. A series of montages showing the appearance of the fracture surface are provided in Figure 6-16. The intergranular crack depth profile measured on the fracture face is shown in Figure 6-17. Figure 6-18 are SEM photomicrographs showing the general nature of the indication. These micrographs clearly indicate the degradation originated at the OD surface. The transition from intergranular SCC to ductile tearing is seen at higher magnification, as are ductile ligaments. The maximum depth of intergranular cracking was 28.7 mils or 61% through-wall based on a 47-mil original wall thickness. The average depth of the indication was determined to be 20.3 mils or 42.3% through-wall. As noted previously, the fracture face exhibited multiple intergranular short cracks interconnected with ductile ligaments. No effort was made to determine the area of the ductile ligaments or to perform EDS analyses of the fracture face.

As noted above, the burst did not occur at the location of the SCI, but in the freespan above the indication. This burst pressure was 13,028 psi. This burst pressure is similar to that observed for a non-degraded freespan section. The axial burst was located approximately 1.8 inches above the TTS and had an azimuthal orientation of 300°. The burst opening measured 1.728 inches in length and 0.342 inches in width. The burst facture face was totally ductile with no evidence of corrosion. SEM photomicrographs illustrating the appearance of the fracture face are shown in Figure 6-19. EDS analyses are provided in Figure 6-20. No unusual species were noted.

R11C41 HL - Piece 3B2 – Section 3B2A (HO2 Plate)

Based on field and laboratory eddy current inspections, no indications were reported at the H02 plate intersection of the R11C41 HL tube. Nevertheless, a burst test was performed to support the Watts Bar Unit 1 Alternate Repair Criteria. Following completion of the leak and burst testing, the H02 intersection area was sectioned to allow fractography of the burst opening, as well as the area adjacent to the burst. The azimuthal location of the burst opening was 220°. A 2.0- inch long piece containing the burst opening was cut from the burst specimen. A longitudinal section containing the burst fracture was removed to facilitate the examination of the burst plane. The burst face presented both intergranular and ductile fracture features. Intergranular cracking was not seen outside of the H02 plate to tube intersection. A montage showing the burst fracture face is shown in Figure 6-21 while the intergranular fracture profile is shown in Figure 6-22. The general appearance of the intergranular fracture face is shown in Figure 6-23. The delineation between the intergranular fracture near the OD surface and the ductile fracture near the ID surface is easily seen. The fracture face near the OD has a "rock-candy" appearance which is typical of Alloy 600 intergranular cracking. The fracture face near the ID exhibits the "dimpled" appearance characteristic of ductile tearing. The overall length of the observed cracking was approximately 0.11 inch. The maximum depth of IGSCC was 23.9 mils with an average depth of 12.4 mils. Based on an original wall thickness of 44.5 mils, the maximum through-wall depth was 53.7% with an average depth of 27.9%. The original wall thickness was determined by averaging the thickness obtained at the ends of the burst specimen at or near the azimuthal orientation of the burst.

Based on examination of the fracture face, evidence of ductile ligaments and likely multiple crack initiation locations is observed. The dimensions of these ductile ligaments are summarized in Table 6-3, while photomicrographs illustrating the general appearance of the ligaments are provided in Figure 6-24. The appearance of the OD surface adjacent to the fracture face is shown in Figure 6-25.

Results of EDS analyses of IGSCC, ductile, and OD surface areas are presented in Table 6-2 and Figure 6-26. No significant concentrations of unexpected species were noted. Iron, nickel, and chromium, along with carbon and oxygen were identified on all surfaces. Aluminum, silicon, calcium, titanium, manganese, and copper were seen on the IGSCC areas, while the ductile fracture showed the additional presence of magnesium, aluminum, and silicon. Calcium, titanium, manganese, or copper were not detected on the ductile fracture face. In addition to the above noted species, phosphorus and sulfur were identified on the OD surface. It should be pointed out that the detection of species other than iron, nickel, and chromium is not unusual and that the species noted above are normally detected on the fracture face of ODSCC specimens.

<u>R11C41 HL - Piece 4B2 – Section 4B2A (H03 Plate)</u>

The H03 plate intersection of the R11C41 HL tube was identified to contain an SAI by both field and laboratory eddy current inspections. Following completion of the leak and burst testing, the burst specimen from the H03 plate was sectioned to allow fractography of the burst opening, as well as the area adjacent to the burst. The azimuthal location of the burst opening was 60°. A 1.6-inch long piece containing the burst opening was cut from the burst specimen. A longitudinal section containing the burst fracture was removed to facilitate the examination of the burst plane. The burst face contained both intergranular and ductile fracture features. The length of the axial cracking was approximately 0.63 inch and did not extend outside the H03 plate to tube intersection region. A montage showing the burst fracture face is shown in Figure 6-27 while the intergranular fracture profile is shown in Figure 6-28. Examination of the fracture profile confirmed the through-wall extent of the intergranular cracking, as well as illustrating multiple crack fronts. One location on the fracture face exhibited through-wall intergranular cracking. The average depth of the intergranular cracking over the length of the indication was 22 mils or 47.8% through-wall based on an original wall thickness of 46 mils in the area of the indication. The original wall thickness was determined by averaging the thickness obtained at the ends of the burst specimen at or near the azimuthal orientation of the burst.

Examination of the fracture face showed a number of ductile ligaments within the intergranular regions. The dimensions of these ductile ligaments are summarized in Table 6-3, while photomicrographs illustrating the general appearance of the ligaments are provided in Figure 6-29. Figure 6-30 illustrations the intergranular nature of the fracture face at the region of through-wall penetration. The somewhat rounded appearance of the grain facets seen in Figure

6-30 suggests a thick surface oxide or deposit. This appearance is typical for OD-initiated stress corrosion cracking of mill annealed Alloy 600.

Results of EDS analyses of IGSCC, ductile, and OD surface areas are presented in Table 6-2 and Figure 6-31. No significant concentrations of unexpected species were noted. Iron, nickel, and chromium, along with carbon and oxygen were identified on all surfaces. Aluminum, silicon, calcium, titanium, manganese, and copper were seen on the IGSCC areas, while the ductile fracture showed the additional presence of magnesium, aluminum, and silicon. Calcium, titanium, manganese, or copper were not detected on the ductile fracture face. In addition to the above noted species, phosphorus and sulfur were identified on the OD surface. It should be pointed out that the detection of species other than iron, nickel, and chromium is not unusual and that the species noted above are normally detected on the fracture face of ODSCC specimens.

R11C41 HL - Piece 5A2 – Section 5A2A (Freespan)

A section of tube above the 2nd TSP was burst tested to determine the non-degraded burst strength of the R10C39 tube material. The azimuthal location of the burst opening was 330°. A 2.0-inch long piece containing the burst opening was cut from the burst specimen. A longitudinal section containing the burst fracture was removed to facilitate the examination of the burst plane. The burst face exhibited 100% ductile fracture with evidence of intergranular fracture features. An SEM photomicrograph of the ductile fracture is shown in Figure 6-32, while the appearance of the OD surface adjacent to the burst is shown in Figure 6-33. EDS results are provided in Table 6-2. No abnormal species were noted on the fracture face or on the OD surface adjacent to the burst opening.

Table 6-1 Summary of EDS Analyses for R10C39 HL

	Element															
	C	O	Mg	Al	Si	P	S	V	Ca	Ti	Cr	Mn	Fe	Ni	Cu	Pb
Piece 3B - Section 3B2A (1st TSP [HO2])																
IGSCC (Area 1)	0.69	30.30	-	0.60	0.87	-	-	-	0.95	0.26	12.79	-	10.66	42.05	-	-
IGSCC (Area 3)	0.34	25.25	-	-	0.53	-	-	-	0.55	-	2.00	2.01	64.18	3.99	1.16	-
IGSCC (Area 4)	0.58	29.53	-	0.60	1.07	-	-	-	0.10	0.23	10.99	0.42	5.04	51.43	-	-
Ductile (Area 5)	0.76	0.59	1.18	0.76	0.50	-	-	-	-	-	14.84	-	7.02	74.37	-	-
OD (Area 6)	3.77	39.87	3.51	7.31	6.84	0.56	0.15	-	8.36	-	0.85	-	26.61	1.93	0.26	-
OD (Area 7)	1.97	33.05	0.73	1.43	1.18	-	0.65	-	0.53	0.21	10.55	-	19.18	29.35	1.17	-
Piece 4B - Section 4B2A (2nd TSP [HO3])																
IGSCC (Area 1)	0.38	1.12	-	0.66	0.53	-	-	-	0.24	0.27	15.38	0.42	7.38	73.63	-	-
IGSCC (Area 2)	1.26	31.27	-	0.64	3.23	-	-	-	0.33	0.15	8.78	0.62	5.37	48.35	-	-
IGSCC (Area 3)	0.92	2.48	-	1.20	1.00	-	-	-	1.18	0.24	14.78	0.59	8.38	69.24	-	-
Ductile (Area 5)	0.45	0.71	-	0.81	0.44	-	-	-	0.18	0.31	15.84	0.60	7.26	73.39	-	-
OD (Area 5)	1.45	34.35	1.10	2.40	2.10	-	-	-	0.68	0.38	12.62	1.21	9.13	33.08	1.50	-
OD Area 6)	1.25	33.35	1.14	1.96	1.24	-	-	-	0.54	0.32	13.06	1.19	10.18	34.03	1.74	-
Piece 3C (Freespan)																
OD (Area 1)	-	-	-	-	-	-	-	-	-	0.35	21.09	0.82	9.92	67.83	-	-
OD (Area 2)	-	-	-	-	-	-	-	0.05	-	0.33	21.73	0.81	10.47	66.62	-	-
Ductile (Area 1)	-	-	-	-	-	-	-	0.26	-	0.47	16.49	1.03	8.17	73.55	-	-
Ductile (Area 2)	-	-	-	-	-	-	-	0.12	-	0.43	16.55	0.69	8.17	74.04	-	-

Note: The vanadium identified on Piece 3B is likely related to foreign material pick-up during handling of the specimen.

Table 6-2 Summary of EDS Analyses for R11C41HL

	Element																
	C	O	Mg	Al	Si	P	S	V	K	Ca	Ti	Cr	Mn	Fe	Ni	Cu	Pb
Piece 3B - Section 3B2A (1st TSP [HO2])																	
IGSCC	0.45	0.75	-	0.58	0.40	-	-	-	-	0.41	0.26	15.19	0.43	7.77	72.43	1.32	-
IGSCC	0.73	1.41	-	0.69	0.64	-	-	-	-	1.38	0.21	14.60	0.42	8.21	70.57	1.15	-
Ductile	0.54	0.67	-	0.87	0.45	-	-	-	-	-	0.26	17.00	0.45	7.56	72.19	-	-
OD	1.70	34.49	1.83	2.57	2.77	-	-	-	-	1.97	0.32	10.55	0.97	10.97	30.27	1.59	-
OD	2.22	36.95	1.89	4.12	4.20	-	-	-	-	2.59	0.36	9.54	1.14	15.54	20.19	1.27	-
Piece 4B - Section 4B2A (2nd TSP [HO3])																	
IGSCC	0.43	29.78	-	0.97	2.28	-	-	-	-	0.12	-	10.19	0.44	5.01	50.79	-	-
IGSCC	0.50	1.49	-	4.35	0.92	-	0.21	-	0.31	0.17	-	14.76	0.64	7.41	69.24	-	-
Ductile	0.33	0.48	-	1.13	0.32	-	-	-	-	-	0.29	15.98	0.55	7.48	73.43	-	-
OD	1.38	35.63	3.85	4.36	6.09	0.33	0.20	-	-	6.29	0.25	1.25	3.64	32.13	3.80	0.81	-
OD	7.97	43.59	0.67	2.05	5.32	-	0.30	-		6.73	0.17	0.78	1.15	27.24	3.84	0.19	-
OD	0.24	30.66	0.75	1.66	1.34	-	-	-	-	0.69	0.20	12.39	1.15	8.62	38.91	3.39	-
OD	0.93	33.38	0.89	2.23	2.69	-	-	-	-	0.92	0.31	12.54	0.99	9.25	33.74	2.13	-
Piece 5B - Section 5B2A (Freespan)																	
Ductile	-	6.46	-	-	-	-	-	-	-	-	0.42	15.97	-	7.77	69.37	-	-
OD	-	32.54	-	-	-	-	-	-	-	-	0.21	13.69	-	6.67	46.89	-	-

Table 6-3
Dimensions of Ductile Ligaments
Observed Within IGSCC for TSP Burst Specimens

Specimen	Ligament	Length (mils)	Average Width (Area/length - mils)	Area (mils²)
R10C39 - 3B2B (1st TSP)				
	L1	18.2	5.0	91.2
	L2	30.7	4.5	138.9
	L3	21.0	8.3	175.0
	L4	11.8	11.2	132.6
	L5	12.9	4.3	55.1
	L6	4.4	1.9	8.3
	L7	10.1	7.6	76.6
	L8	9.7	5.2	50.8
	AVERAGE:	14.9	6.0	91.1
	TOTAL:	118.8	48.1	728.5
R10C39 - 4B2B (2nd TSP)				
	L1	19.8	1.9	10.2
	L2	82.2	13.7	6
	L3	102.4	5.9	17.3
	Average	68.1	7.2	11.2
	Total	204.4	21.6	33.5
R11C41 - 3B2B (1st TSP)				
	L1	7.1	3.3	23.2
	L2	7.8	5.2	40.5
	L3	18.4	7.2	132.5
	Average	11.1	5.2	65.4
	Total	33.3	15.7	196.2
R11C41 - 4B2B (2nd TSP)				
	L1	13.7	5.2	70.6
	L2	18.8	4.4	82.5
	L3	10.2	2.9	29.1
	L4	2.7	1.7	4.5
	L5	12.7	0.9	12.0
	L6	12.4	2.6	32.1
	L7	9.4	1.2	11.3
	L8	14.1	1.0	13.5
	L9	6.8	1.3	8.8
	L10	14.0	1.9	26.7
	L11	24.3	17.5	425.8
	L12	11.7	1.2	13.6
	AVERAGE:	12.6	3.5	60.9
	TOTAL:	150.8	41.6	730.5

Figure 6-1
R10C39 – Piece 3B2A - Montage of Burst Fracture Face Associated with H02 Plate

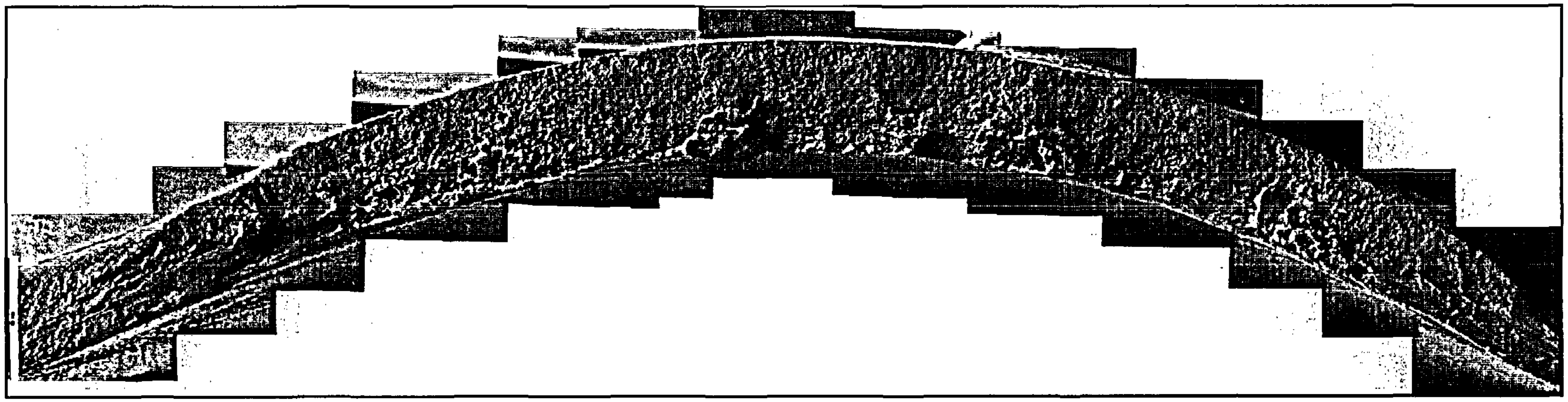

Figure 6-2
R10C39 - Piece 3B - Section 3B2A - Burst Fracture
IGSCC Depth Profile Associated with H02 Plate

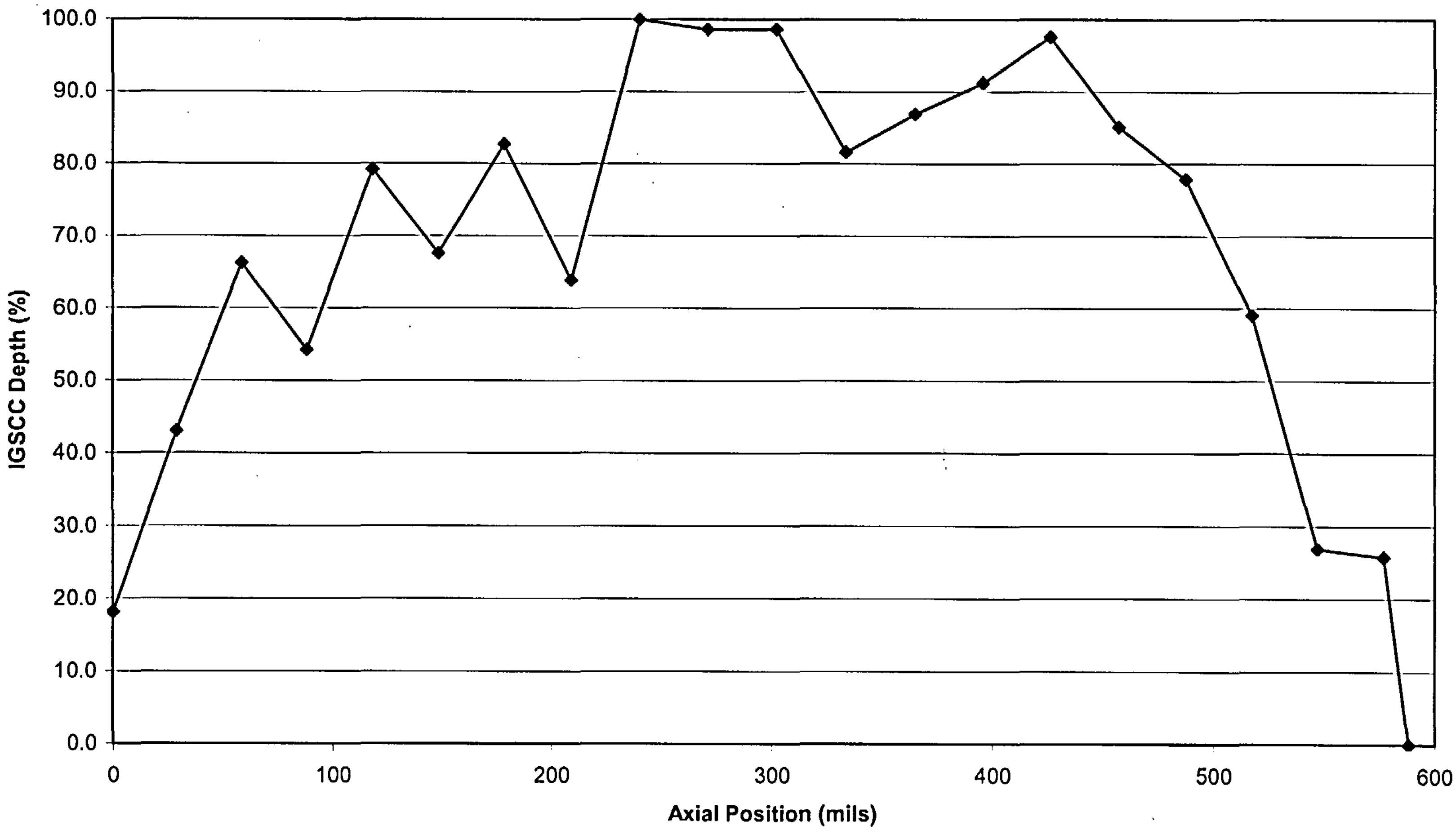

Figure 6 – 3
R10C39 – Piece 3B – Section 3B2A (H02 Plate)
SEM Photographs Showing Through-Wall IGSCC Fracture Features

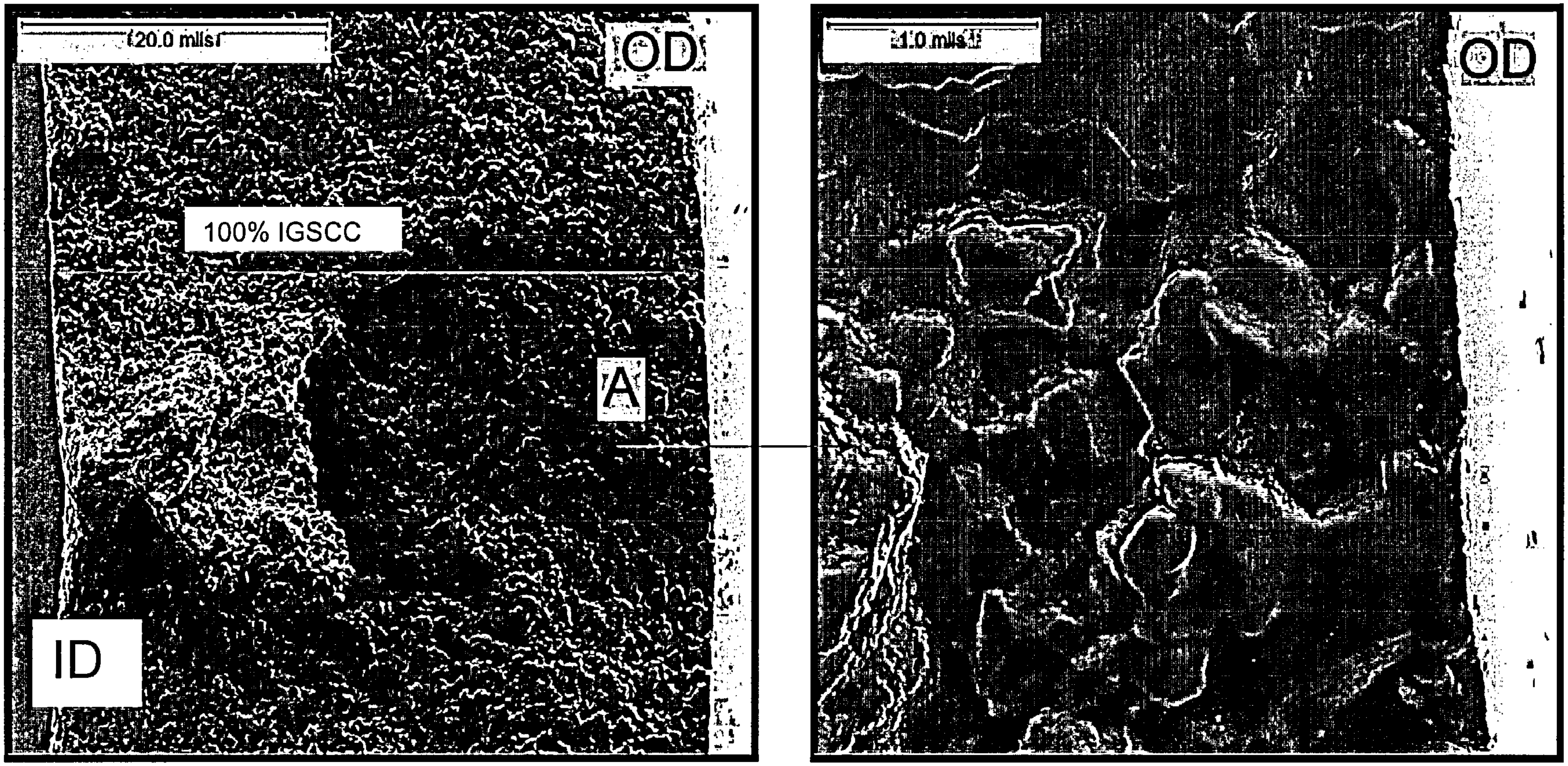

Figure 6 – 4
R10C39 – Piece 3B – Section 3B2A (H02 Plate)
SEM Photographs Showing Ductile to IGSCC Interface Observed on Fracture Face

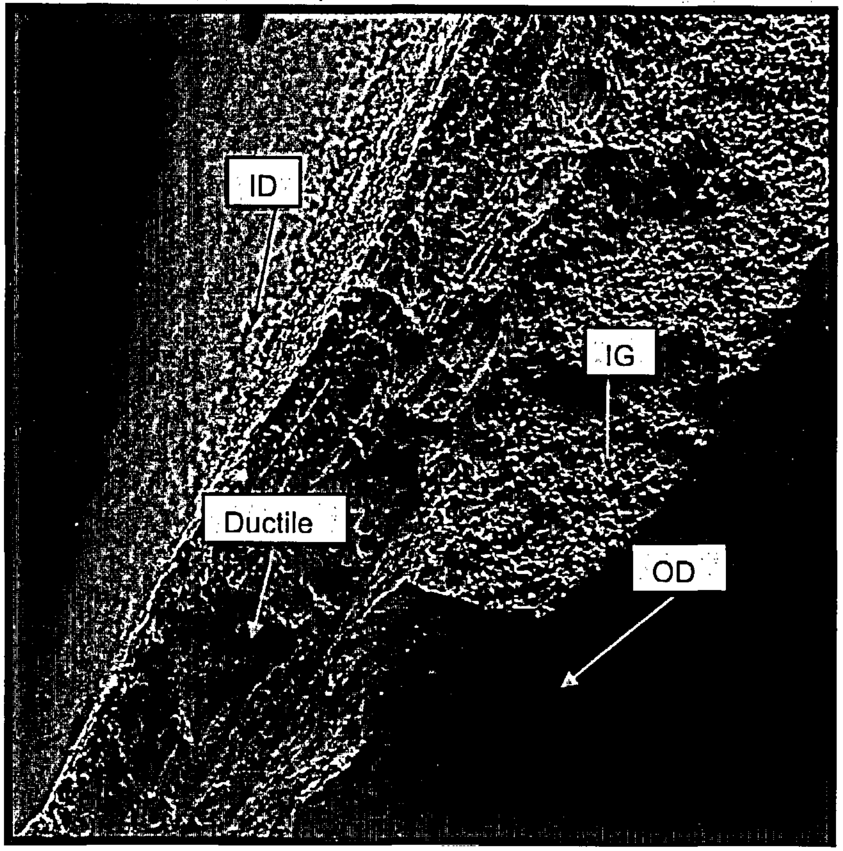

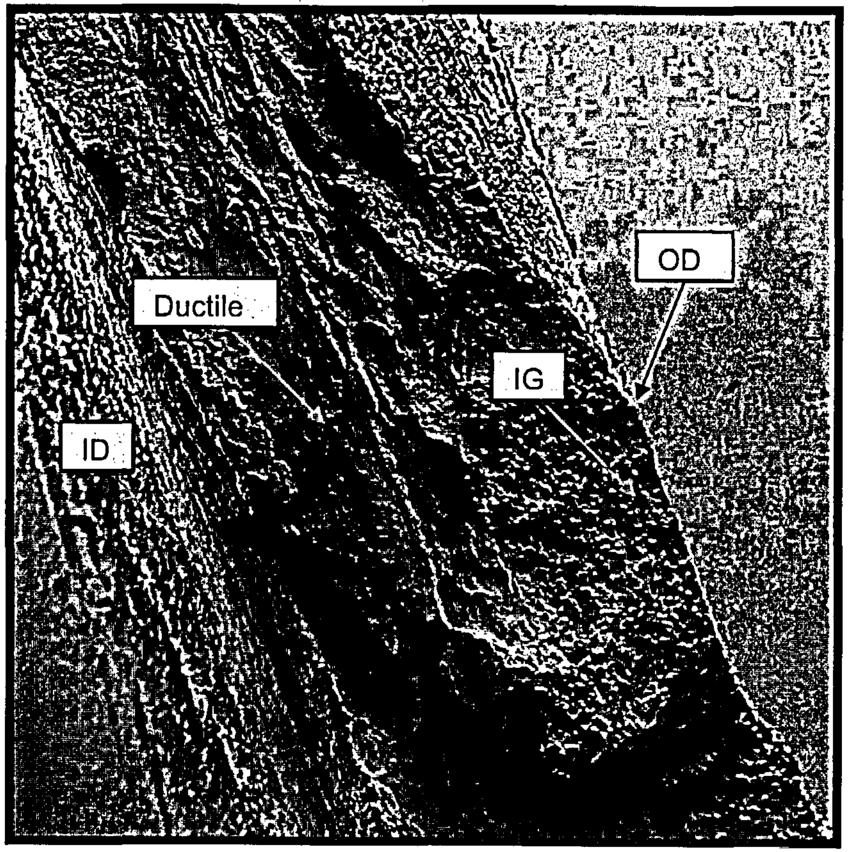

Figure 6 – 5
R10C39 – Piece 3B – Section 3B2A (H02 Plate)
SEM Photographs Showing Ductile Ligaments Observed Within Intergranular Fracture Areas

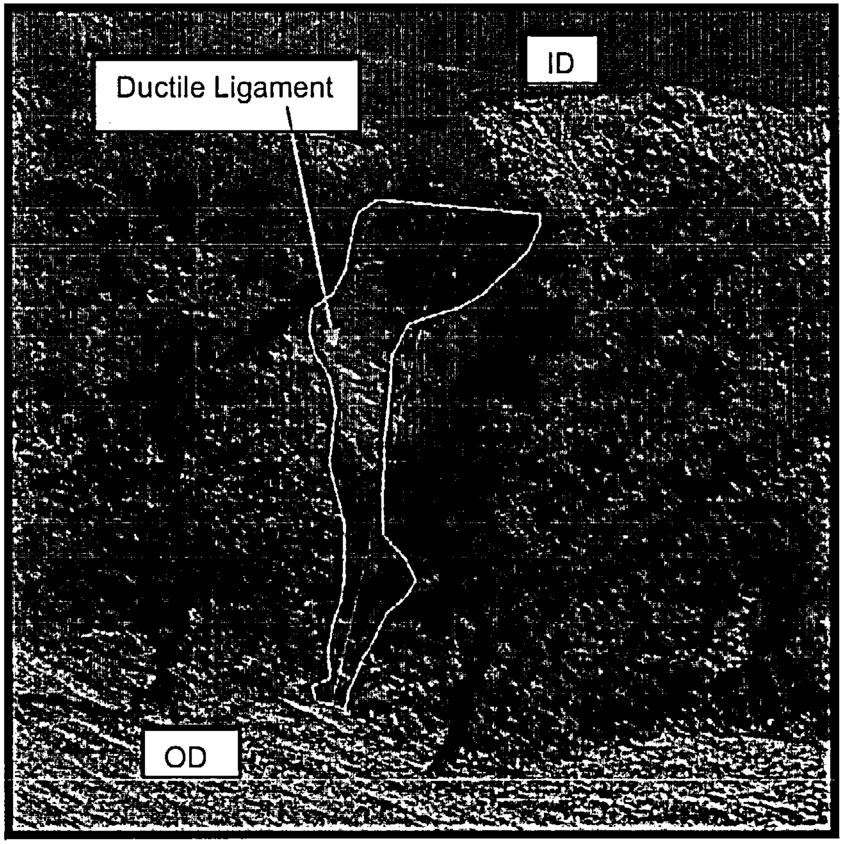

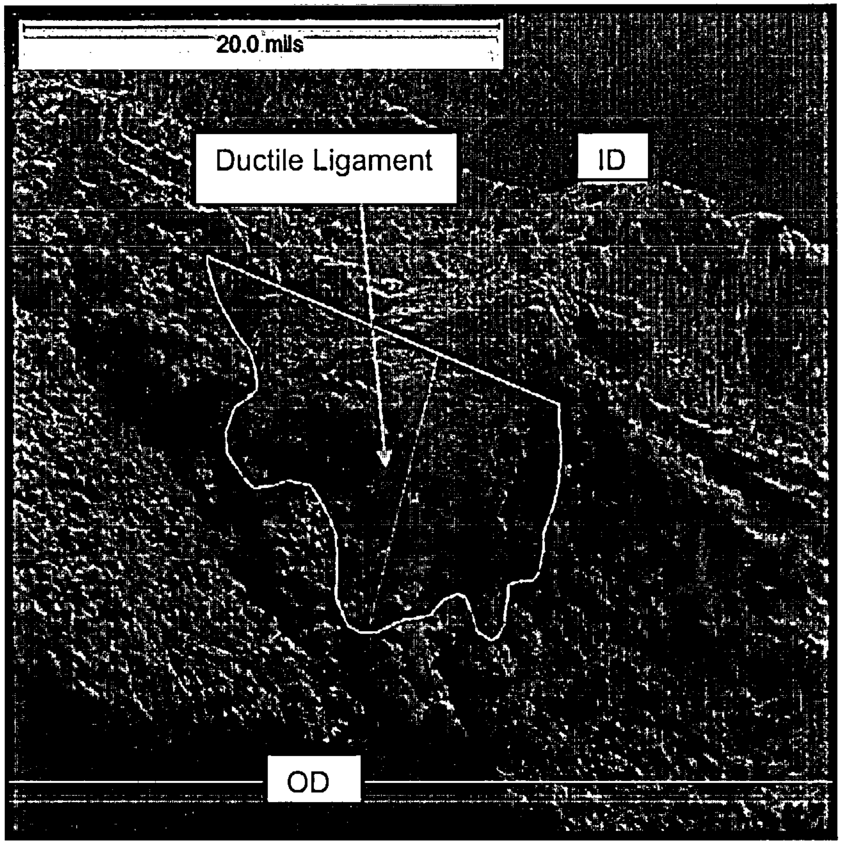

Figure 6 – 6
R10C39 – Piece 3B – Section 3B2A (H02 Plate)
SEM Photographs Showing OD Surface Adjacent to Fracture Face

Note: Axial surface anomaly likely occurred during tube removal

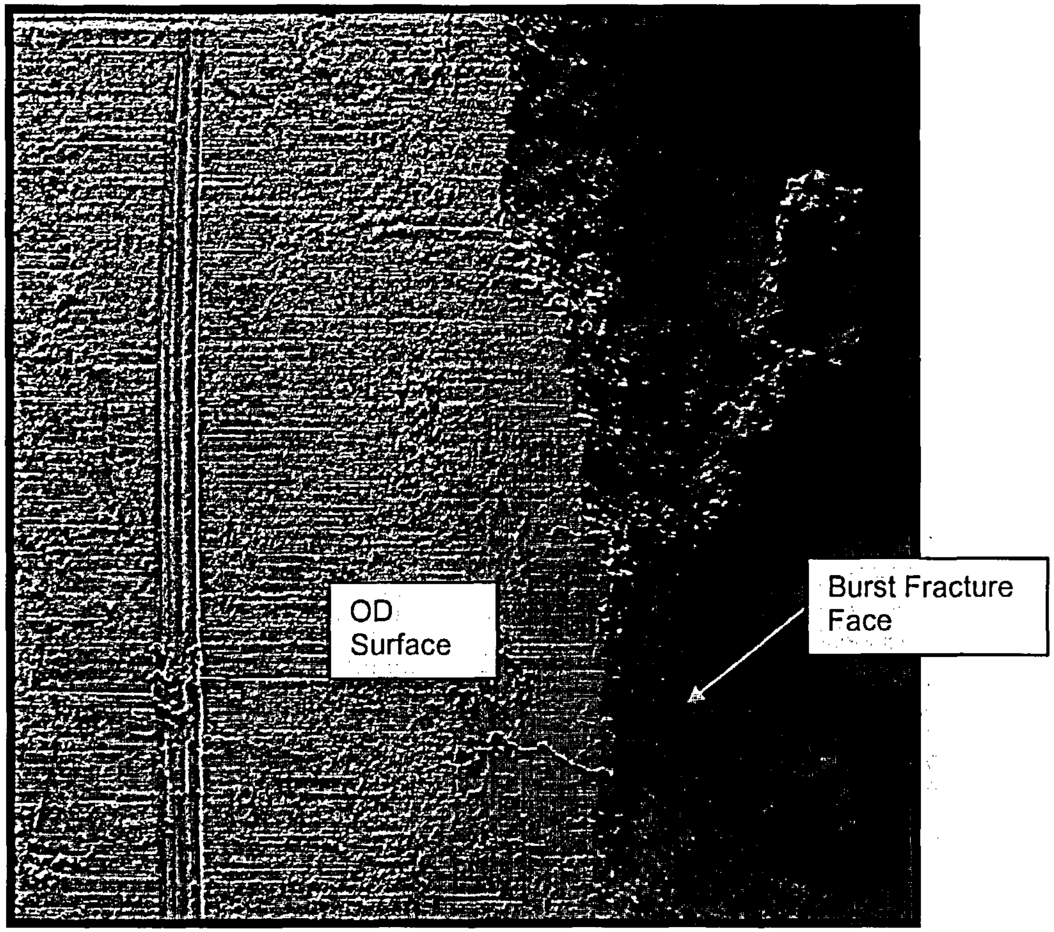

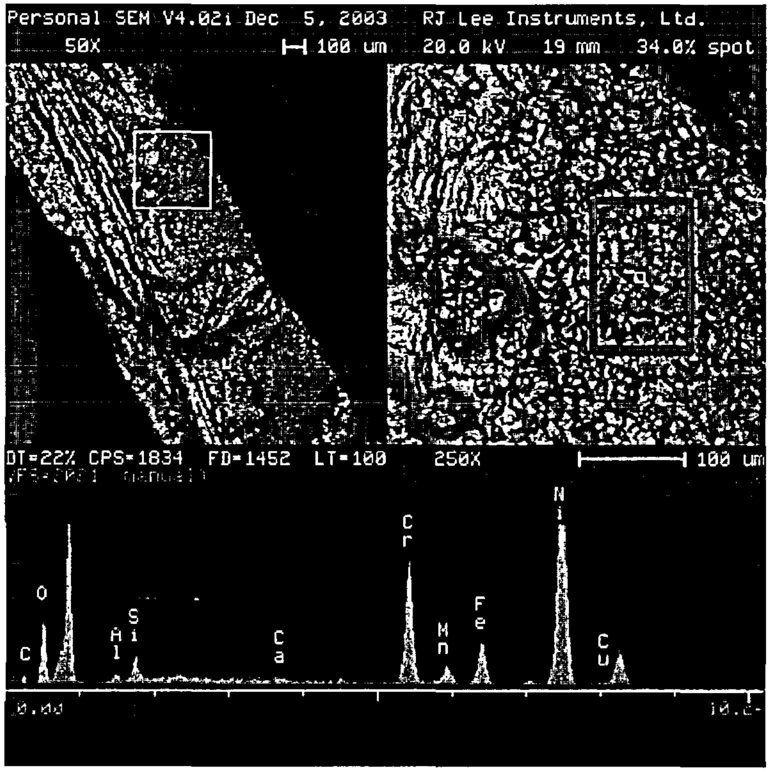

a) IGSCC (Area 1)

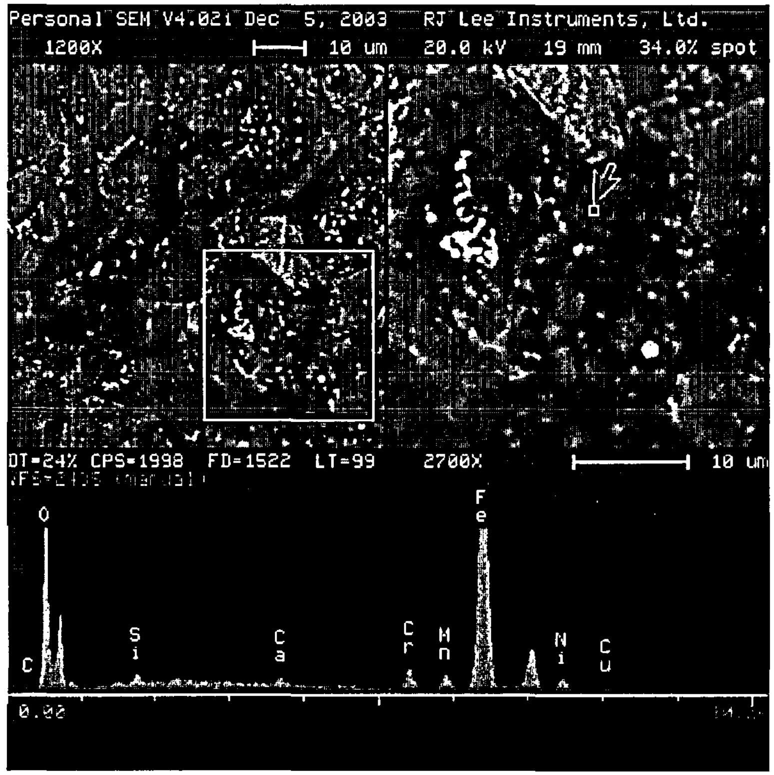

b) IGSCC (Area 3)

Figure 6 – 7
R10C39 – Piece 3B – Section 3B2A (H02 Plate)
SEM Photographs Illustrating Areas Selected for EDS

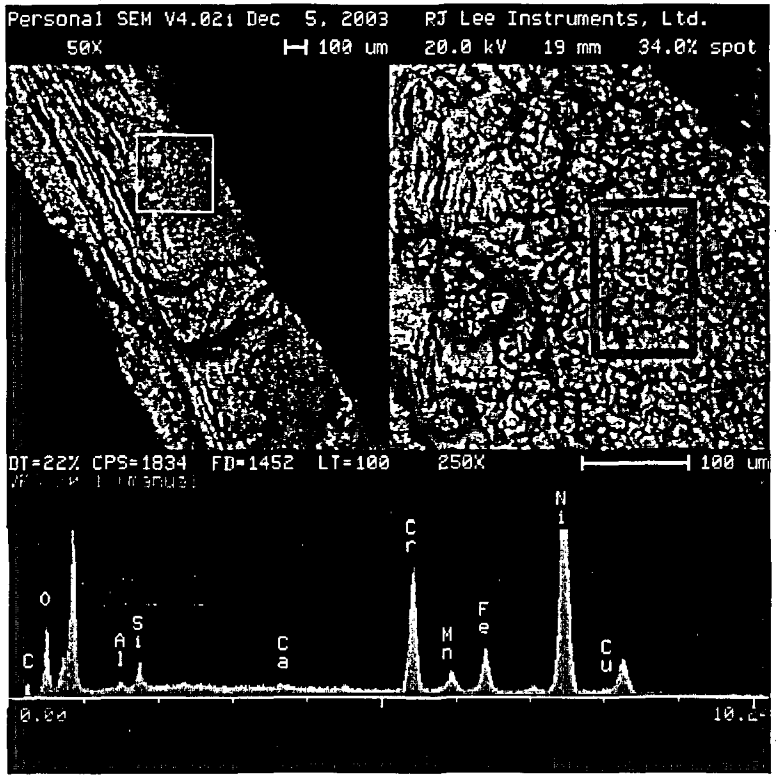

c) IGSCC (Area 4)

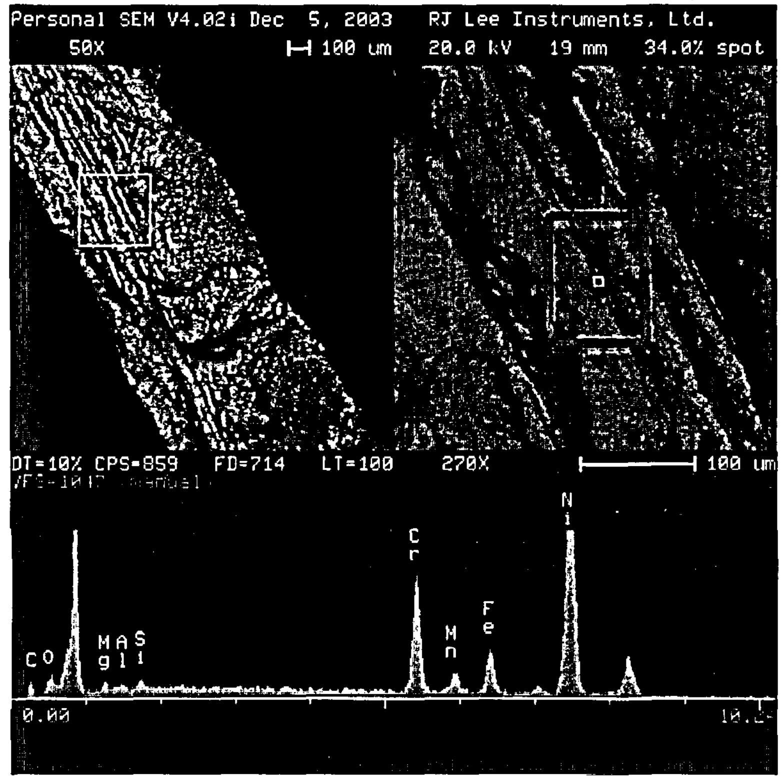

d) Ductile Fracture (Area 5)

Figure 6 – 7 (Cont'd)
R10C39 – Piece 3B – Section 3B2A (H02 Plate)
SEM Photographs Illustrating Areas Selected for EDS

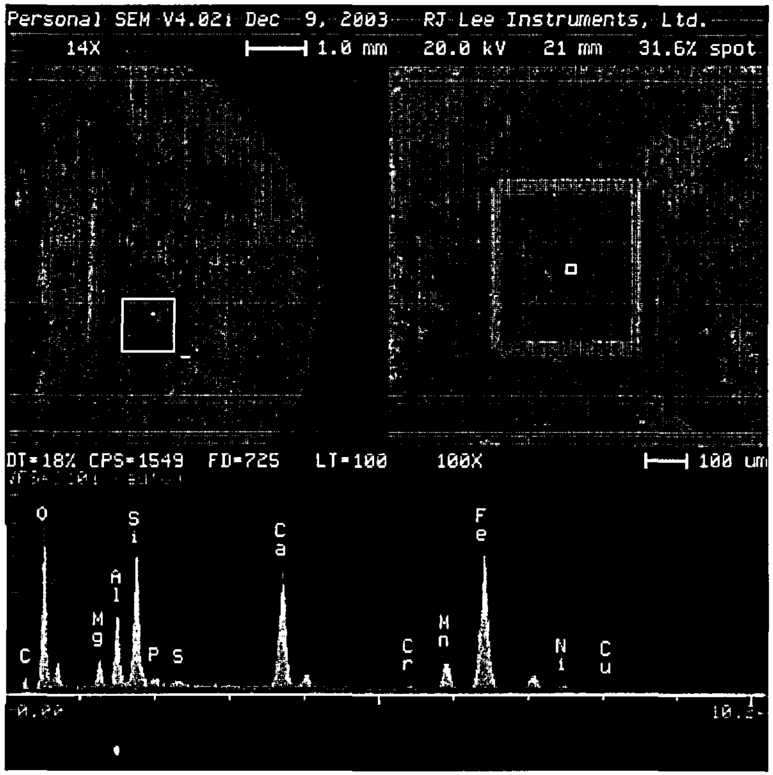

e) OD Surface (Area 6)

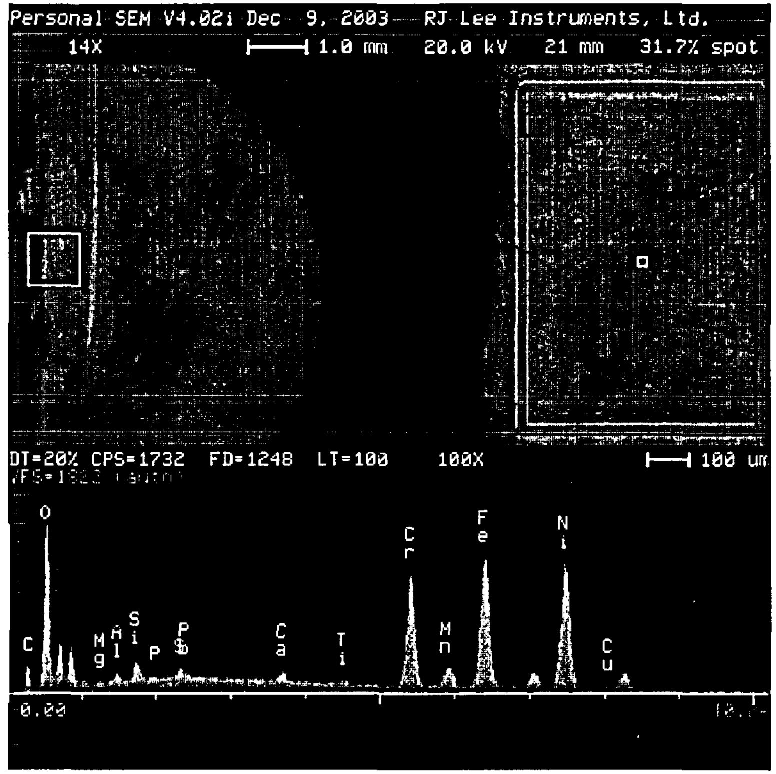

f) OD Surface (Area 7)

Figure 6 – 7 (Cont'd)
R10C39 – Piece 3B – Section 3B2A (H02 Plate)
SEM Photographs Illustrating Areas Selected for EDS

Figure 6 – 8
R10C39 – Piece 3C (Freespan)
SEM Photographs Illustrating Ductile Areas Selected for EDS

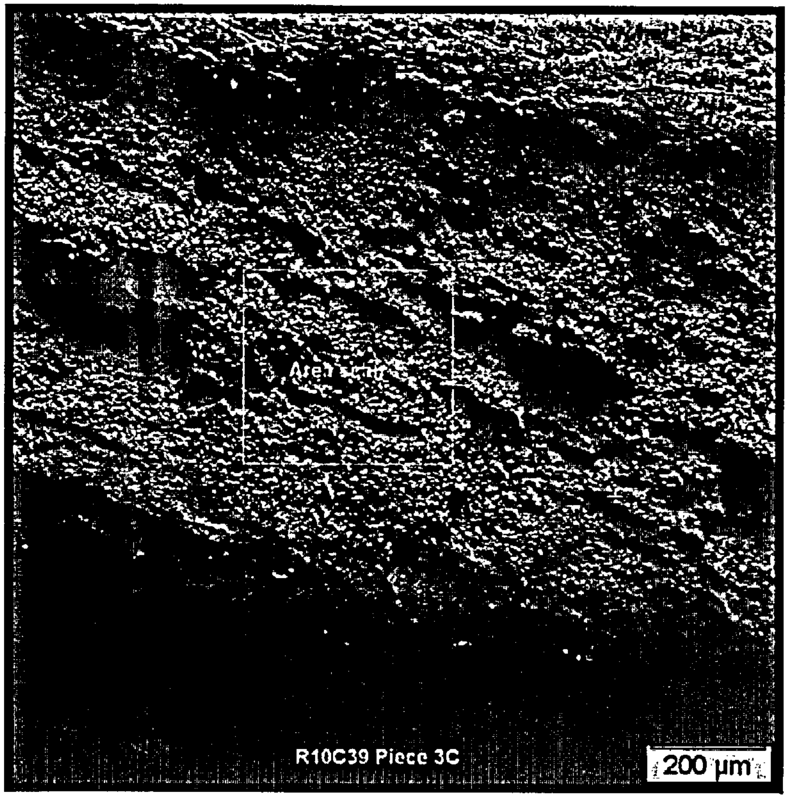

a) Ductile Fracture Face (Area 1)

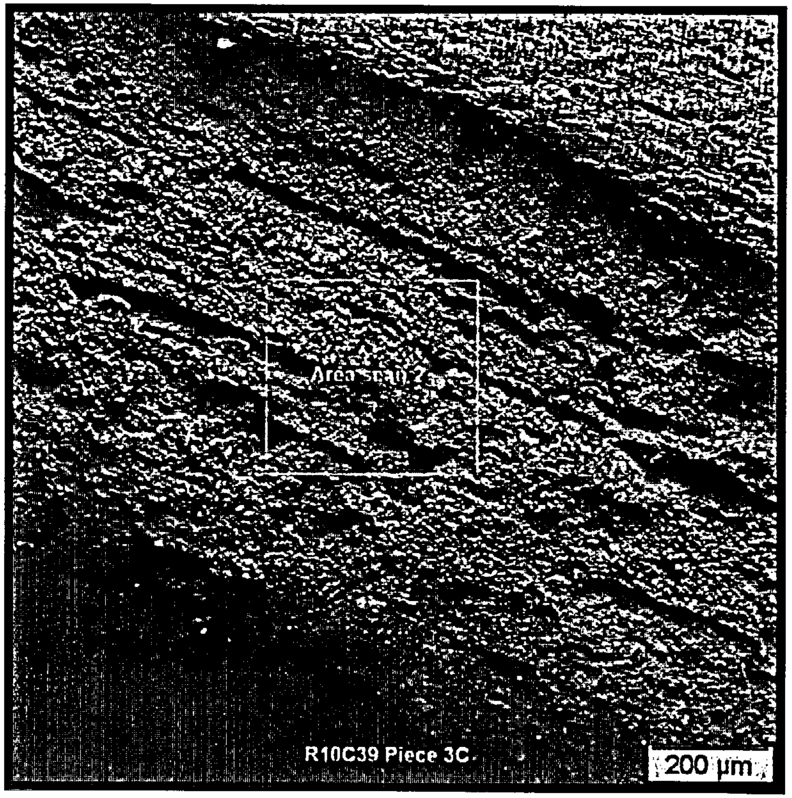

b) Ductile Fracture Face (Area 2)

Figure 6-9

R10C39 – Piece 4B – Section 4B2A – Burst Fracture Montage Associated with H03 Plate

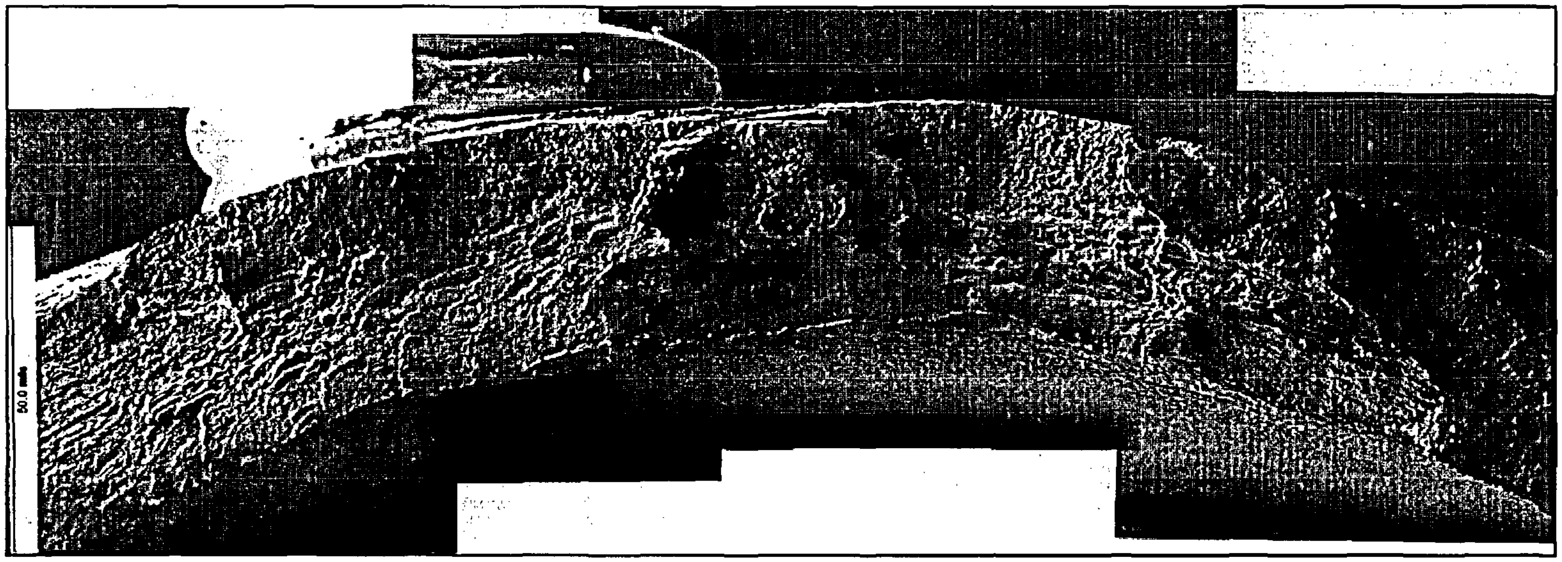

Figure 6-10
R10C39 - Piece 4B - Section 4B2A - Burst Fracture
IGSCC Depth Profile Associated with H03 Plate

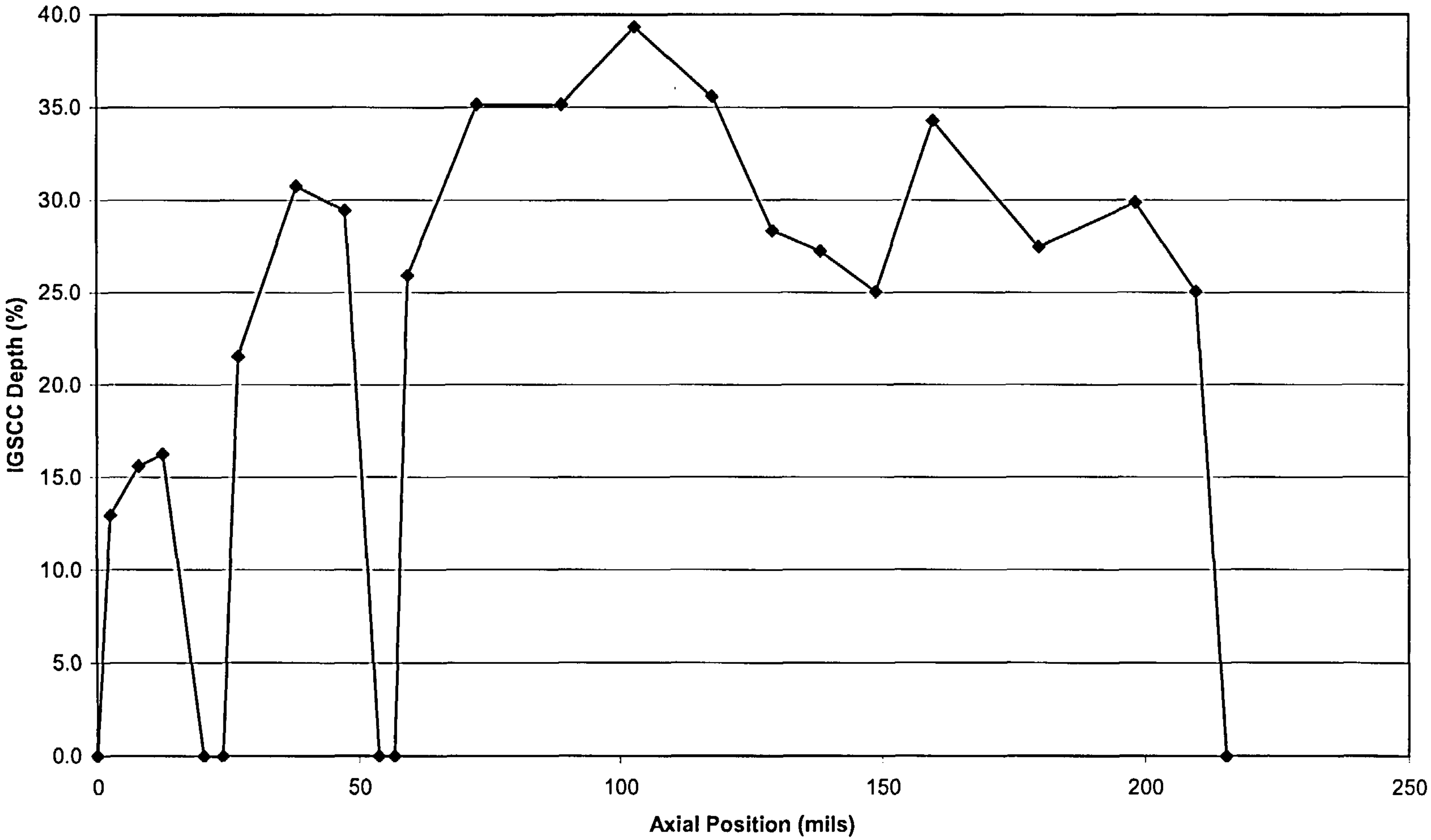

Figure 6 – 11
R10C39 – Piece 4B – Section 4B2A (H03 Plate)
SEM Photographs Showing General Ductile and Intergranular Fracture Features

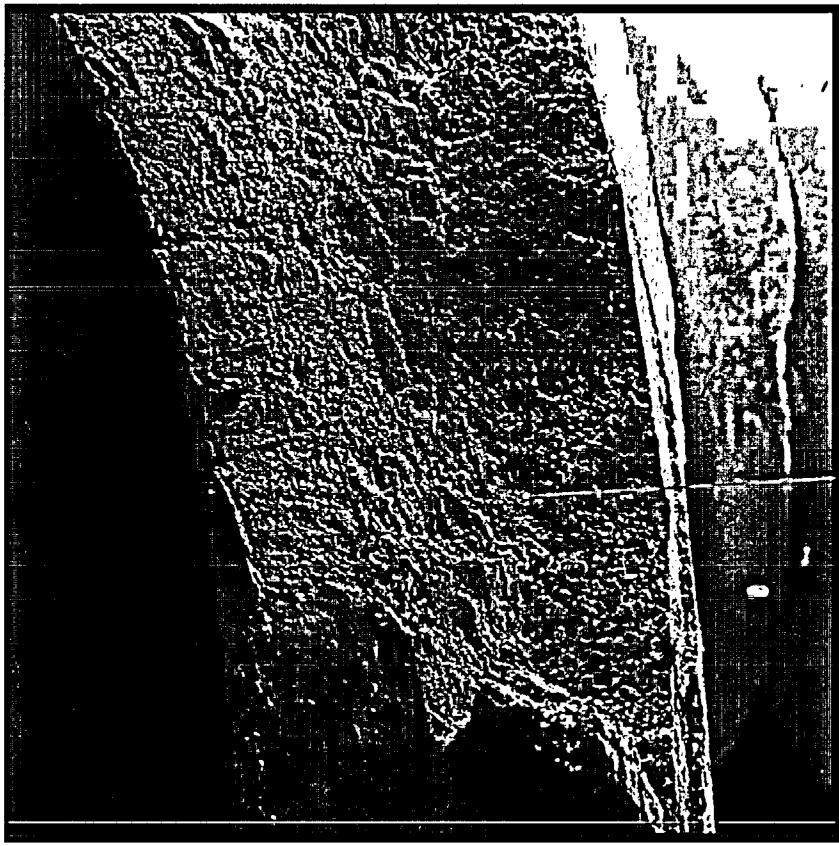

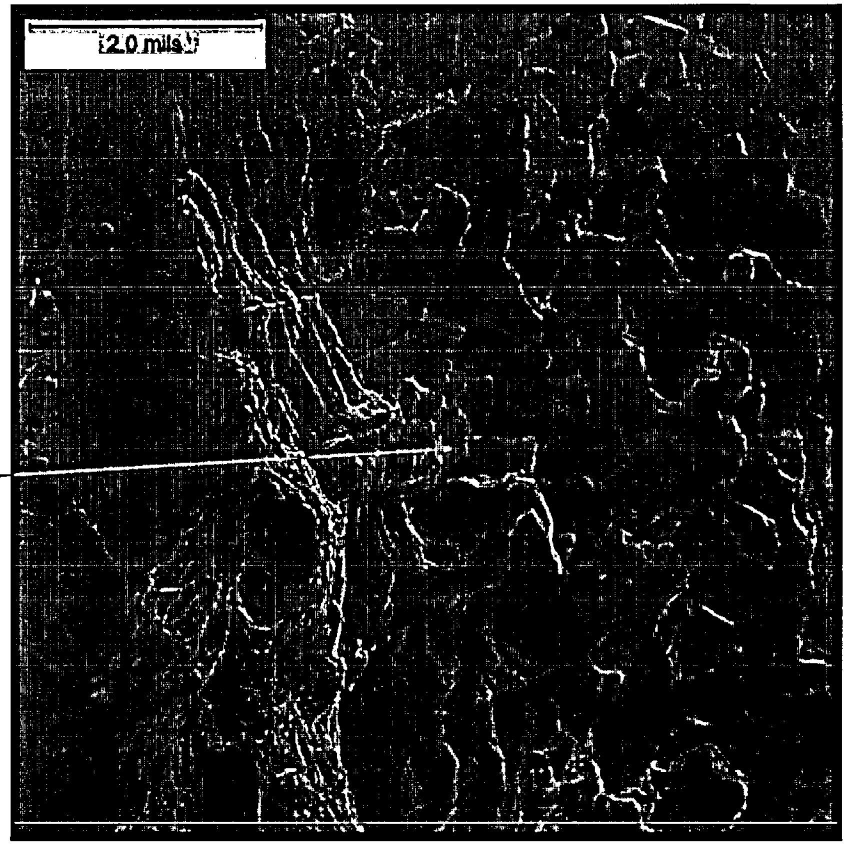

Figure 6 – 12
R10C39 – Piece 4B – Section 4B2A (H03 Plate)
SEM Photograph Showing OD Surface Adjacent to
Burst Fracture

Figure 6 – 13
R10C39 – Piece 4B – Section 4B2A (H03 Plate)
SEM Photograph Showing Ductile Ligaments Observed
Within Intergranular Fracture Areas

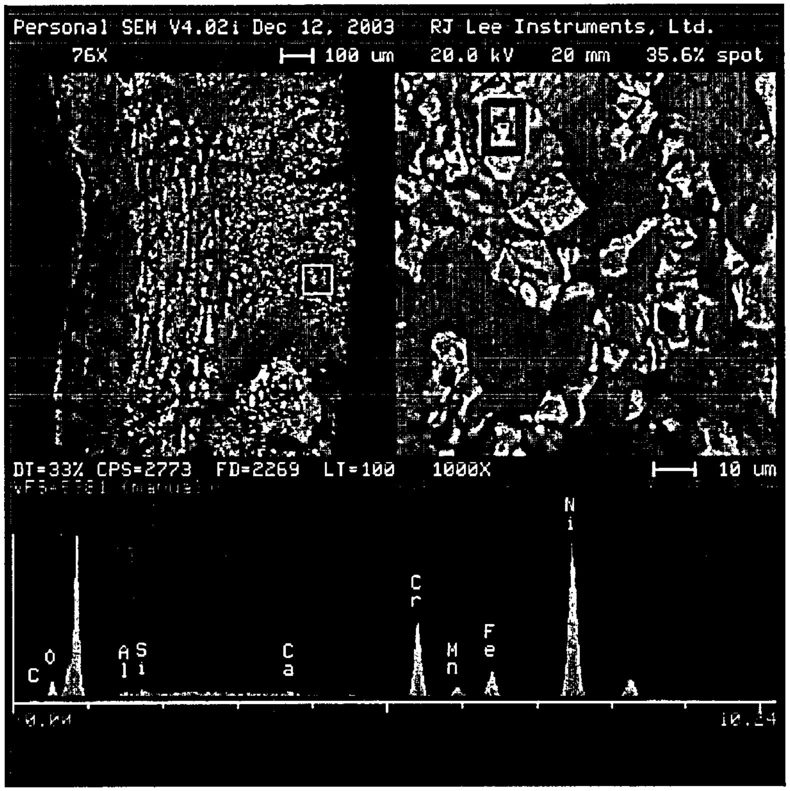

a) IGSCC (Area 1)

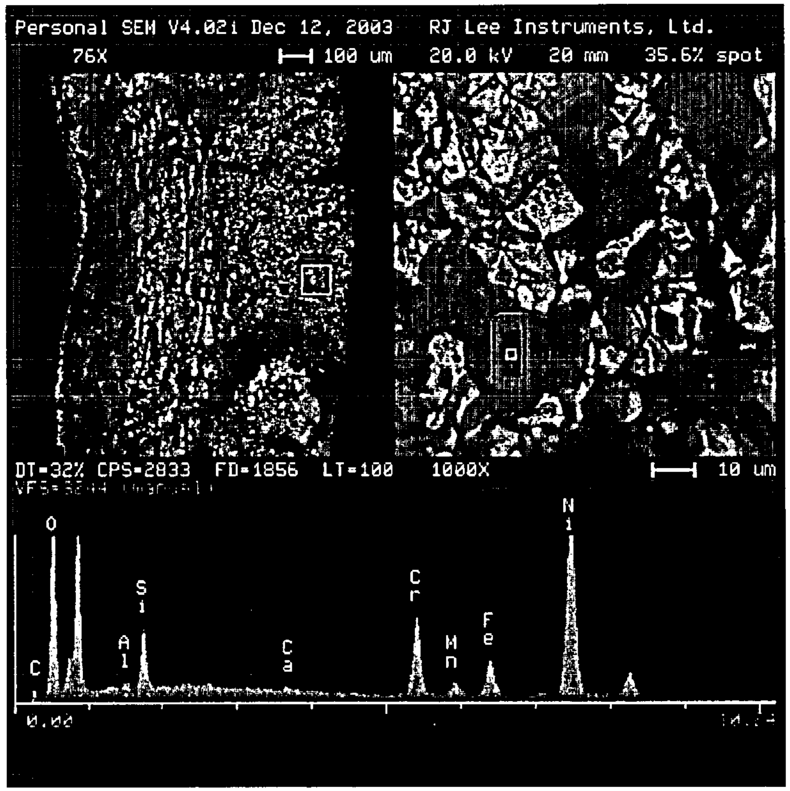

b) IGSCC (Area 2)

Figure 6 – 14
R10C39 – Piece 4B – Section 4B2A (H03 Plate)
SEM Photographs Illustrating Areas Selected for EDS

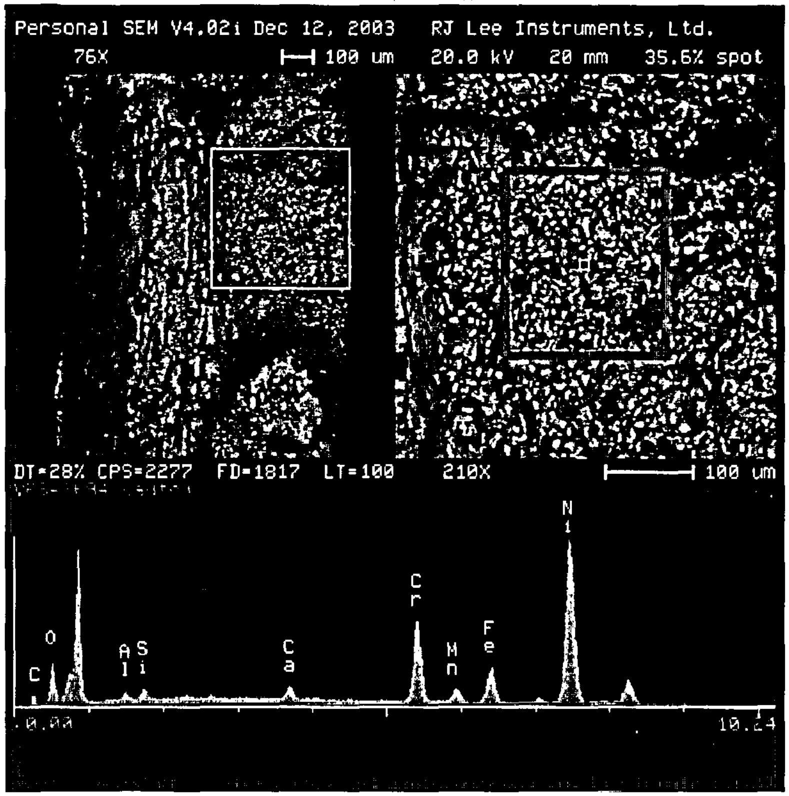

c) IGSCC (Area 3)

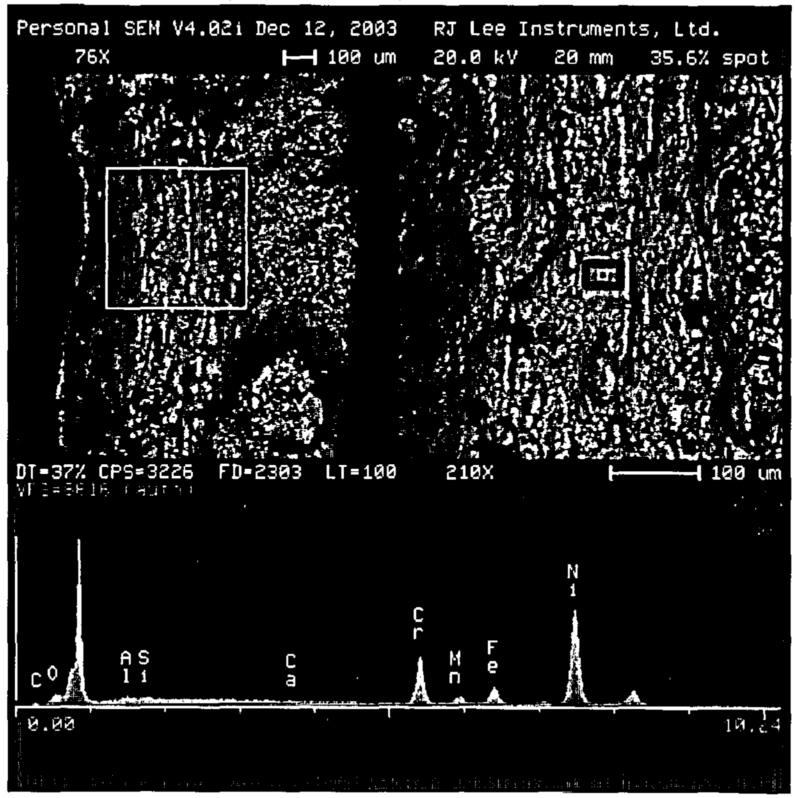

d) Ductile Fracture (Area 4)

Figure 6 – 14 (Cont'd)
R10C39 – Piece 4B – Section 4B2A (H03 Plate)
SEM Photographs Illustrating Areas Selected for EDS

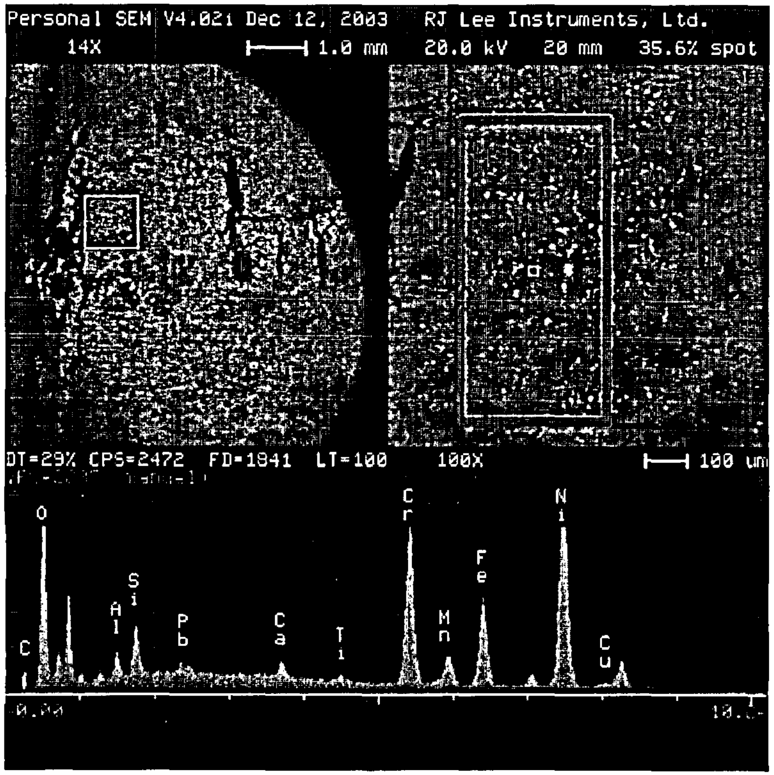

e) OD Surface (Area 5)

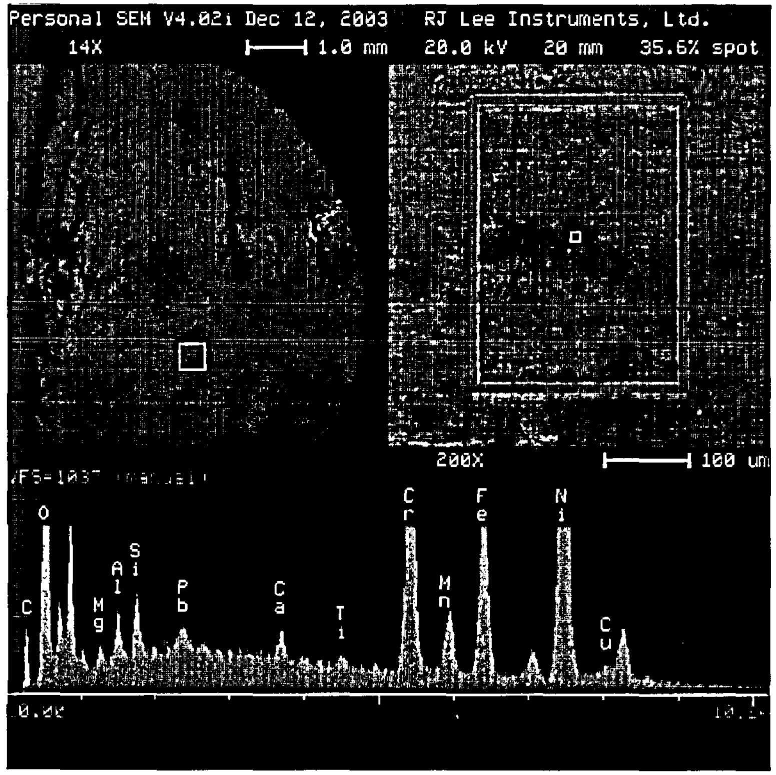

d) Ductile Fracture (Area 6)

Figure 6 – 14 (Cont'd)
R10C39 – Piece 4B – Section 4B2A (H03 Plate)
SEM Photographs Illustrating Areas Selected for EDS

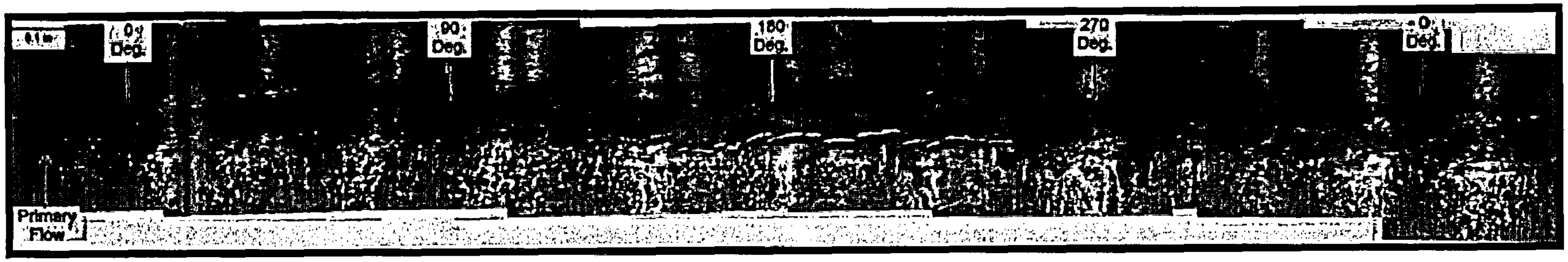

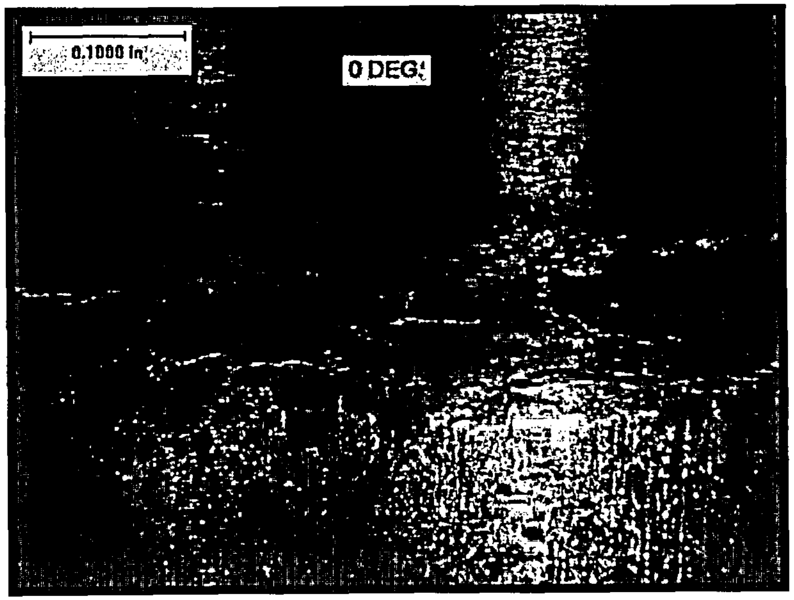

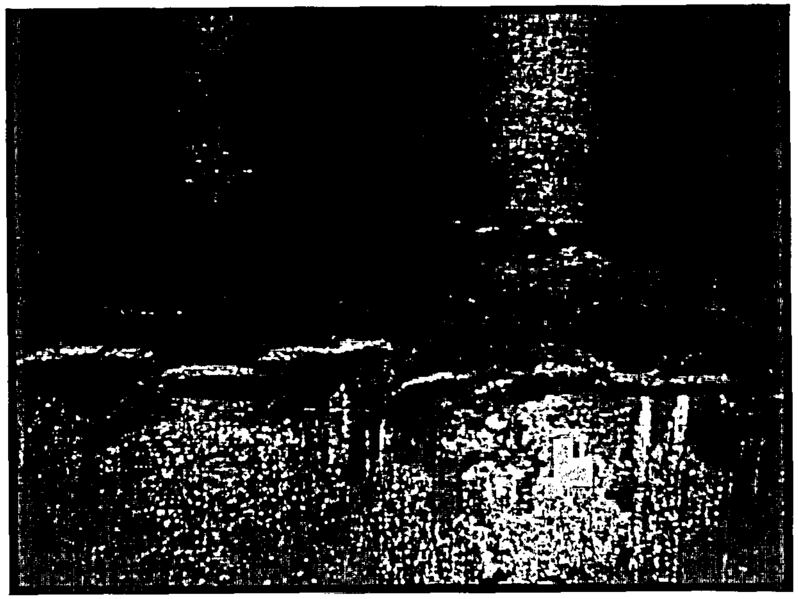

Figure 6 - 15
R11C41 – Piece 2B – Section 2B1
General OD Appearance of Circumferential Indication @ TTS

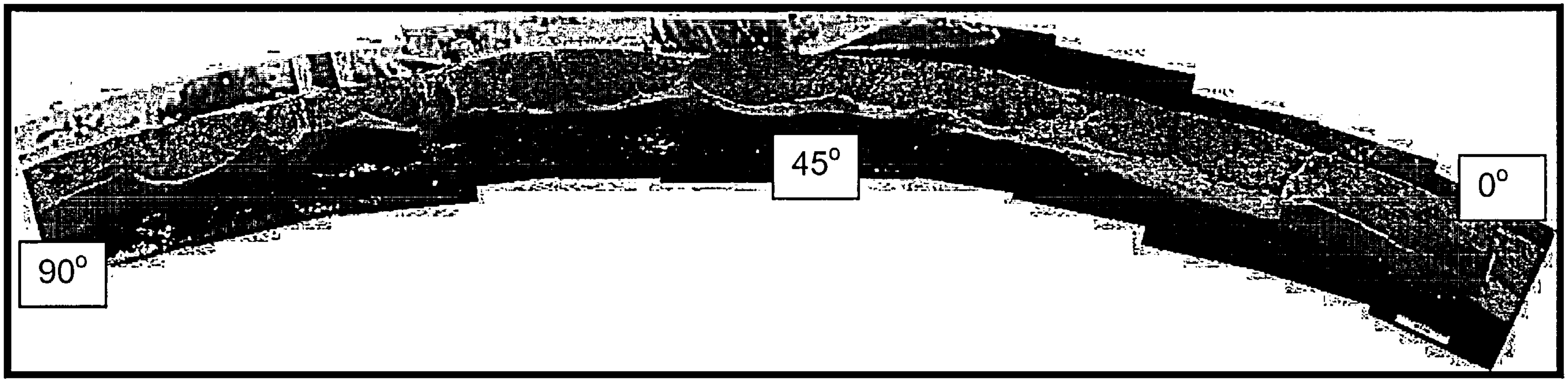

Figure 6 – 16
R11C41 – Piece 2B – Section 2B1B
Fracture Face Montage (0° to 90°) of Circumferential Indication @ TTS

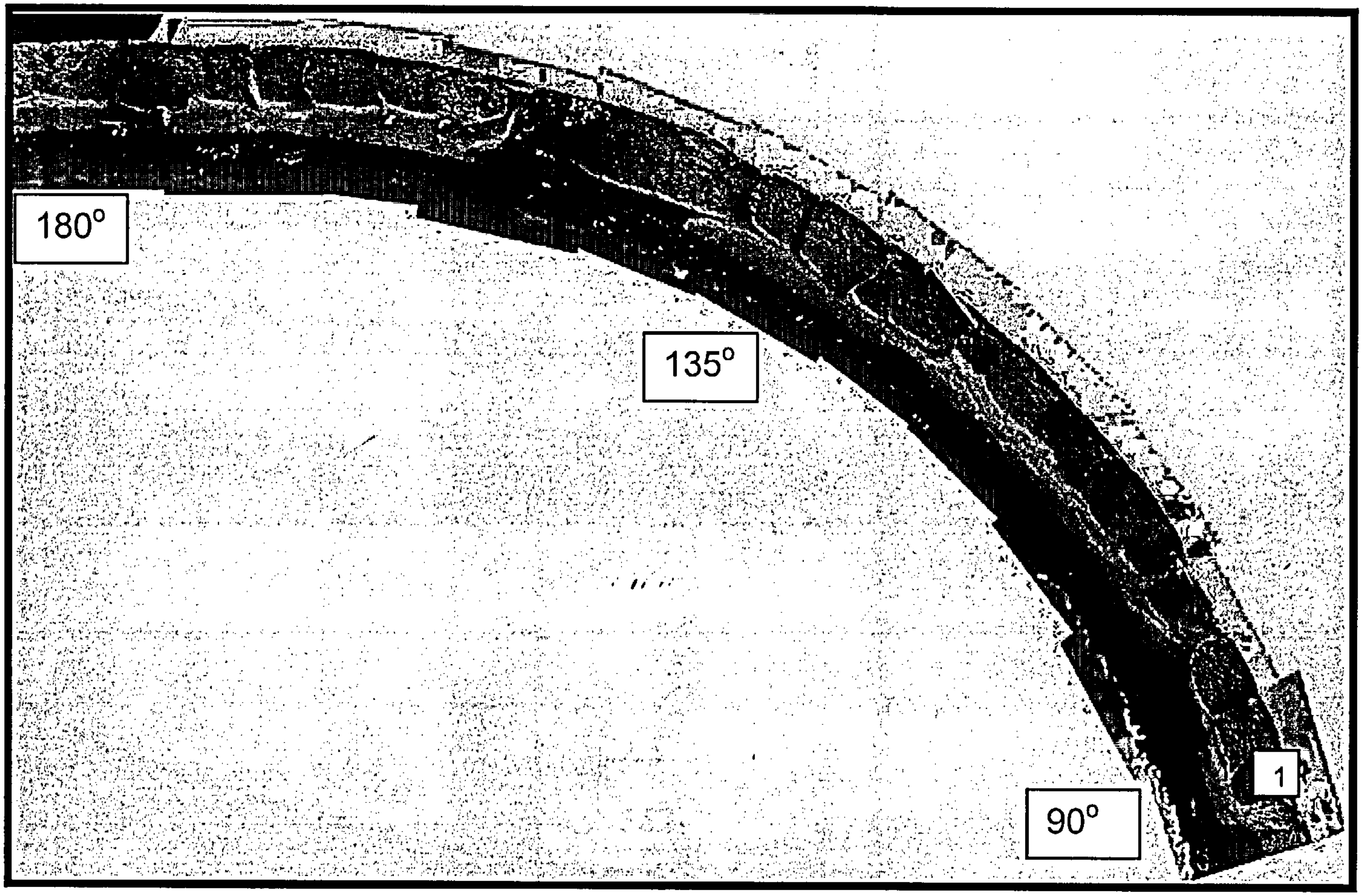

Figure 6 – 16 (Cont'd)
R11C41 – Piece 2B – Section 2B1B
Fracture Face Montage (90° to 180°) of Circumferential Indication @ TTS

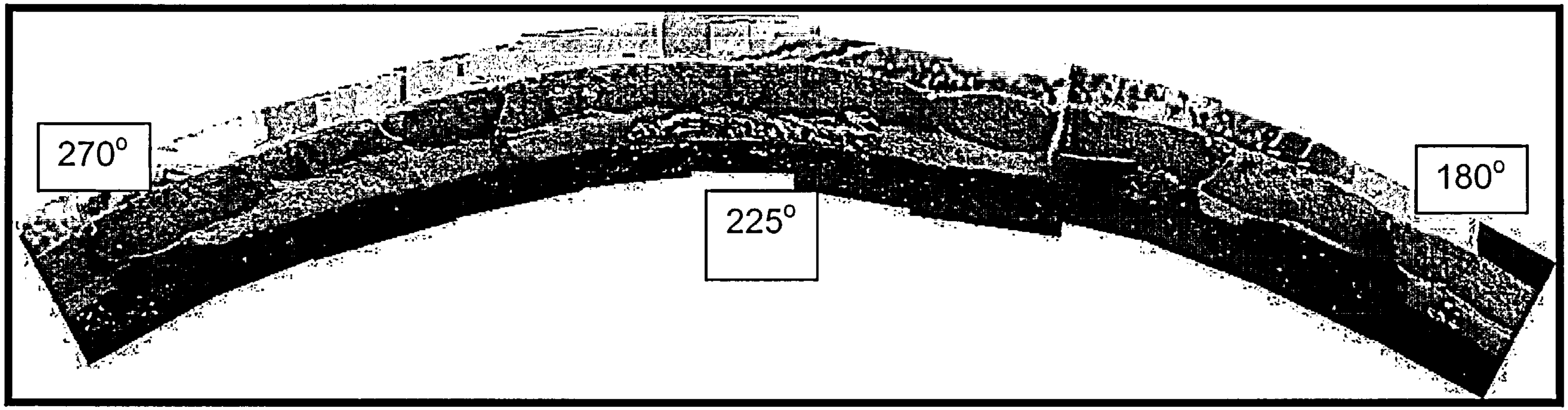

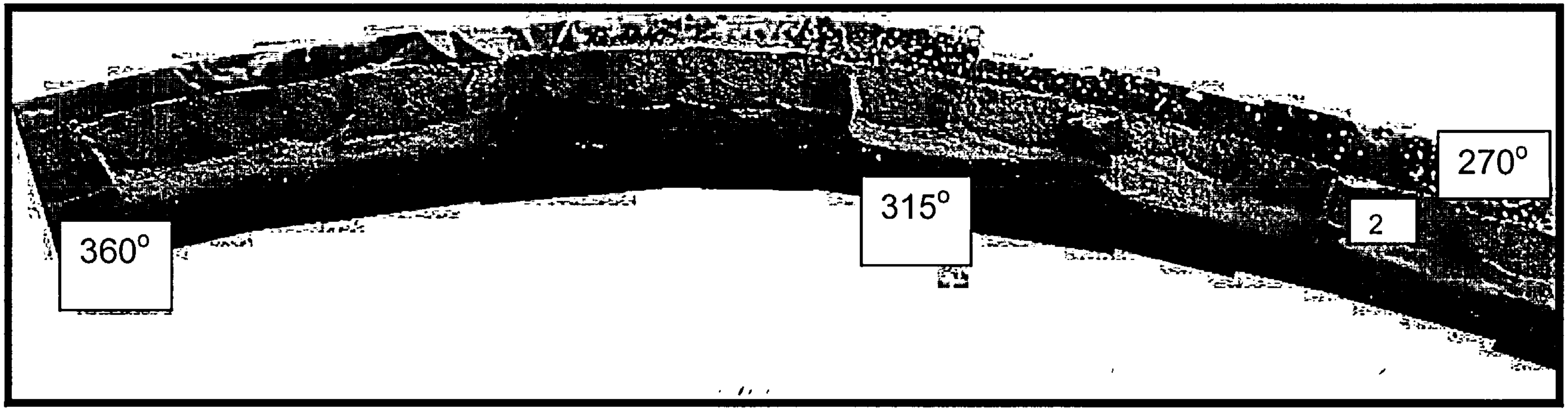

Figure 6 – 16 (Cont'd)
R11C41 – Piece 2B – Section 2B1B
Fracture Face Montage (180° to 360°) of Circumferential Indication @ TTS

Figure 6-17
R11C41 - Piece 2B - Section 2B1B - Intergranular Fracture Depth Following Tensile Loading of Circumferential Indication @ TTS

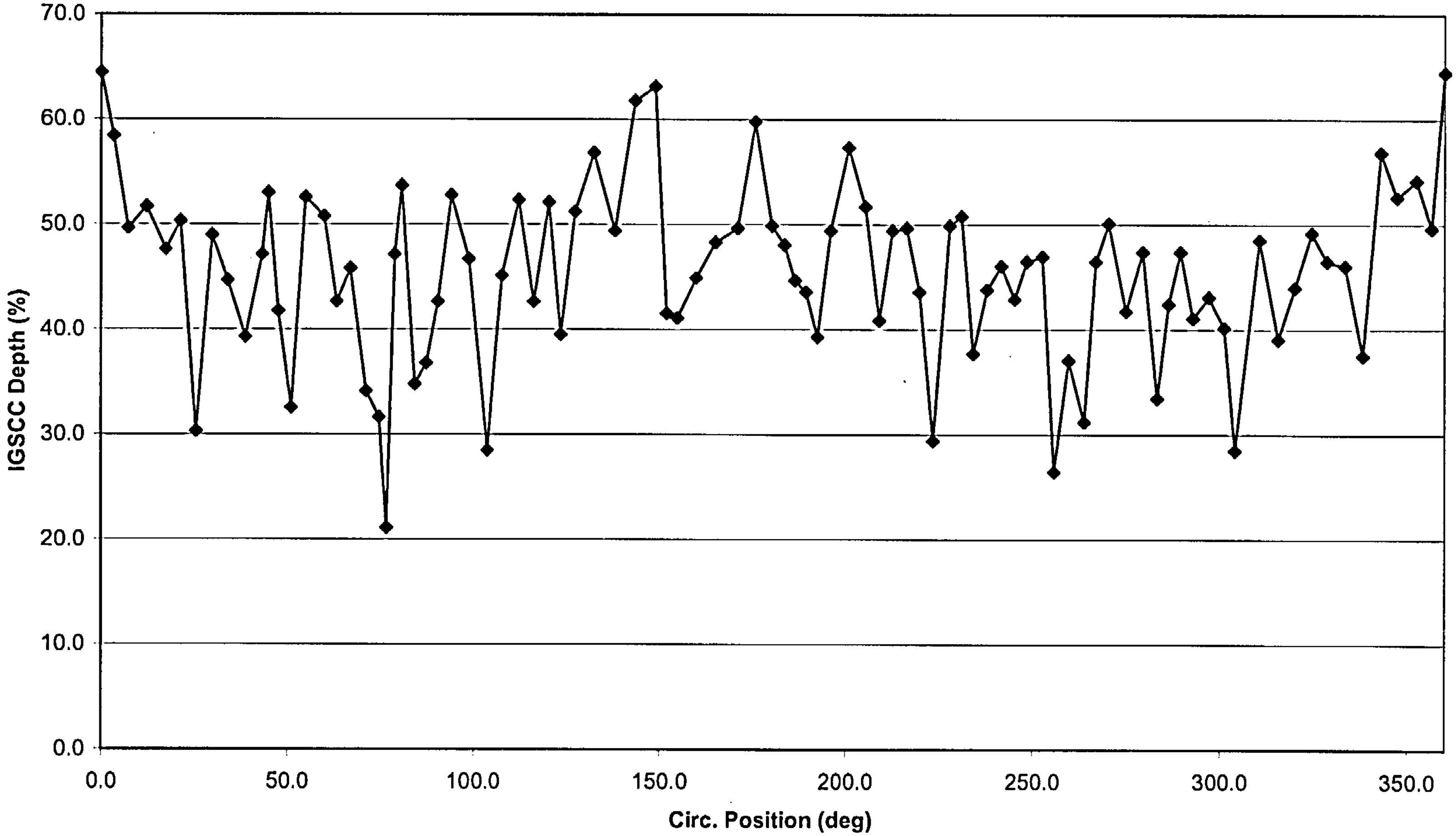

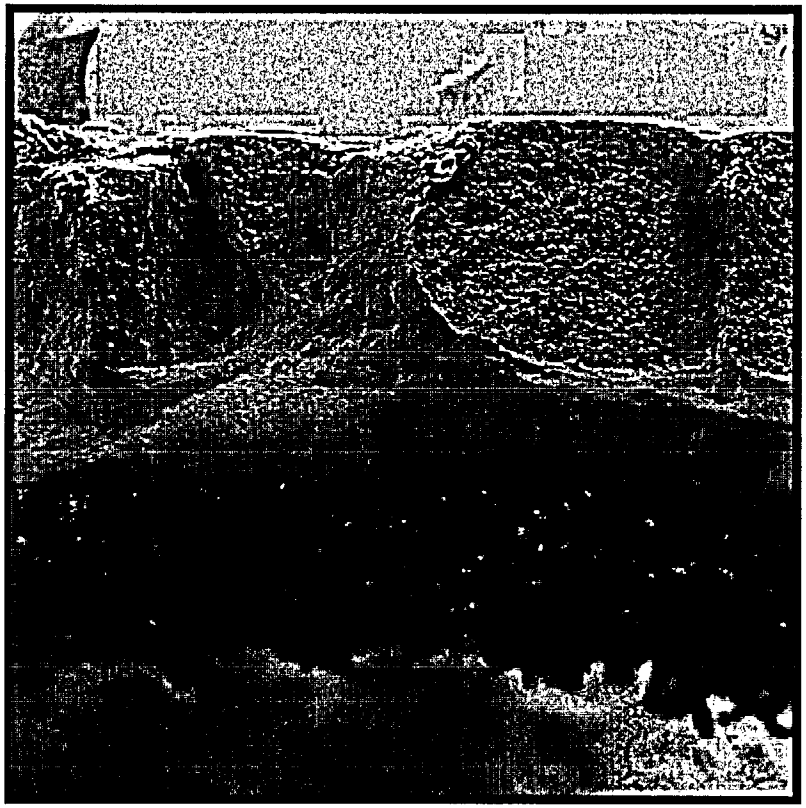

Area 1

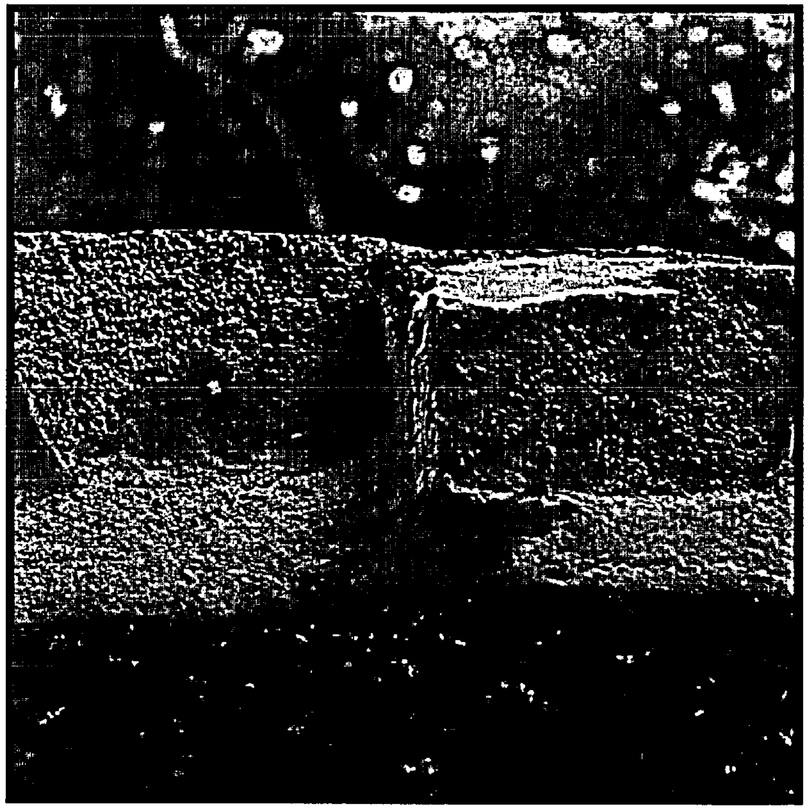

Area 2

Figure 6 – 18
R11C41 – Piece 2B – Section 2B1B (TTS)
SEM Photographs Showing IGSCC Fracture Features
Note: See Figure 6-17 for Area Location

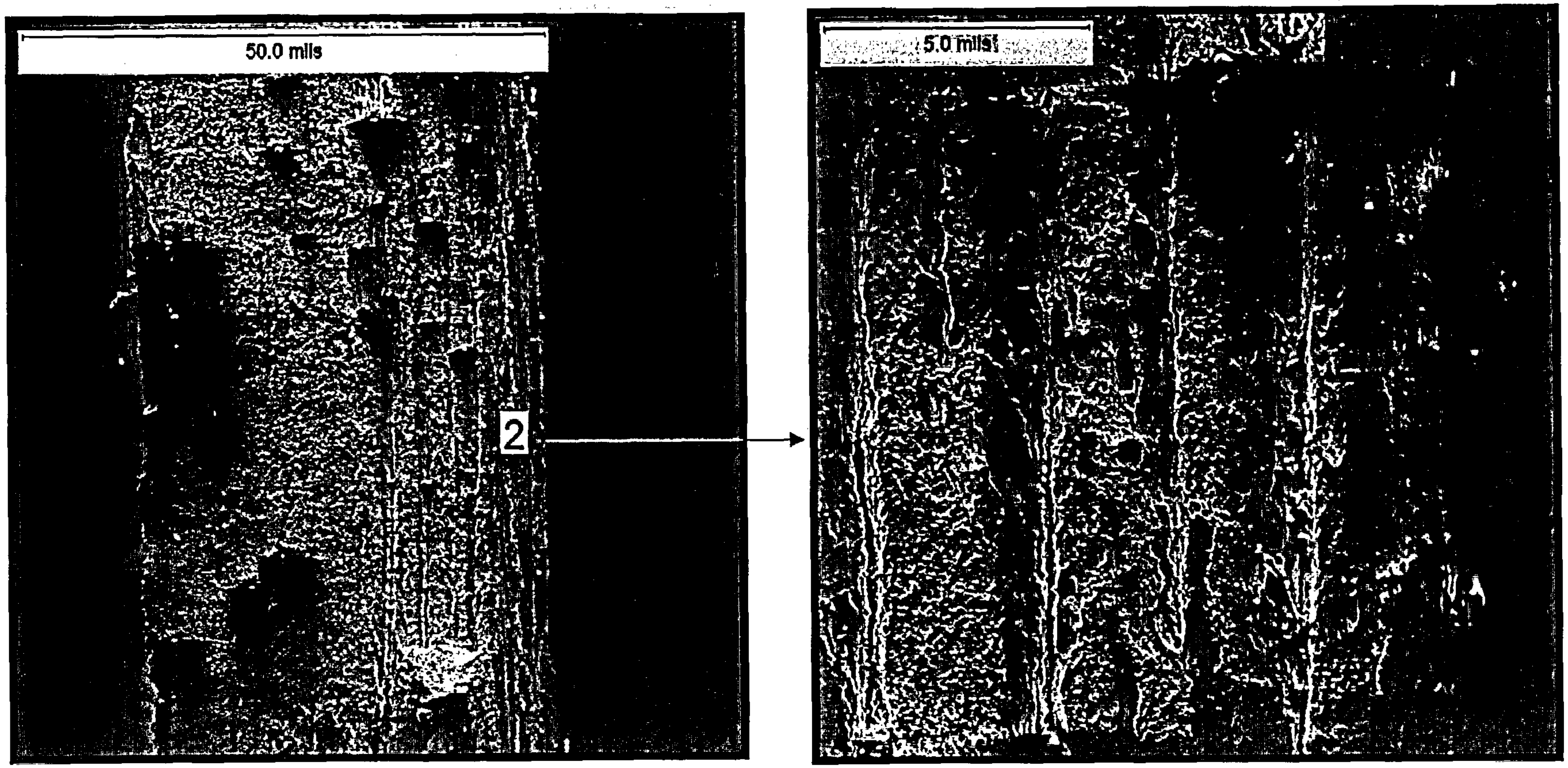

Figure 6-19
R11C41HL – Piece 2B – Section 2B2A
General Appearance of Freespan Burst Fracture Face Located Above TTS

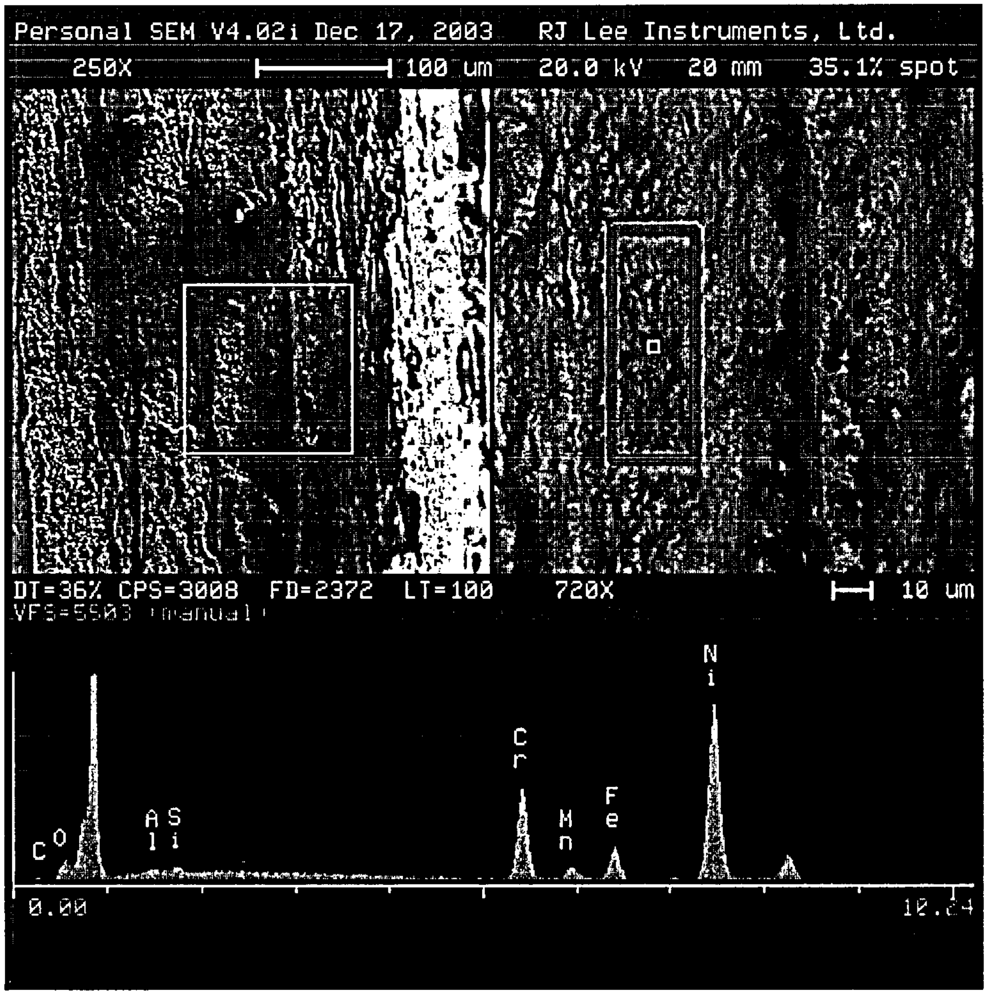

Figure 6-20
R11C41 HL – Piece 2B – Section 2B2A
EDS Results of Axial Burst Fracture Face (Ductile)

Figure 6 – 21
R11C41 – Piece 3B – Section 3B2A
Montage of Burst Fracture Face Associated with H02 Plate

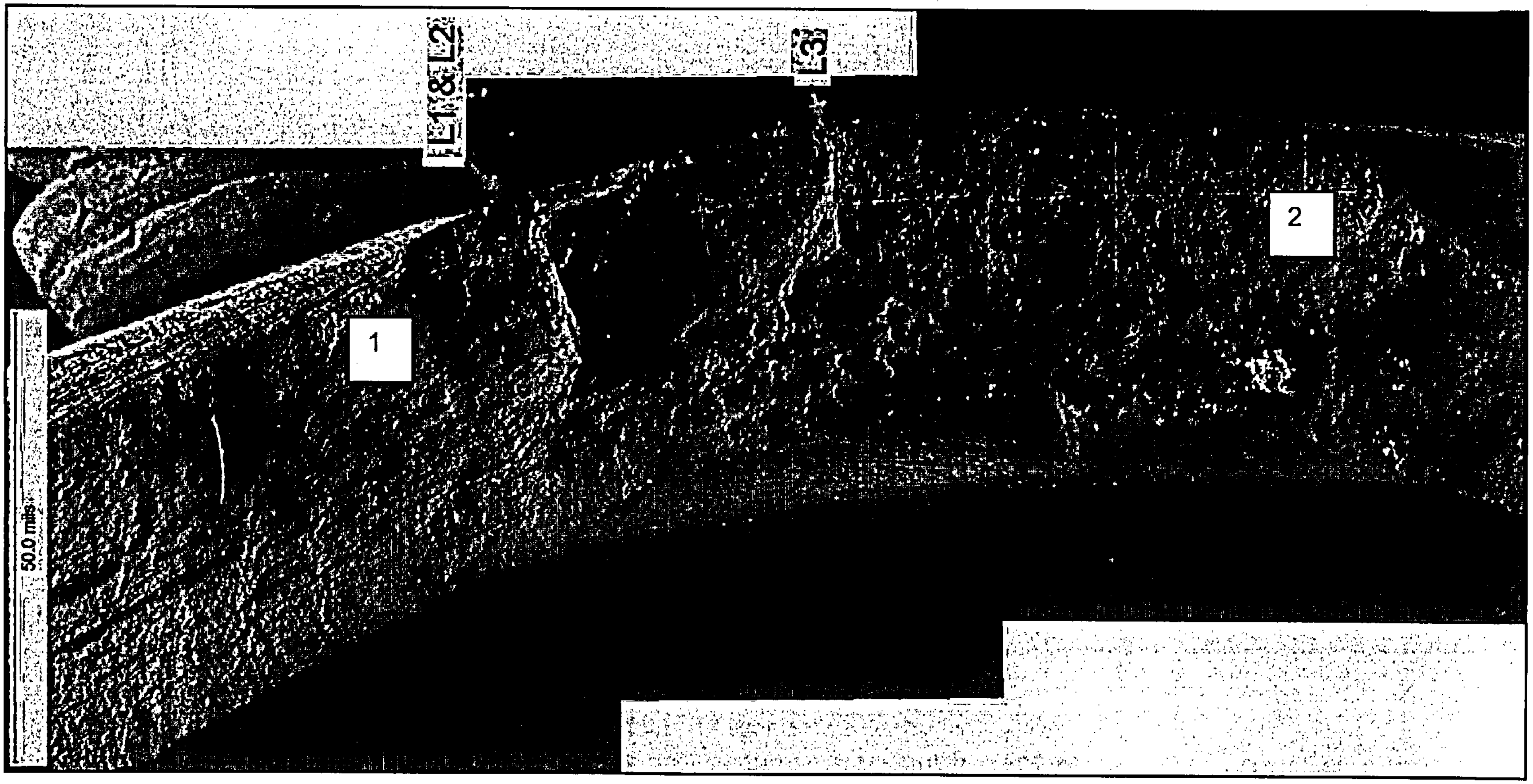

Figure 6-22
R11C41 - Piece 3B - Section 3B2A - Burst Fracture
IGSCC Depth Profile Associated with H02 Plate

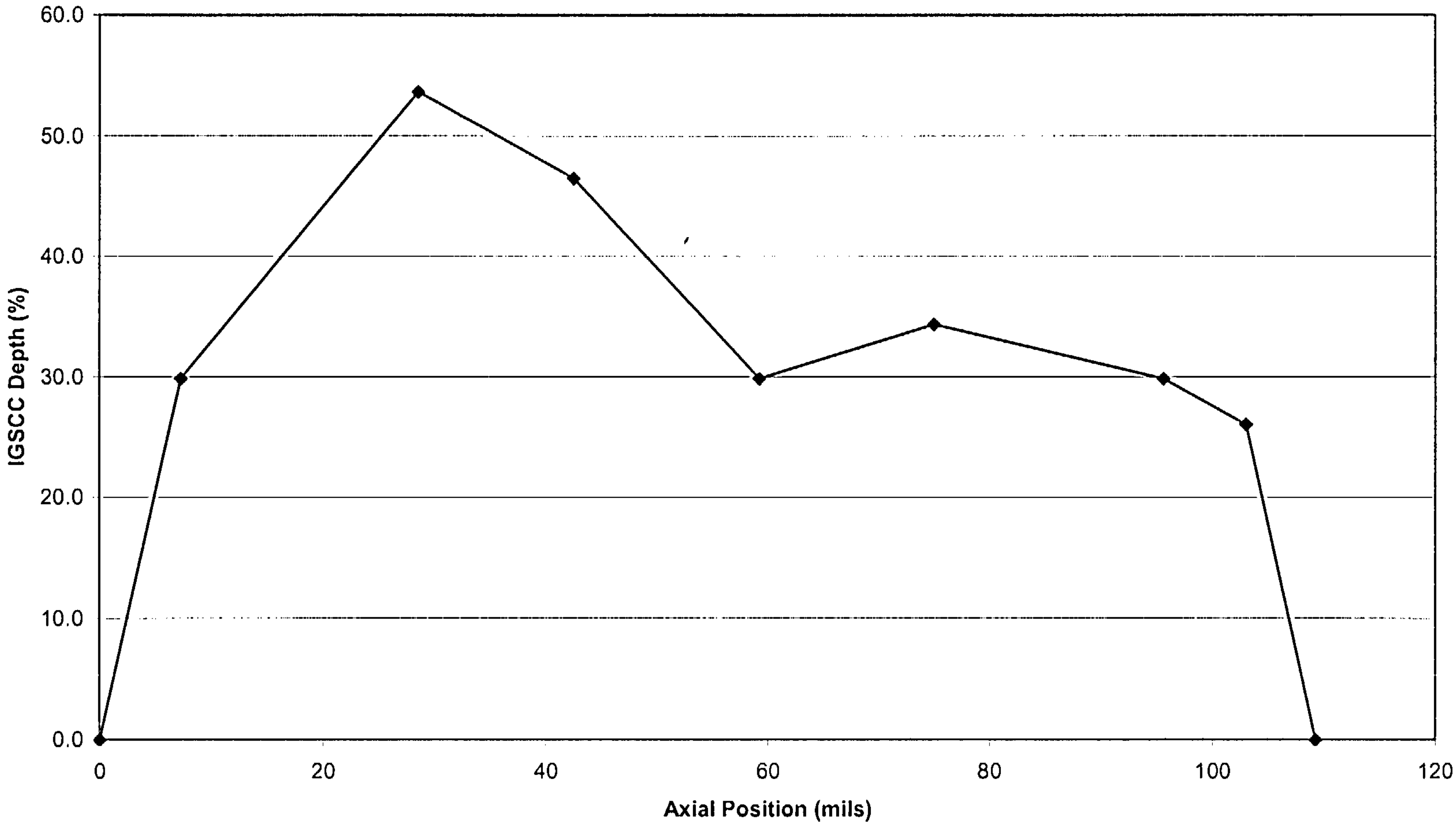

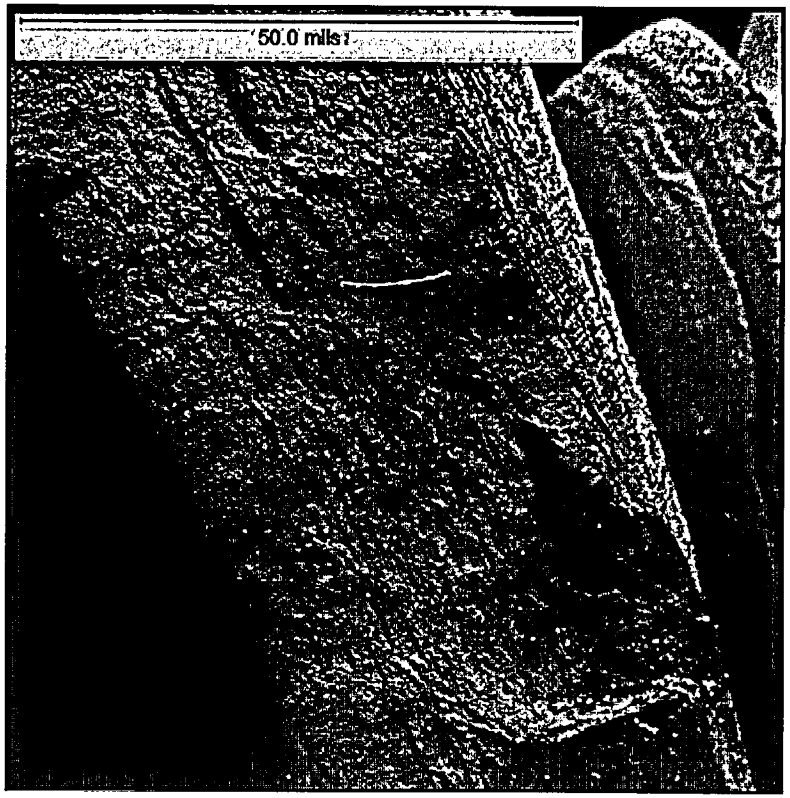

Area 1

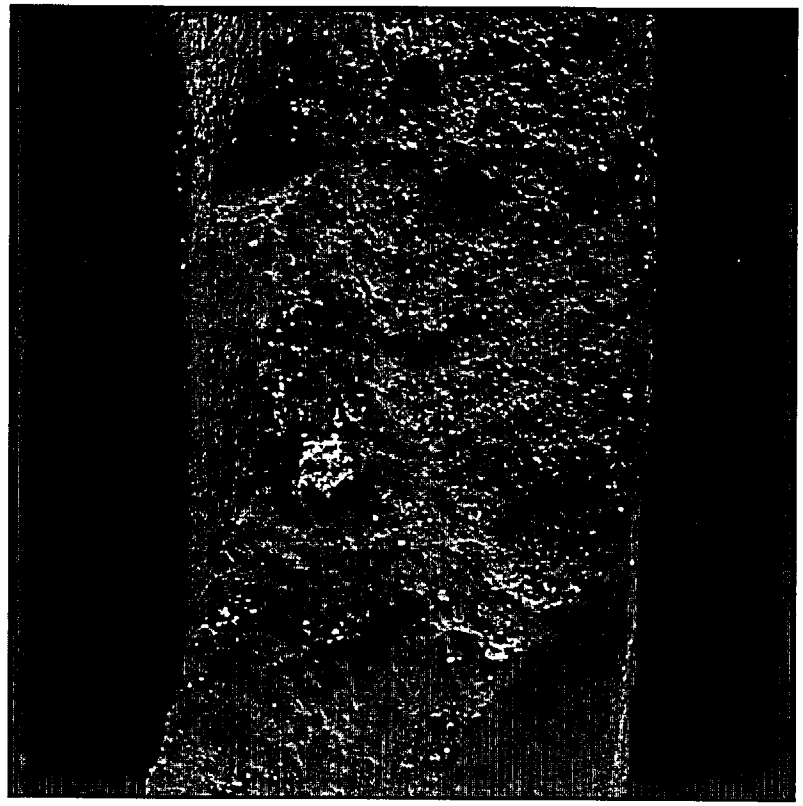

Area 2

Figure 6 - 23
R11C41 – Piece 3B – Section 3B2A (H02 Plate)
General Appearance of IGSCC Fracture Face
Note: Refer to Figure 6-19 for Area Location

Figure 6 – 24
R11C41 – Piece 3B – Section 3B2A (H02 Plate)
SEM Photograph Showing Ductile Ligaments Observed Within Intergranular Fracture Areas

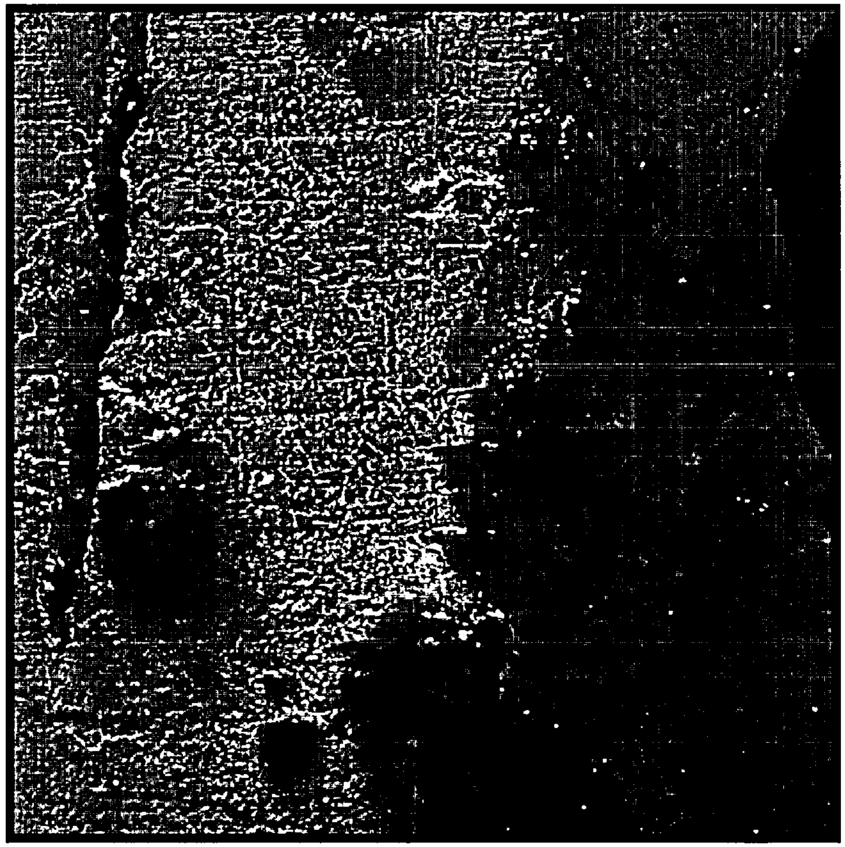

Figure 6 – 25
R11C41 – Piece 3B – Section 3B2A (H02 Plate)
SEM Photograph Showing OD Surface Adjacent to Burst Fracture

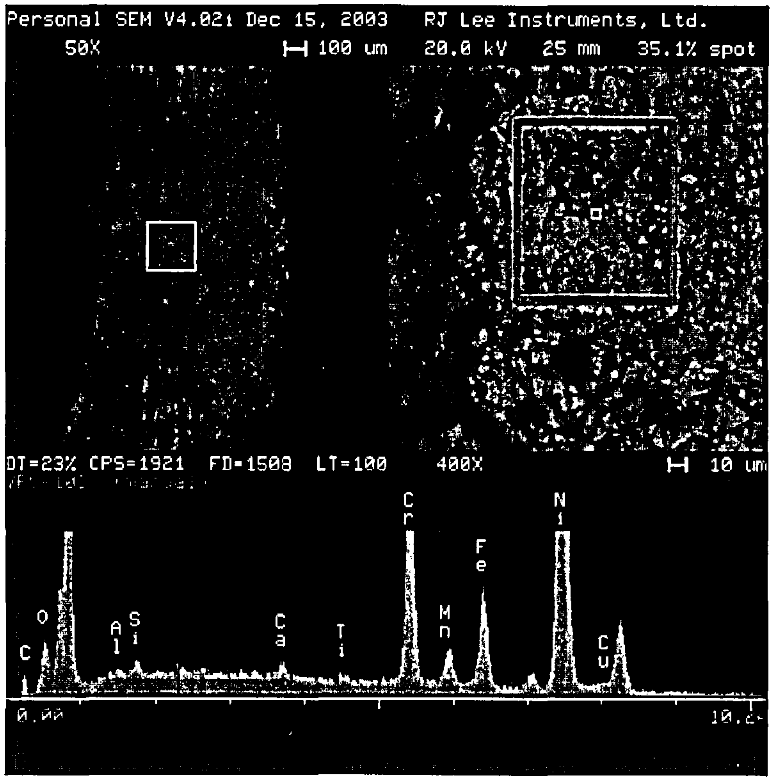

a) Intergranular Near Tip

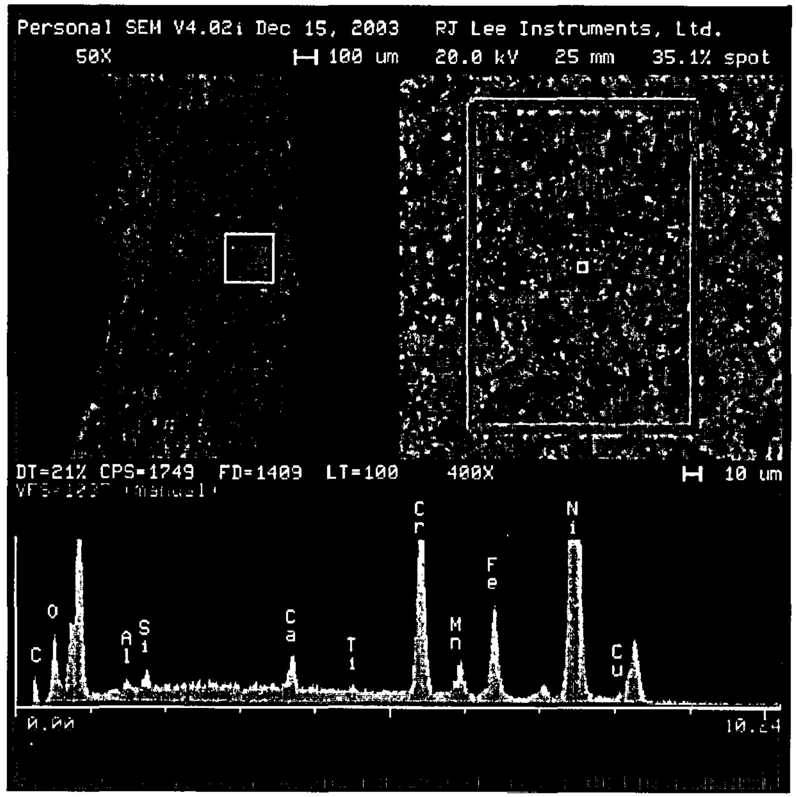

b) Intergranular Near Crack Mouth

Figure 6 – 26
R11C41 – Piece 3B – Section 3B2A (H02 Plate)
SEM Photographs Illustrating Areas Selected for EDS

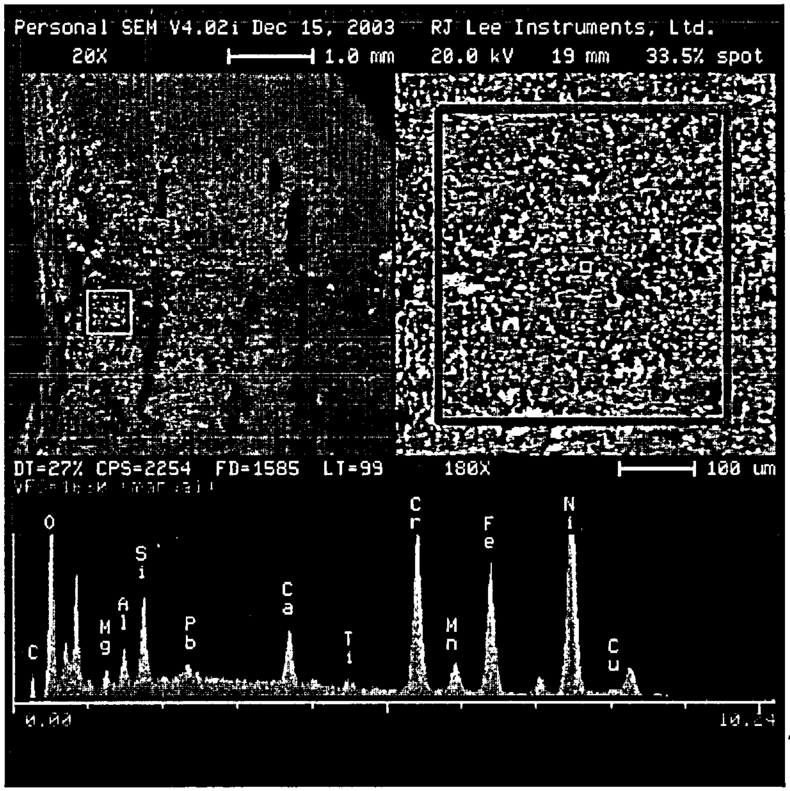

c) OD Surface

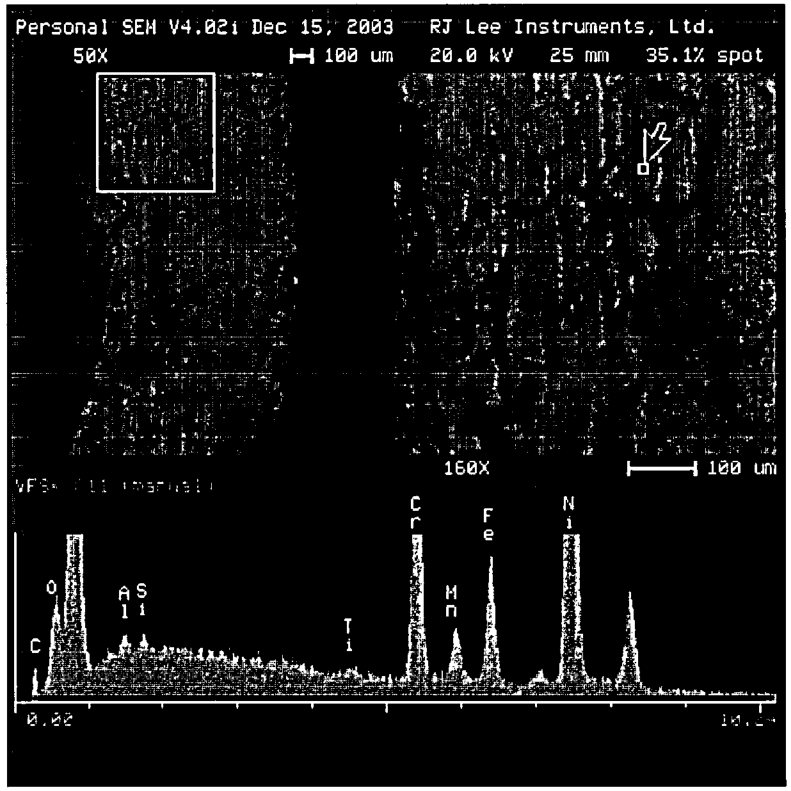

d) Ductile Facture

Figure 6 – 26 (Cont'd)
R11C41 – Piece 3B – Section 3B2A (H02 Plate)
SEM Photographs Illustrating Areas Selected for EDS

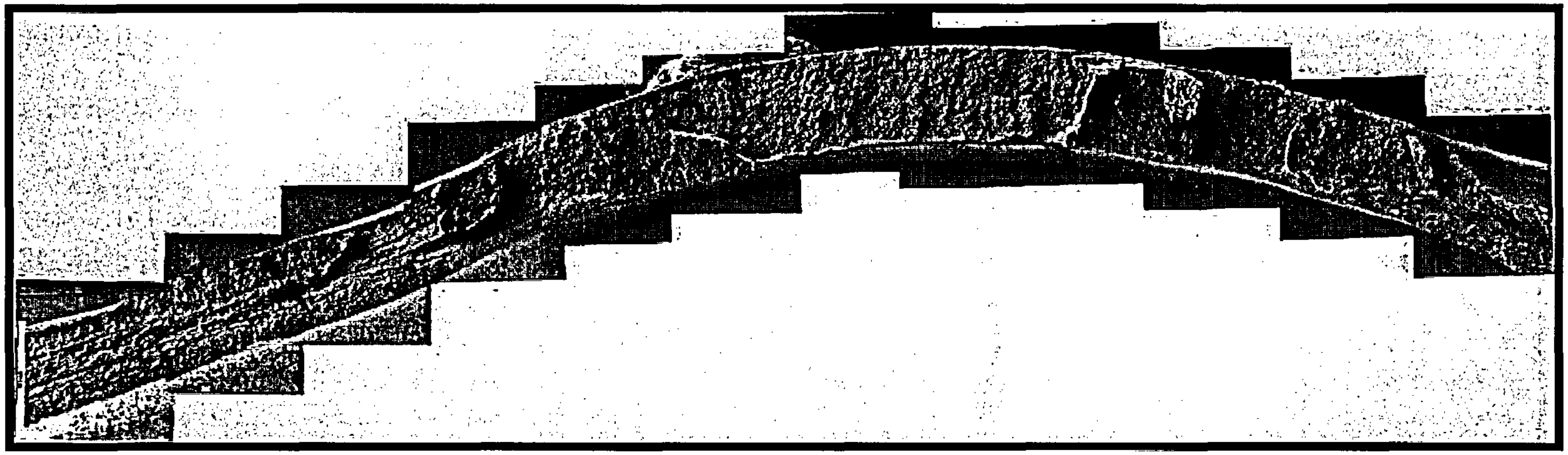

Figure 6-27
R11C41 – Piece 4B – Section 4B2A
Montage of Burst Fracture Face Associated with H03 Plate

Figure 6-28
R11C41 - Piece 4B - Section 4B2A - Burst Fracture
IGSCC Depth Profile Associated with H03 Plate

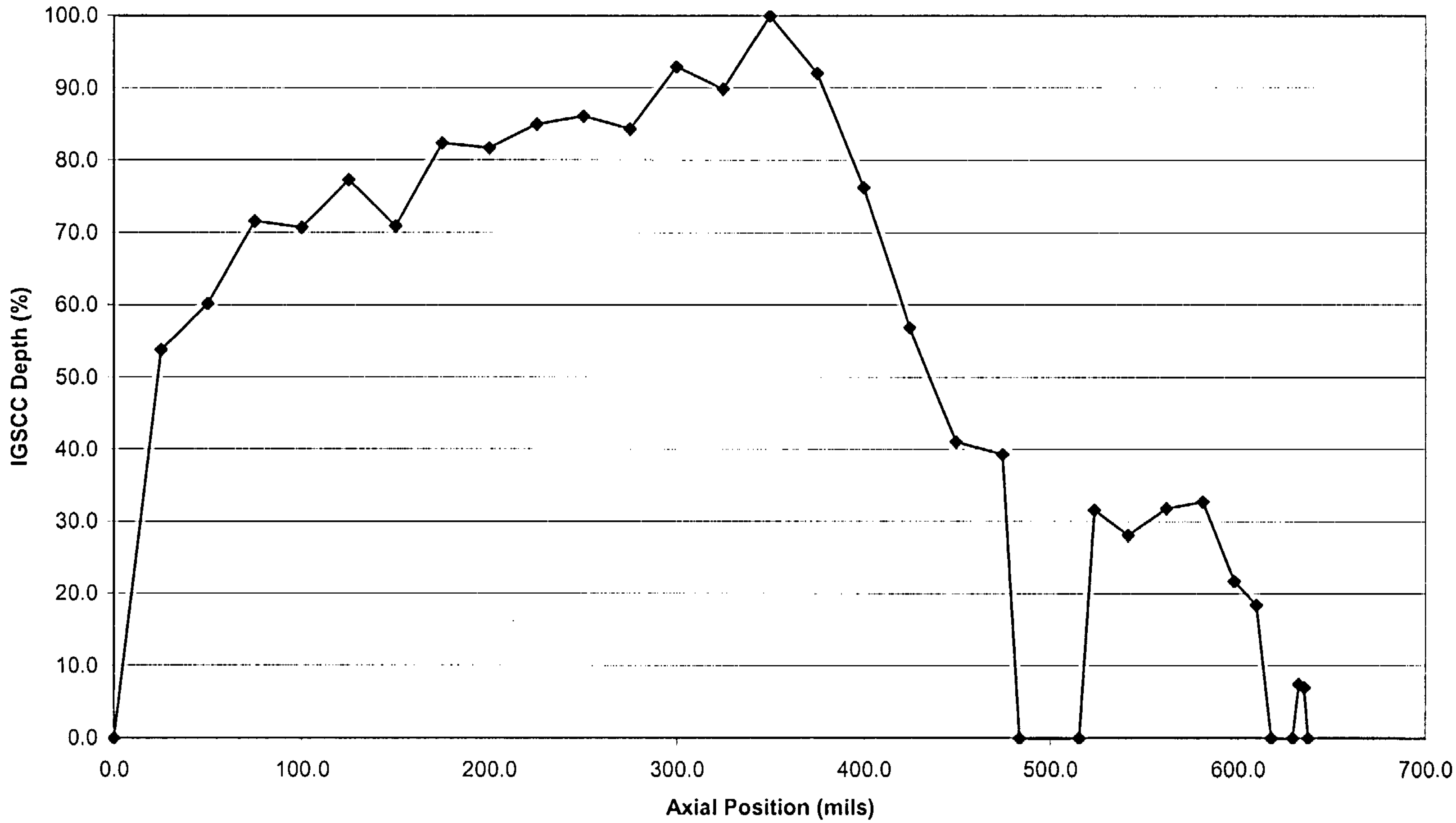

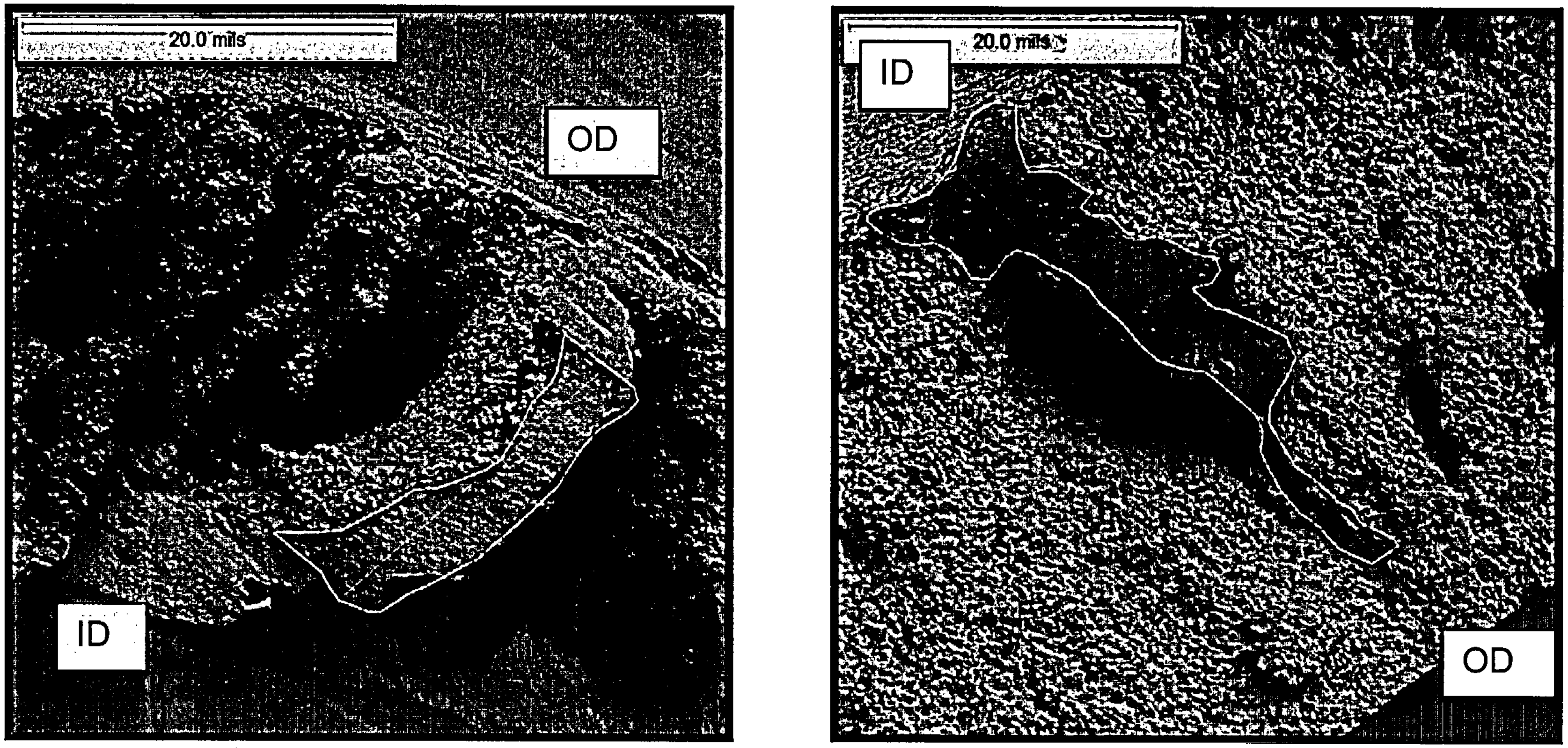

Figure 6 – 29
R11C41 – Piece 4B – Section 4B2A (H03 Plate)
SEM Photographs Showing Ductile Ligaments Observed Within Intergranular Fracture Areas

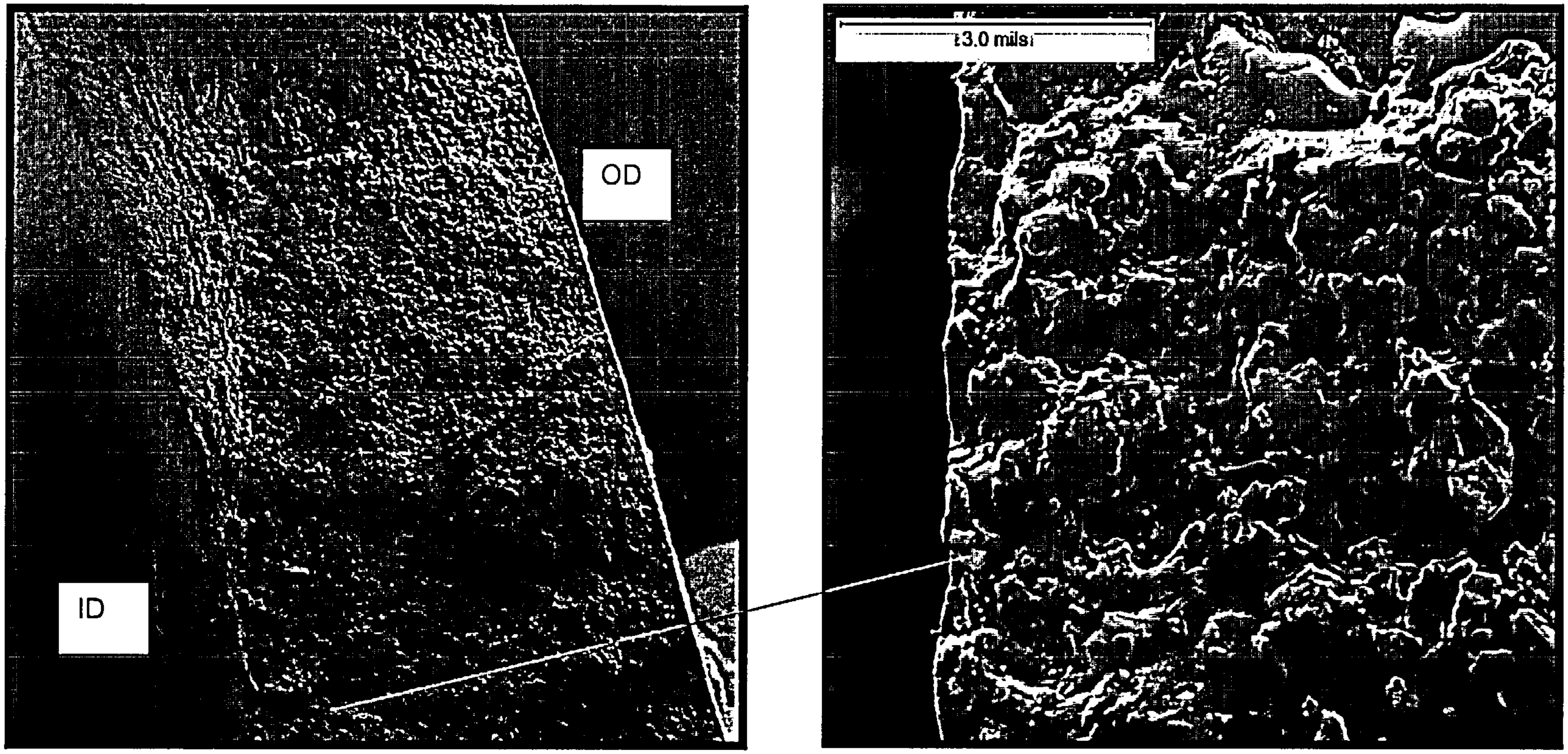

Figure 6 – 30
R11C41 – Piece 4B – Section 4B2A (H03 Plate)
SEM Photographs Illustrating Intergranular Fracture Face

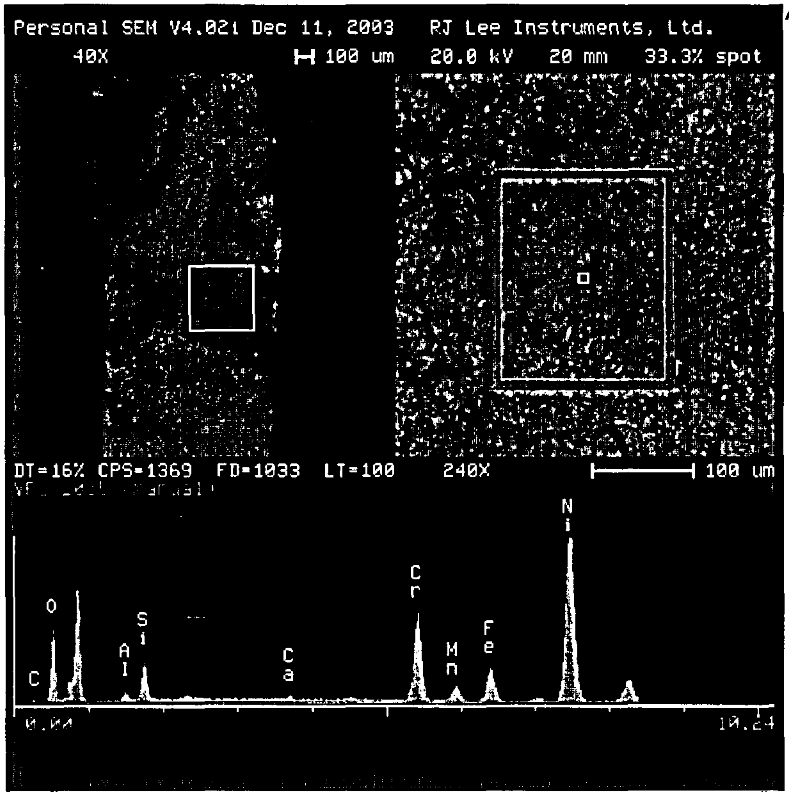

a) Intergranular Near Crack Mouth

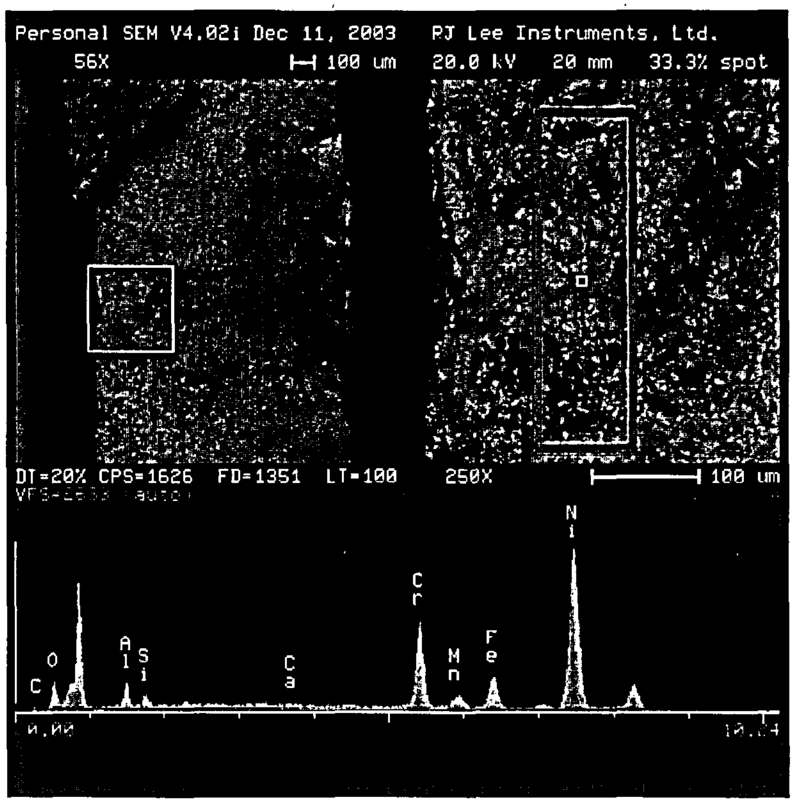

b) Intergranular Near Crack Tip

Figure 6 – 31
R11C41 – Piece 4B – Section 4B2A (H03 Plate)
SEM Photographs Illustrating Areas Selected for EDS

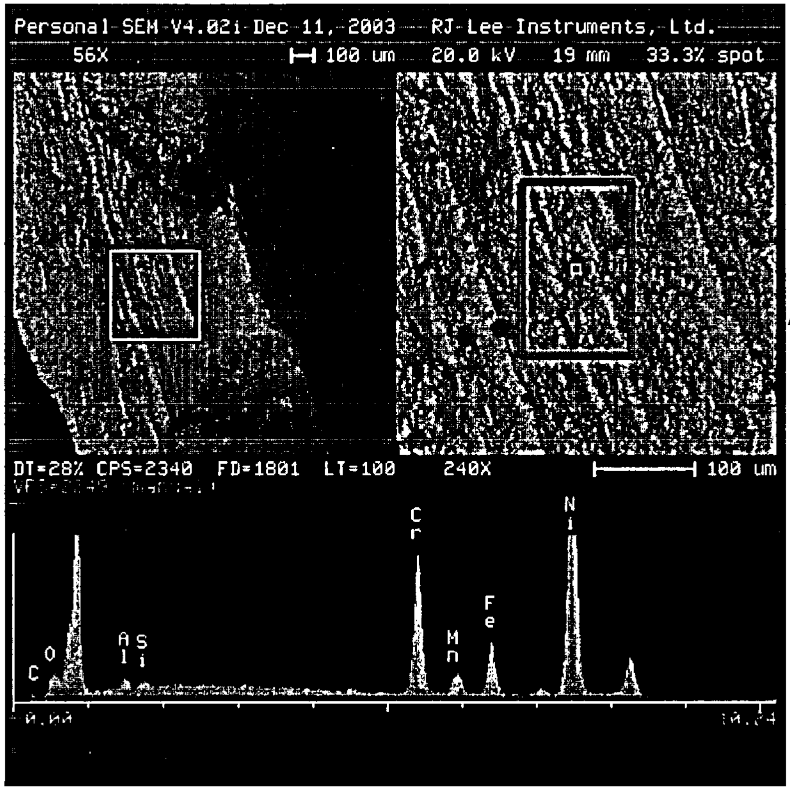

c) Ductile Fracture Face

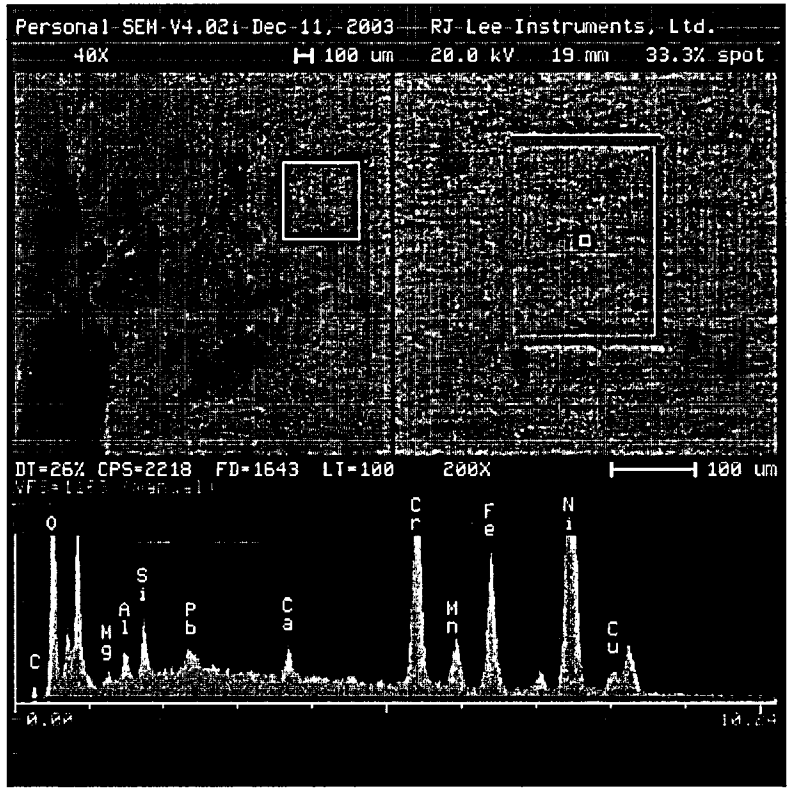

d) OD Surface Near Burst

Figure 6 – 31 (Cont'd)
R11C41 – Piece 4B – Section 4B2A (H03 Plate)
SEM Photographs Illustrating Areas Selected for EDS

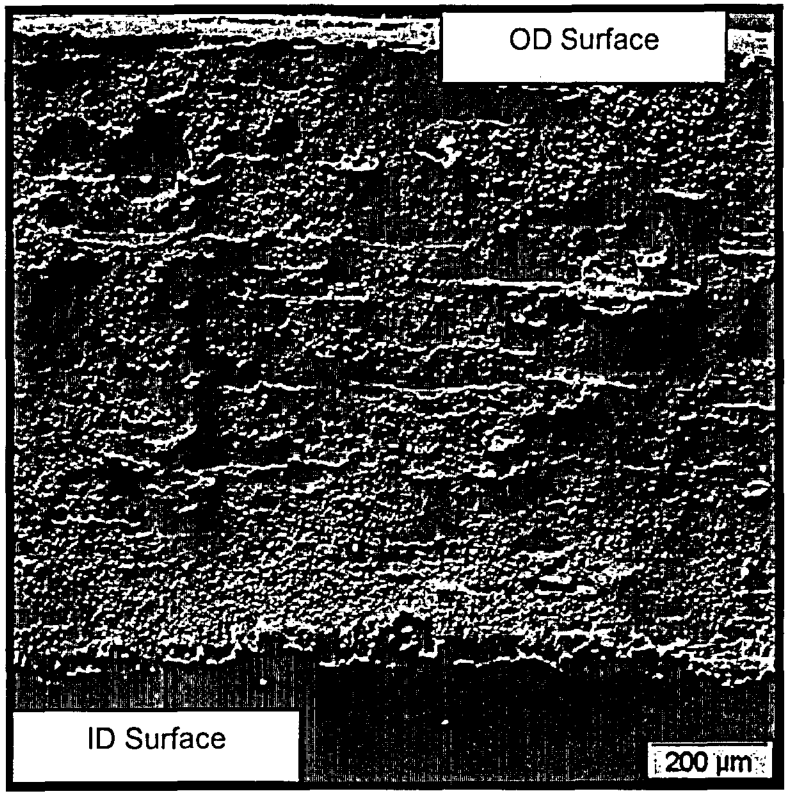

Figure 6 – 32
R11C41 – Piece 5A – Section 5A2A (Freespan)
SEM Photograph Illustrating Ductile Fracture Face

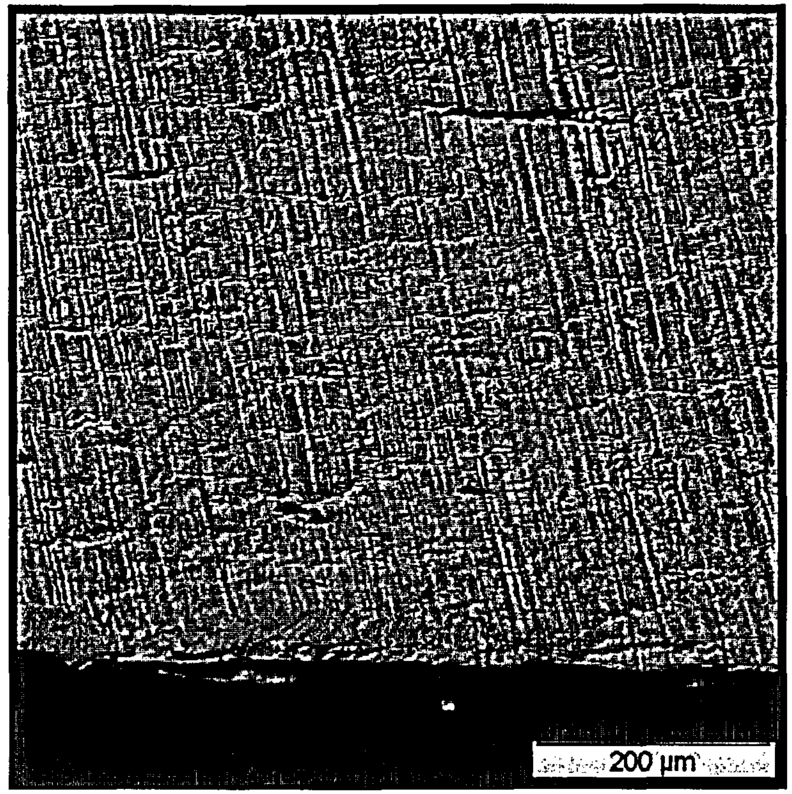

Figure 6 – 33
R11C41 – Piece 5A – Section 5A2A (Freespan)
SEM Photograph of OD Surface

SECTION 7

METALLOGRAPHIC EXAMINATIONS

7.1 Procedure

Following the completion of the burst testing, transverse sections were cut from the 1st and 2nd TSP area and were examined by metallography to verify the presence of corrosion and to determine if any relationship between material condition and the observed corrosion could be established. The specimens were mounted and polished, electrolytically etched in a Nital solution, and viewed with a light microscope. Low magnification photomicrographs were used to document the observed condition and if necessary, higher magnification was utilized to more clearly document the details of the degradation. The following table lists the areas examined metallographically and the objective of the examinations.

Tube	Piece and Location	Specimen Number	Mount Number	Objective
R10C39 HL	Piece 3B – H02	3B2B2	2621	Crack orientation, extent, and morphology
	Piece 4B – H03	4B2B2	2620	Crack orientation, extent, and morphology
R11C41 HL	Piece 3B – H02	3B2B	2619	Crack orientation, extent, and morphology
	Piece 4B – H03	4B2B2	2622	Crack orientation, extent, and morphology

As noted above, the objective of the metallographic examination was to determine the orientation, extent, and morphology of the ODSCC observed in the Watts Bar pulled tube segments. No attempt was made to determine the deepest secondary IGSCC. Maximum crack depths were obtained based on an SEM examination of the burst fracture face (Section 6). Additional mounts were prepared to verify that the metallurgical conditions, i.e., grain size, carbide distribution, and microhardness, of the pulled tubes were consistent with vintage mill annealed material. These results are presented in Section 8.

7.2 Results

The non-destructive and destructive examinations of Watts Bar Unit 1 steam generator tubes R10C39 and R11C41 confirmed the presence of OD-initiated degradation within the support plate crevices and at the top of the tubesheet. The corrosion was limited to the support plate crevices and the crevice at the top of the tubesheet. All four support plate regions had axial intergranular ODSCC. The cracks were intergranular with minimal evidence of IGA. The cracks were discrete with little evidence of branching. Minimal evidence of cellular corrosion was seen.

<u>R10C39 HL – Piece 3B (H02) - Section 3B2B2</u>

The orientation, extent, and morphology of the ODSCC reported at the H02 tube support plate of R10C39 HL were explored by examining a transverse metallographic specimen taken through the center of the axial burst. It should be noted that this region exhibited 100% through-wall IGSCC as determined by examination of the burst fracture face. The area examined is shown in Figure 7-1, while etched photomicrographs representing the ODSCC identified are shown in Figures 7-2 through 7-4. A total of four (4) OD locations were identified with IGSCC. The position 1 shown on Figure 7-1 corresponds to the burst fracture face. It should be noted that the condition shown in these figures is after the area has been pressurized to 4,931 psi. No attempt was made to find the deepest secondary crack. As seen in Figure 7-1, the observed cracking was limited to the quadrant of the tube that was likely in contact with the TSP and thereby promoted the buildup of deposits and the subsequent of secondary side chemicals. Figures 7-2 and 7-3 show the deepest crack seen on this specimen. Minimal evidence of branching or cellular corrosion was observed. Figure 7-4 illustrates the only additional region where IGSCC was seen on this specimen. Once again, minimal cellular corrosion or IGA was noted. The approximate depth of the IGSCC shown in Figure 7-4 was 0.014 inch.

<u>R10C39 HL – Piece 4B (H03) - Section 4B2B2</u>

The orientation, extent, and morphology of the ODSCC reported at the H03 tube support plate of R10C39 HL were characterized by examining a transverse metallographic specimen taken through the center of the axial burst. This region exhibited 40% through-wall IGSCC as determined by examination of the burst fracture face. The area examined is shown in Figure 7-5, while etched photomicrographs representing the ODSCC identified are shown in Figures 7-6 and 7-7. Only two (2) OD locations were identified with IGSCC. Position 1 shown on Figure 7-5 corresponds to the burst fracture face. It should be noted that the condition shown in these figures is after the area has been pressurized to 12,058 psi. No attempt was made to find the deepest secondary crack. As seen in Figure 7-5, the observed cracking was limited to burst fracture area and an area near the burst face. Figure 7-6 shows that the IGSCC associated with the burst fracture face had none to minimal evidence of branching cracks or cellular corrosion. As is seen in Figure 7-6, the burst face is characterized by both intergranular and ductile fracture features. The only other evidence of IGSCC seen on this specimen was two (2) shallow indications seen near the burst fracture, Figure 7-7. The indications are intergranular in nature, with minimal evidence of cellular corrosion. The indications are blunted due to burst test pressurization. Once again, no appreciable evidence of intergranular penetration was noted on the OD surface.

<u>R11C41 HL – Piece 3B (H02) – Section 3B2B2</u>

The orientation, extent, and morphology of the ODSCC reported at the H02 tube support plate of R11C41 HL were determined by examining a transverse metallographic specimen taken through the center of the axial burst. This region exhibited 50% through-wall IGSCC as determined by examination of the burst fracture face. The area examined is shown in Figure 7-8, while etched photomicrographs representing the ODSCC identified are shown in Figures 7-9 through 7-11. A total of three (3) OD locations were identified with IGSCC. Position 1 shown on Figure 7-8 corresponds to the burst fracture face. The condition shown in these figures is after the area has been pressurized to 12,649 psi. No attempt was made to find the deepest secondary crack. Figure 7-9 shows that the IGSCC associated with the burst fracture face had none to minimal evidence of branching cracks or cellular corrosion. As is seen in Figure 7-9, the burst face is characterized by both intergranular and ductile fracture features. Two other regions of OD-initiated IGSCC are shown in Figures 7-10 and 7-11. The indications are intergranular in nature, with minimal evidence of cellular corrosion. The indications are blunted due to burst test pressurization. Once again, no appreciable evidence of intergranular penetration was noted on the OD surface.

<u>R11C41 HL – Piece 4B (H03) – Section 4B2B2</u>

The orientation, extent, and morphology of the ODSCC reported at the H03 tube support plate R11C41 HL were explored by examining a transverse metallographic specimen taken through the center of the axial burst. The area examined is shown in Figure 7-12, while photomicrographs representing the ODSCC identified are shown in Figures 7-13 through 7-17. A total of five (5) OD locations were identified with IGSCC. Position 1 shown in Figure 7-12 corresponds to the burst fracture face. It should be noted that the condition shown in these figures is after the area has been pressurized to 6,999 psi. No attempt was made to find the deepest secondary crack. As is seen in Figure 7-13, the burst face is characterized by both intergranular and ductile fracture features, although this specimen did produce a small leak during the elevated temperature leak test. SEM depth profiles of the burst opening confirmed a through-wall IGSCC. The remaining areas exhibiting OD-initiated IGSCC are shown in Figures 7-14 through 7-17. In all cases the indications are relatively shallow and exhibit a blunt tip due to the burst pressurization. The IGSCC cracks had no or few branches and minimal cellular corrosion. Once again, no appreciable evidence of intergranular penetration was noted on the OD surface.

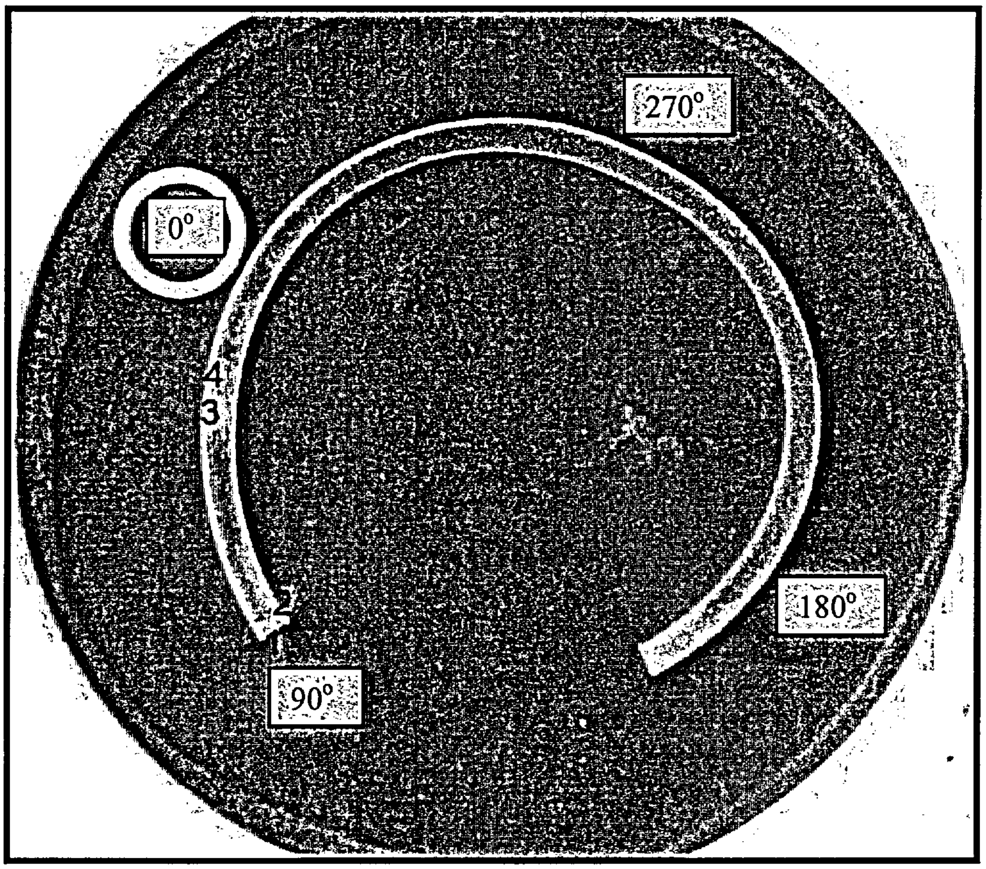

Figure 7-1

Transverse Section of R10C39 HL- Piece 3B – Specimen 3B2B2 (Mount 2621) Showing IGSCC Locations Associated with H02 Plate Intersection

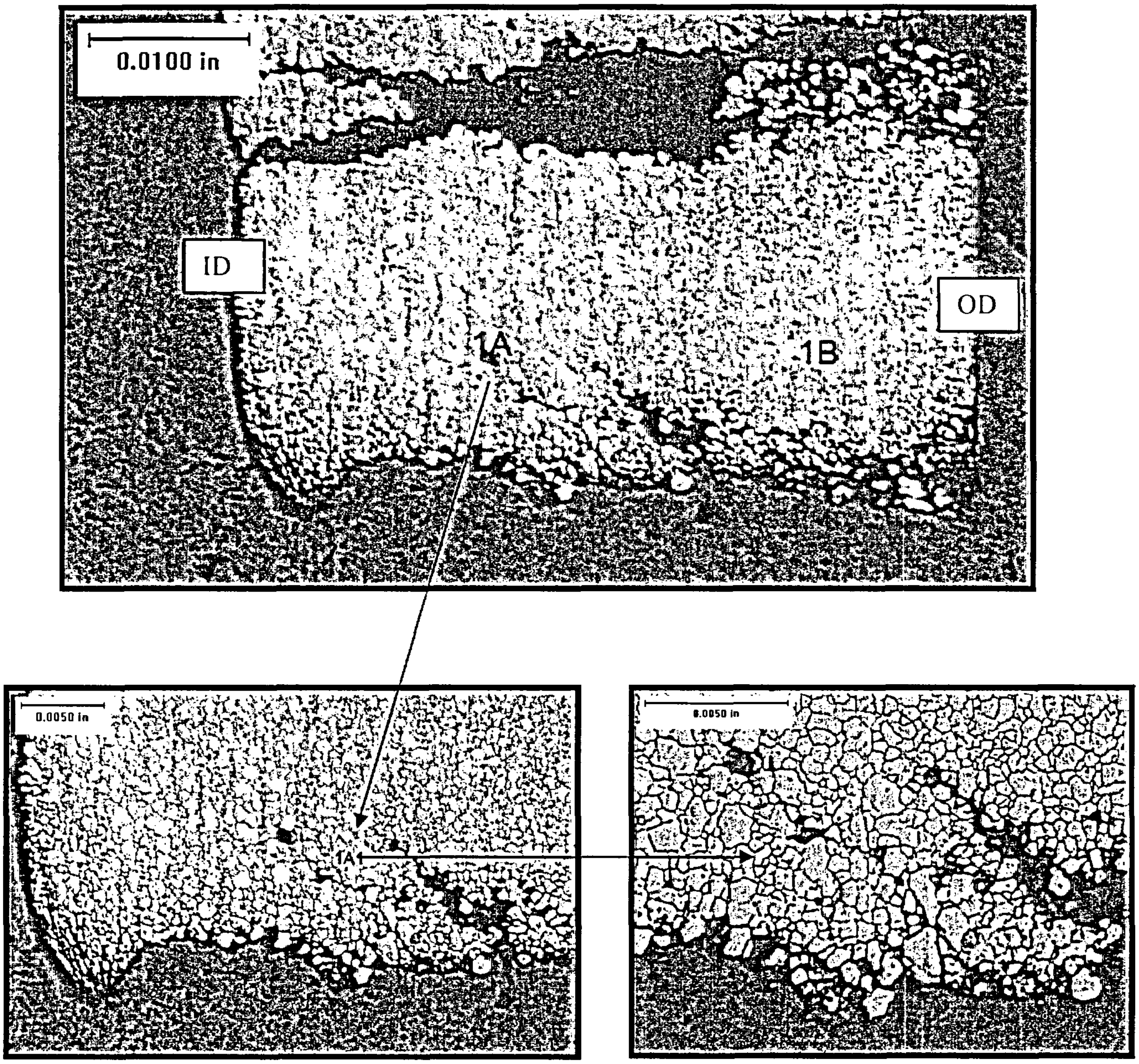

Figure 7-2

R10C39 HL- Piece 3B (H02 Plate) – Specimen 3B2B2

Etched Transverse Section Showing IGSCC on Burst Face

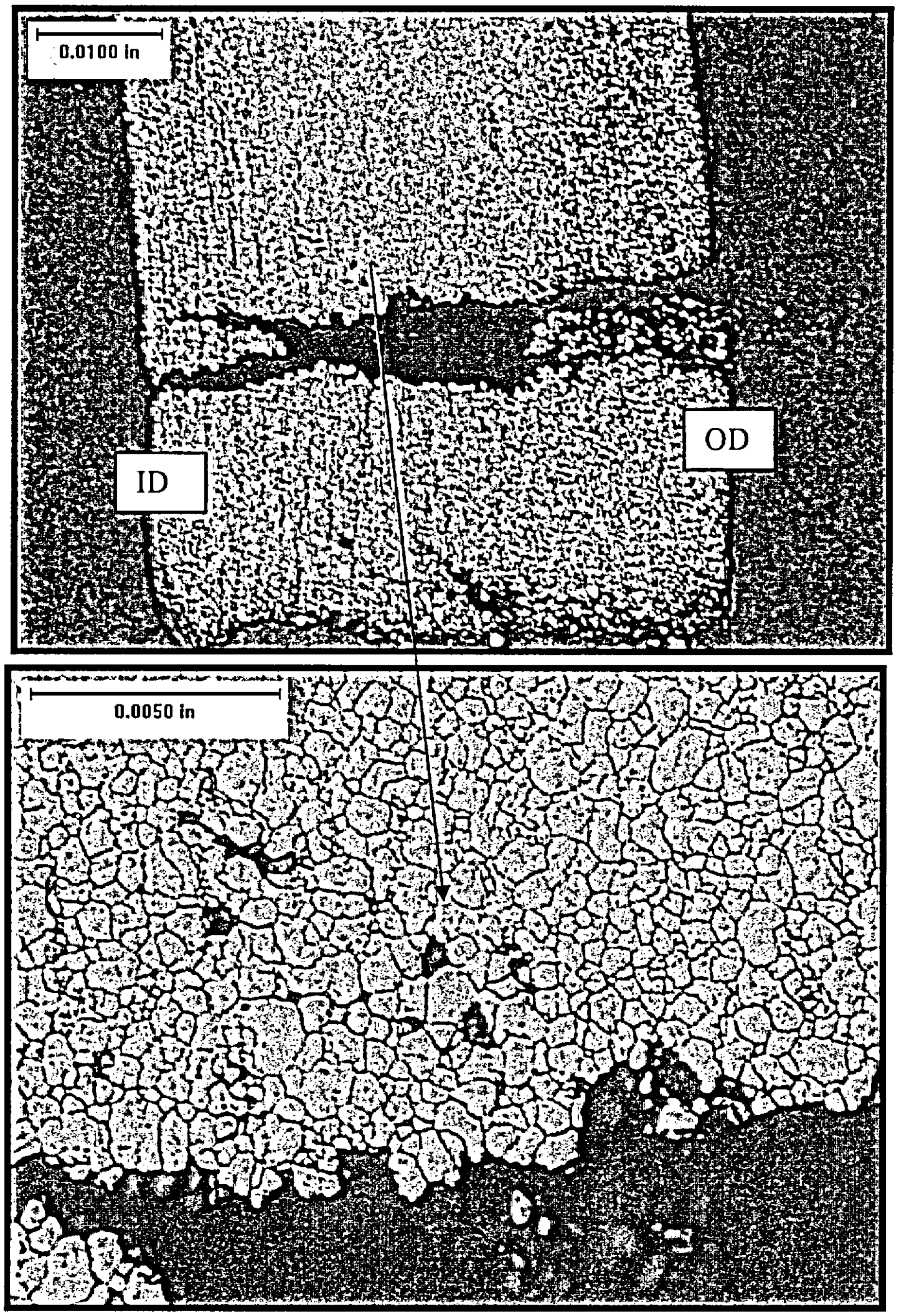

Figure 7-3

R10C39 HL- Piece 3B (H02 Plate) – Specimen 3B2B2

Transverse Section Showing IGSCC Adjacent to Burst Face

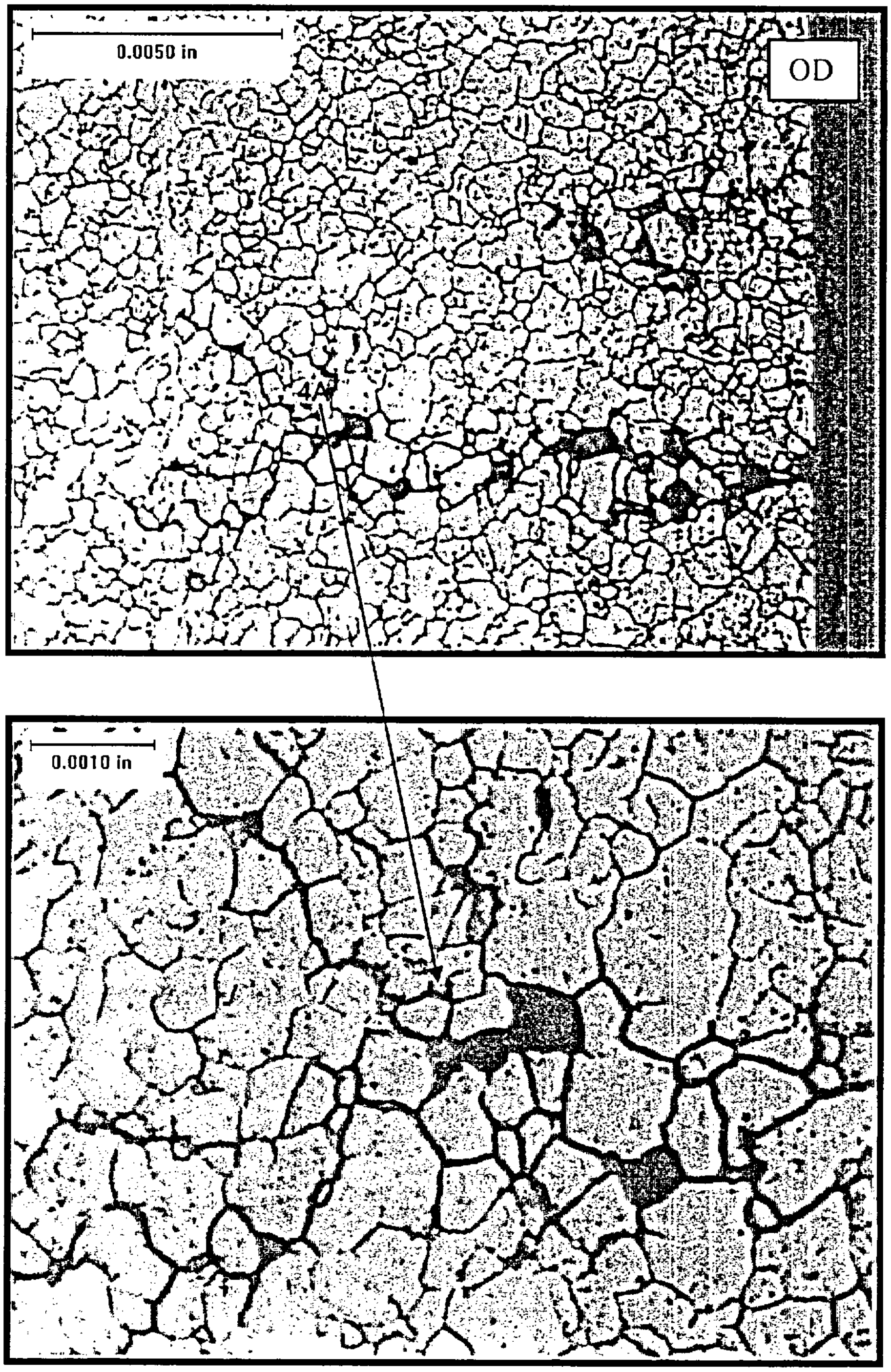

Figure 7-4

R10C39 HL- Piece 3B (H02 Plate) – Specimen 3B2B2

Transverse Section Showing IGSCC Away From Burst Face

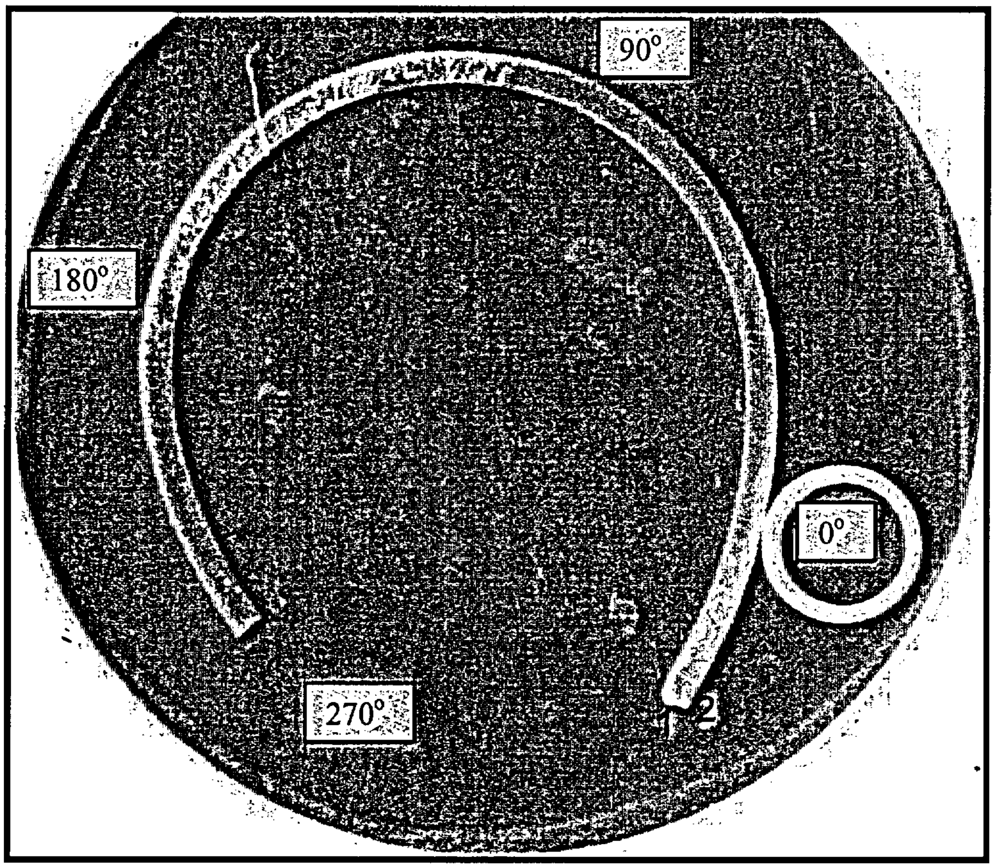

Figure 7-5

Transverse Section of R10C39 HL- Piece 4B – Specimen 4B2B2 (Mount 2620) Showing IGSCC Locations Associated with H03 Plate Intersection

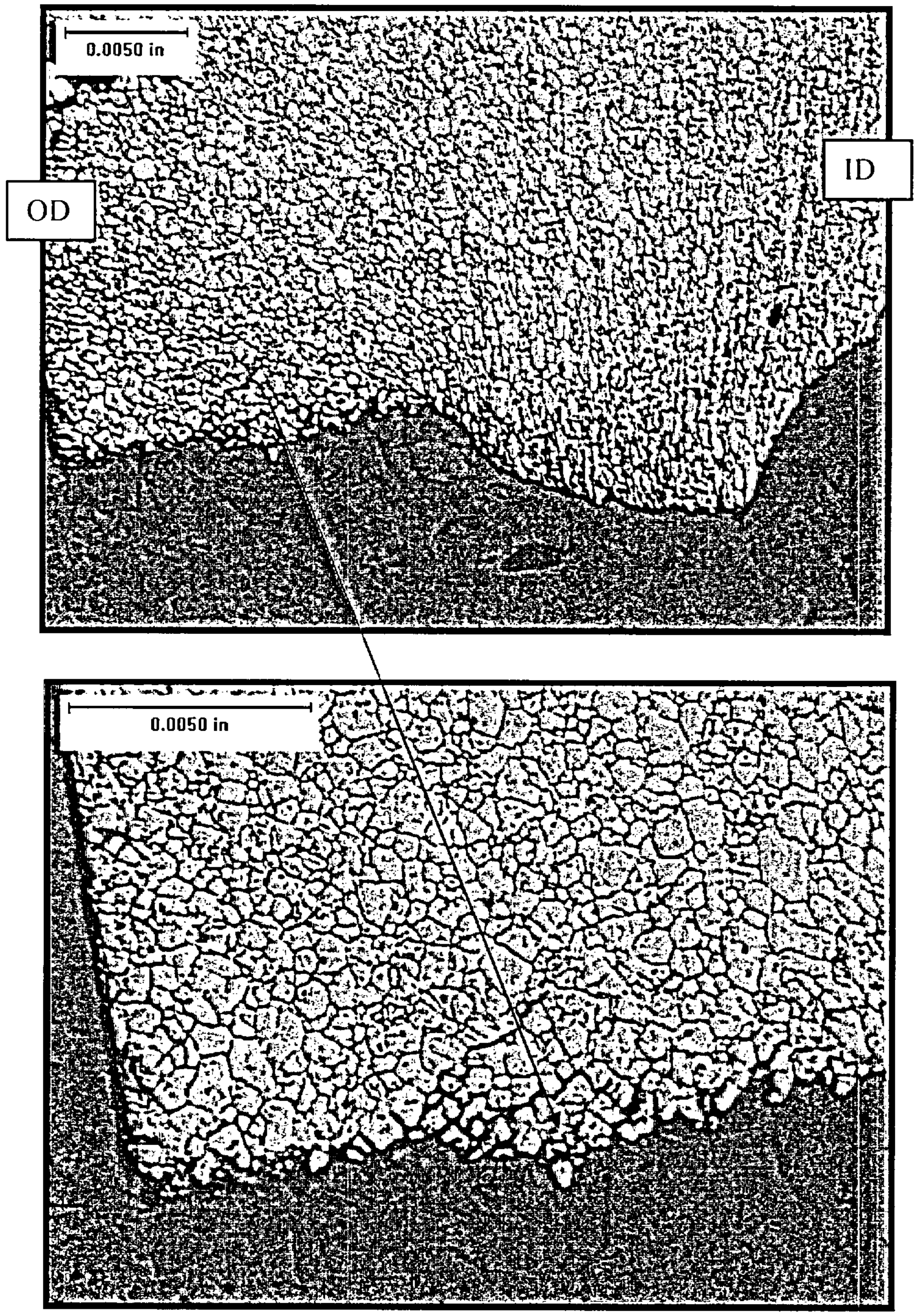

Figure 7-6

R10C39 HL- Piece 4B (H03 Plate) – Specimen 4B2B2 – Position 1

Transverse Section Showing IGSCC on Burst Fracture Face

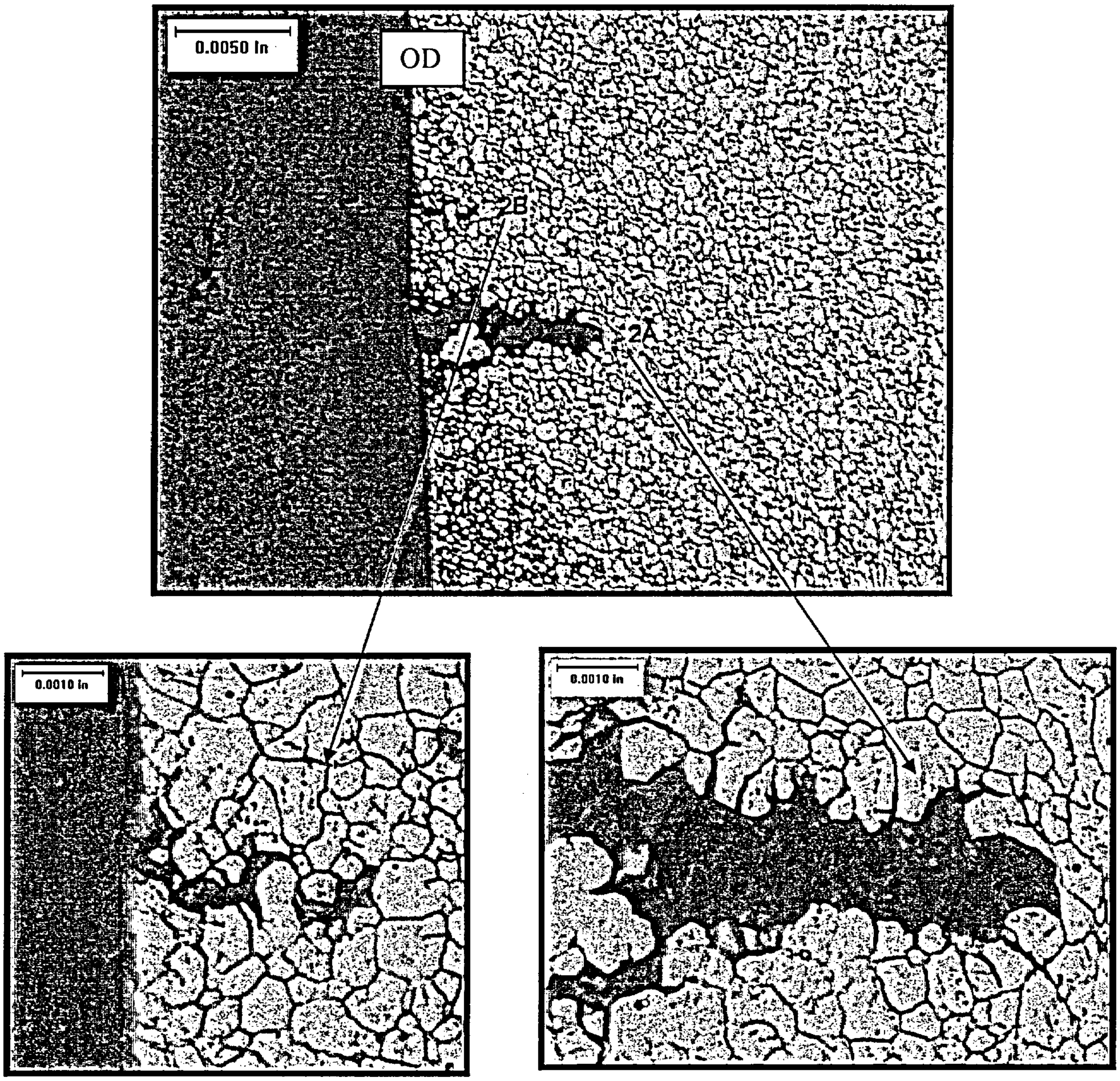

Figure 7- 7

R10C39 HL- Piece 4B (H03 Plate) – Specimen 4B2B2 – Position 2

Transverse Section Adjacent to Burst Face Showing IGSCC

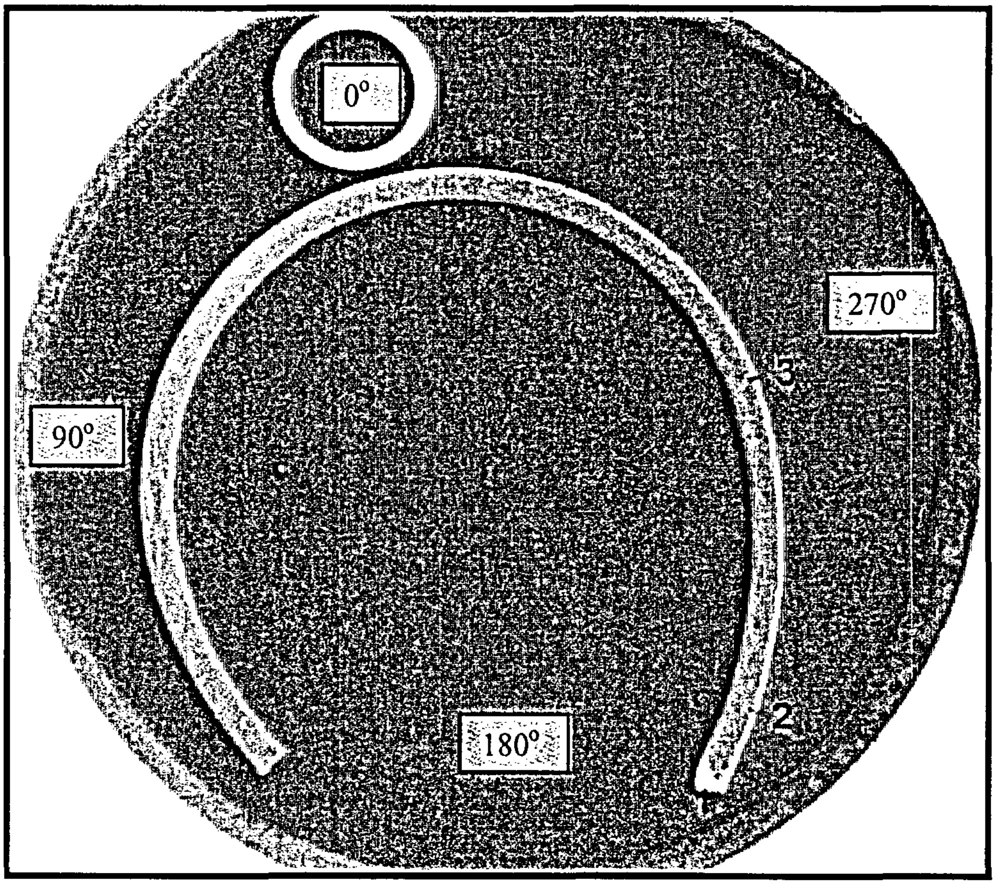

Figure 7-8

Transverse Section - R11C41HL- Piece 3B – Specimen 3B2B2 (Mount 2619)

Showing IGSCC Locations Associated with H02 Plate Intersection

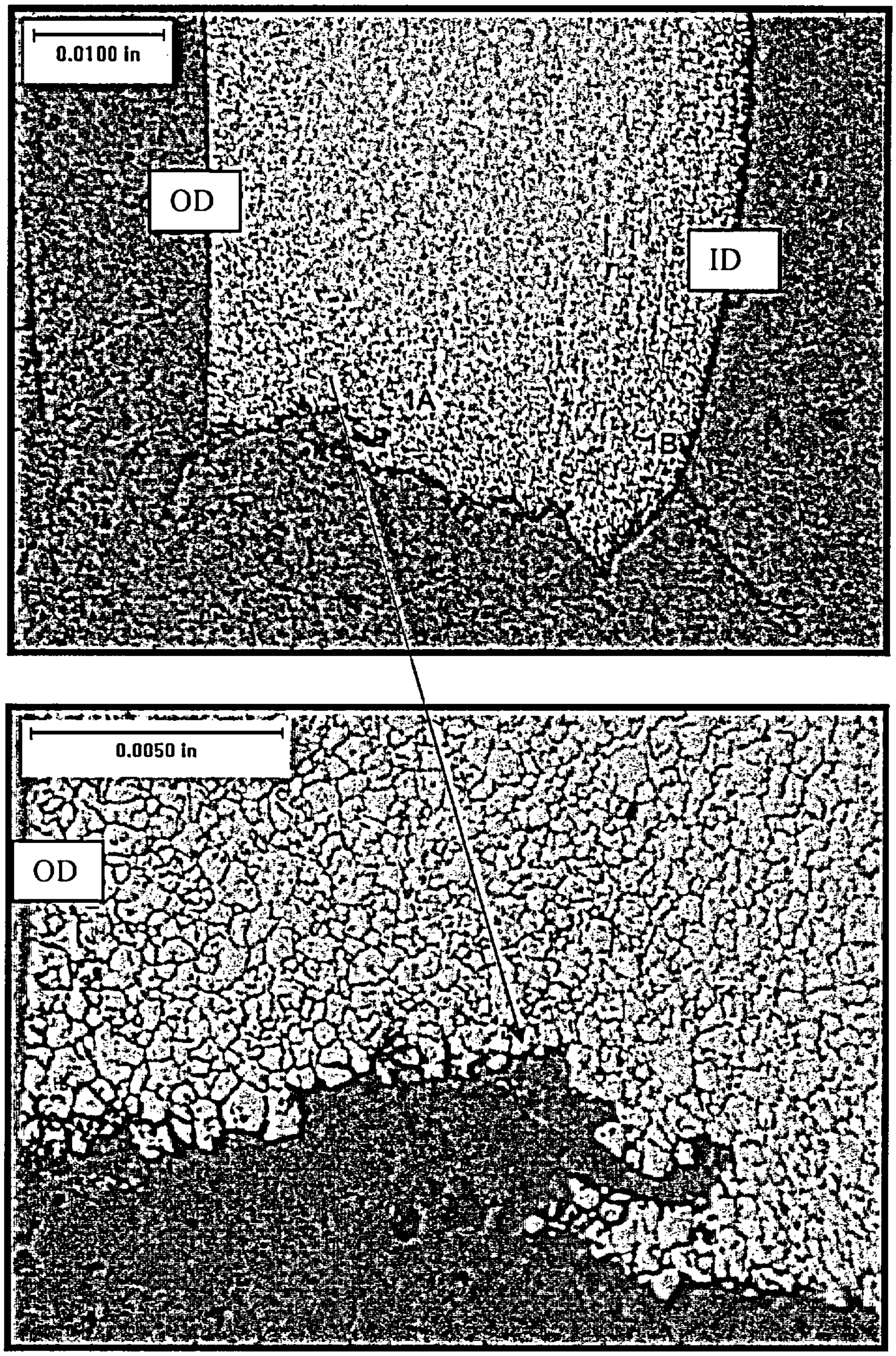

Figure 7-9

R11C41HL- Piece 3B (H02 Plate) – Specimen 3B2B2 – Position 1

Etched Transverse Section Showing IGSCC on Burst Fracture Face

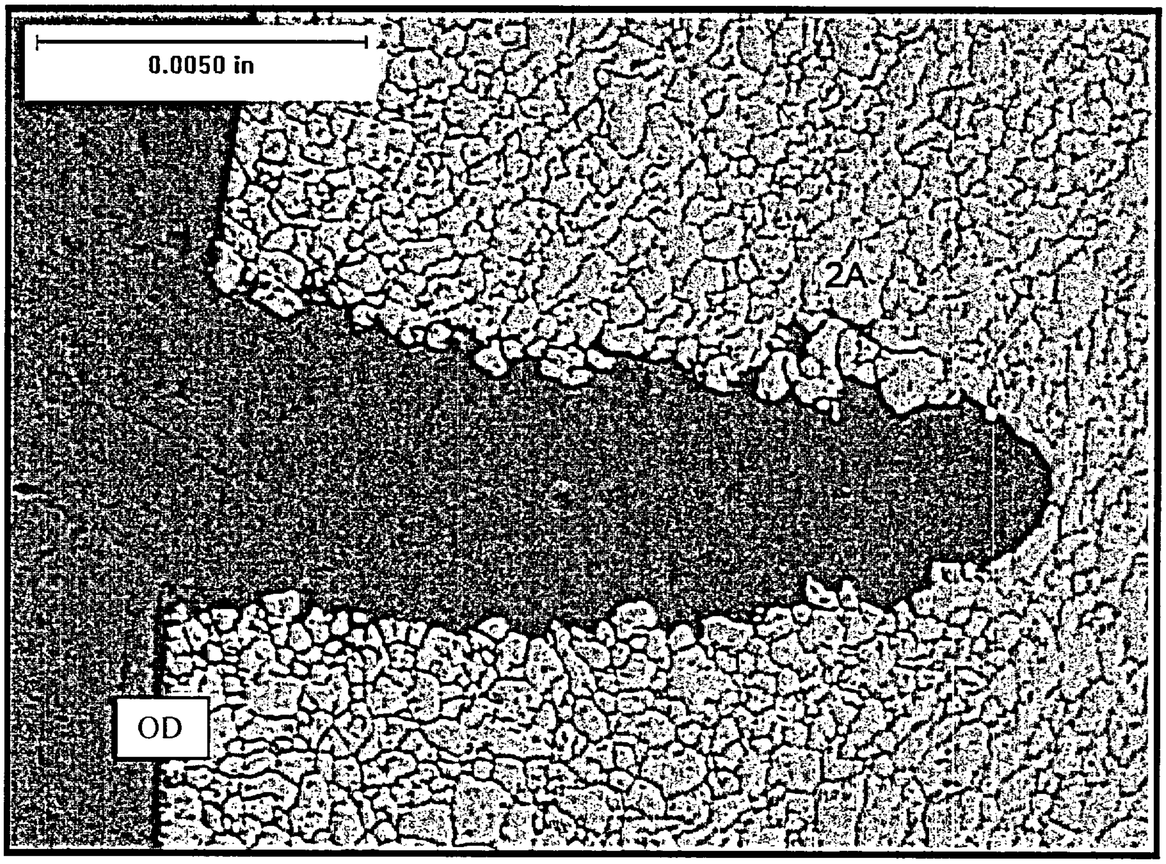

Figure 7-10

R11C41HL- Piece 3B (H02 Plate) – Specimen 3B2B2 – Position 2

Etched Transverse Section Adjacent to Axial Burst

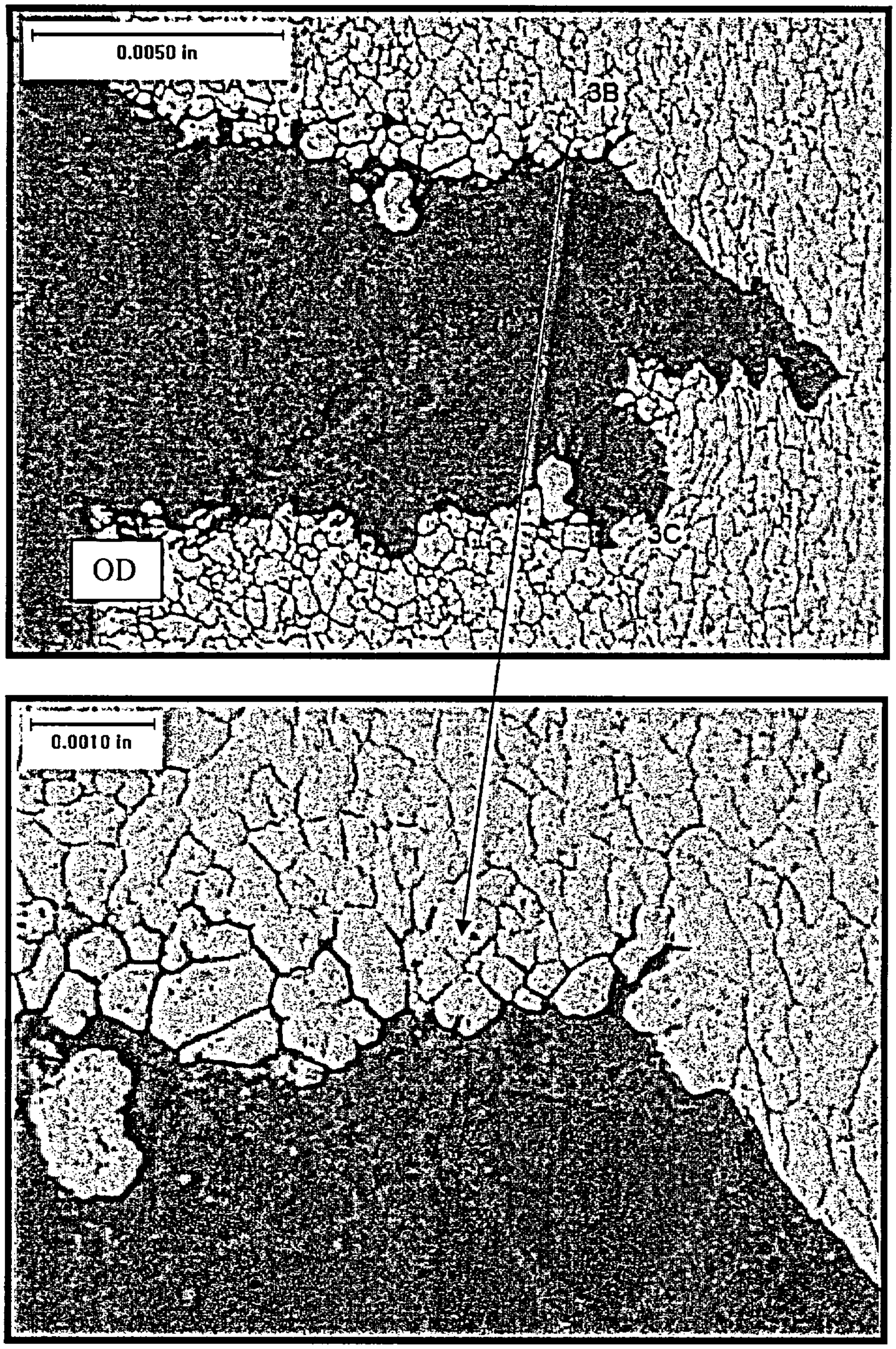

Figure 7-11

R11C41HL- Piece 3B (H02 Plate) – Specimen 3B2B2 – Position 3

Etched Transverse Section Adjacent to Axial Burst

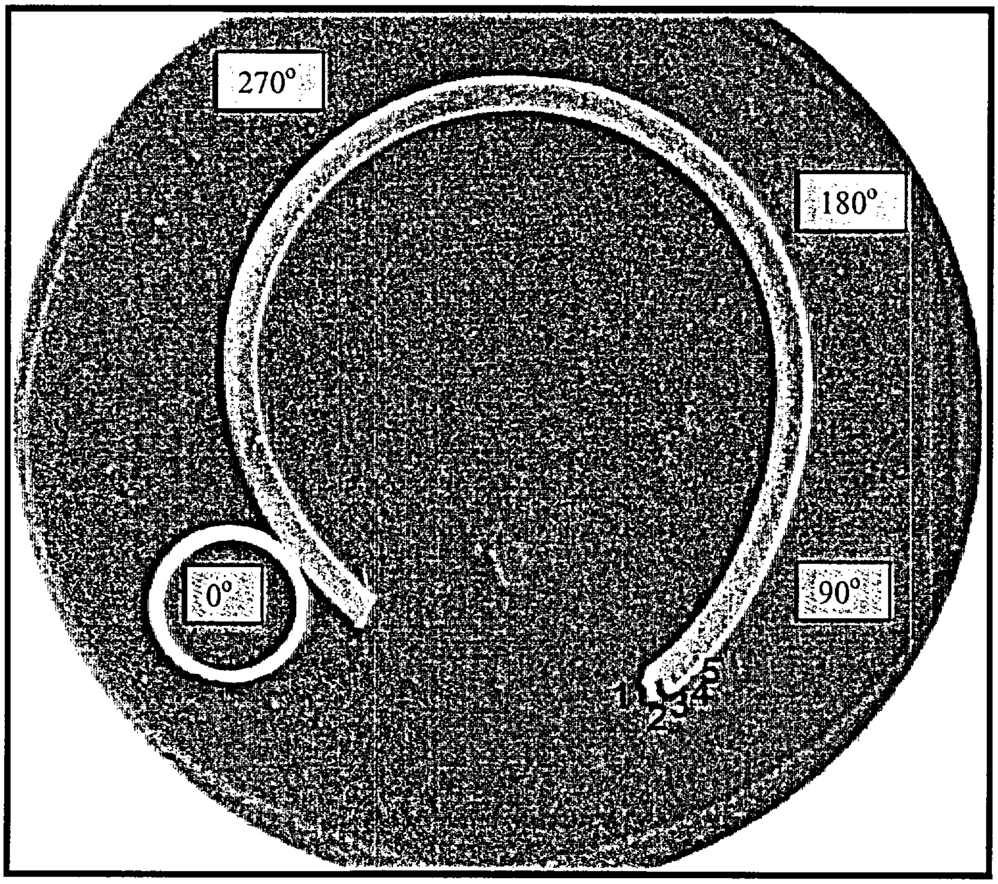

Figure 7-12

Transverse Section - R11C41HL- Piece 4B – Specimen 4B2B2 (Mount 2622)

Showing IGSCC Locations Associated with H03 Plate Intersection

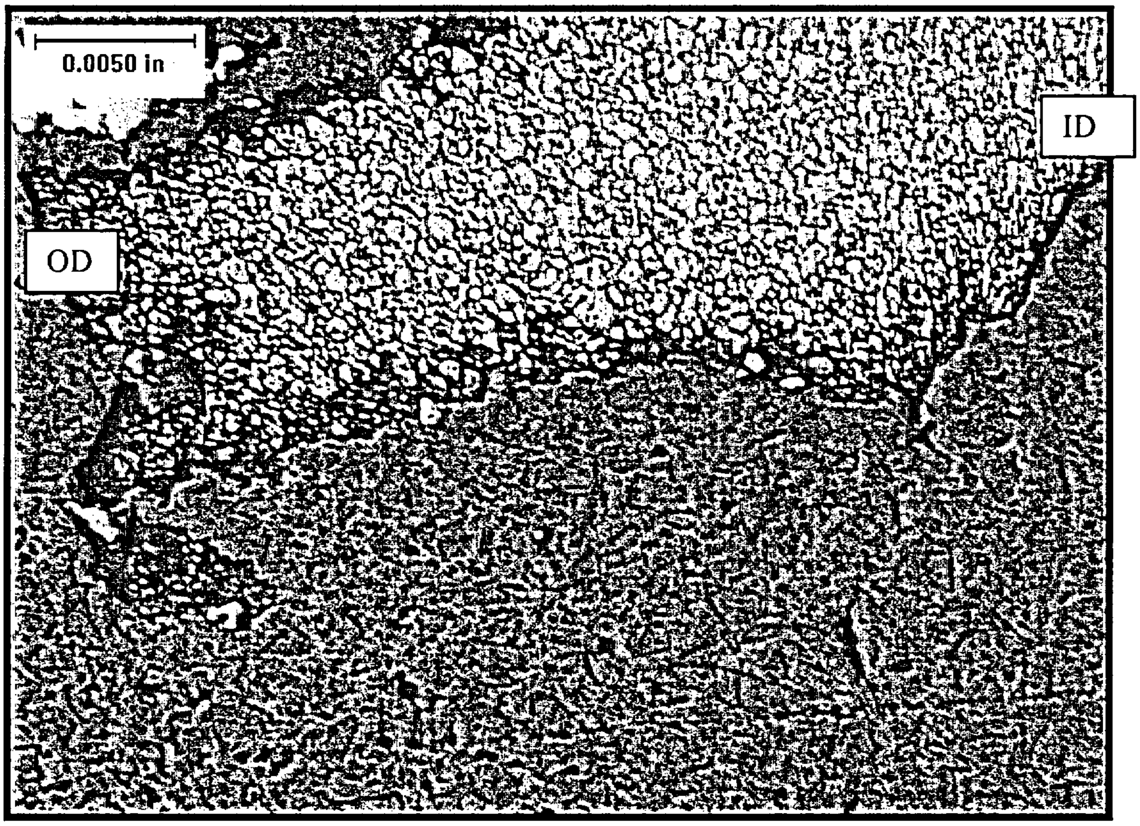

Figure 7-13

R11C41HL- Piece 4B (H03 Plate) – Specimen 4B2B2 – Position 1

Etched Transverse Section Showing IGSCC on Burst Fracture Face

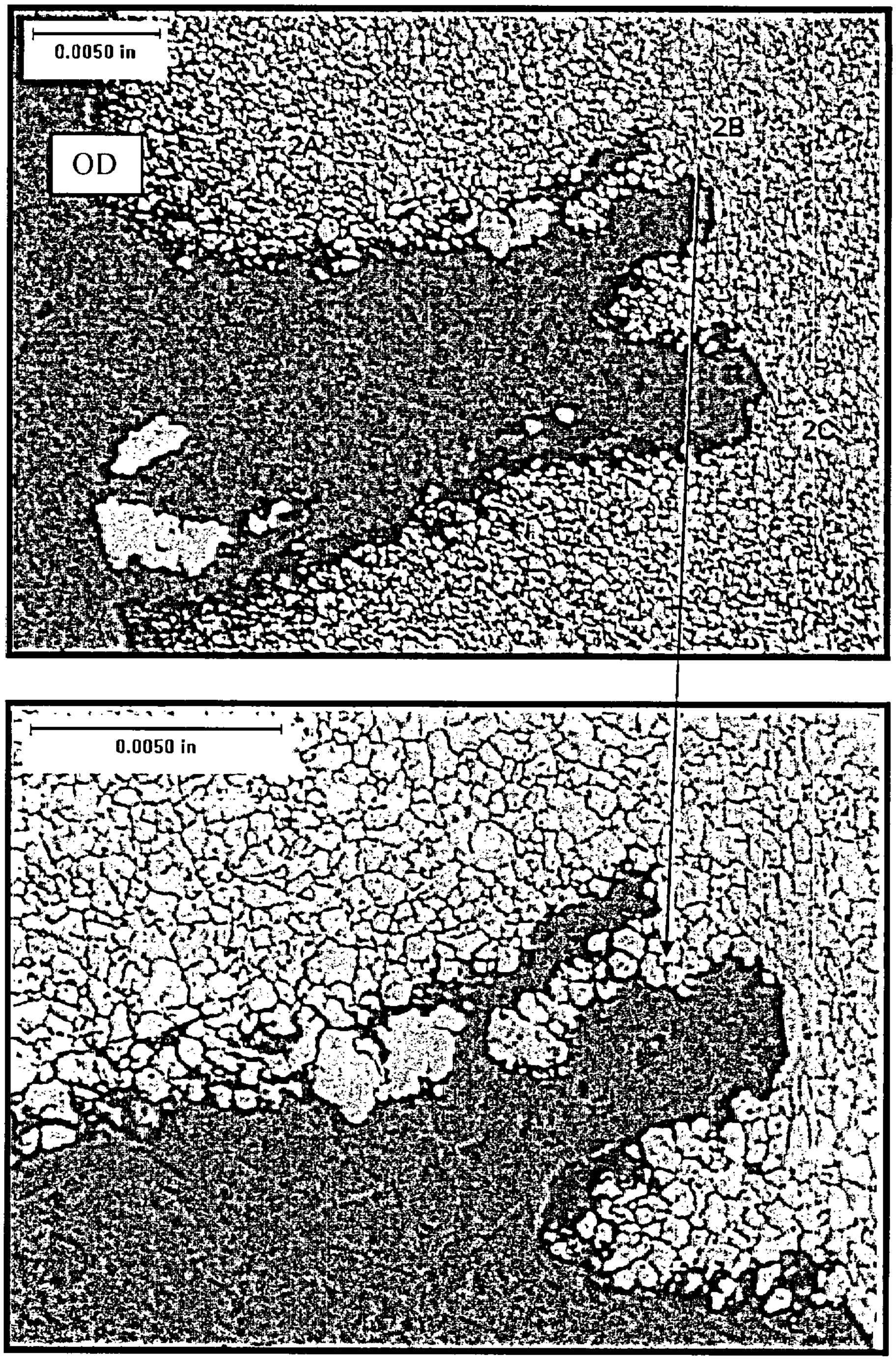

Figure 7-14

R11C41HL- Piece 4B (H03 Plate) – Specimen 4B2B2 – Position 2

Etched Micrographs Showing Observed ODSCC Adjacent to Burst Fracture

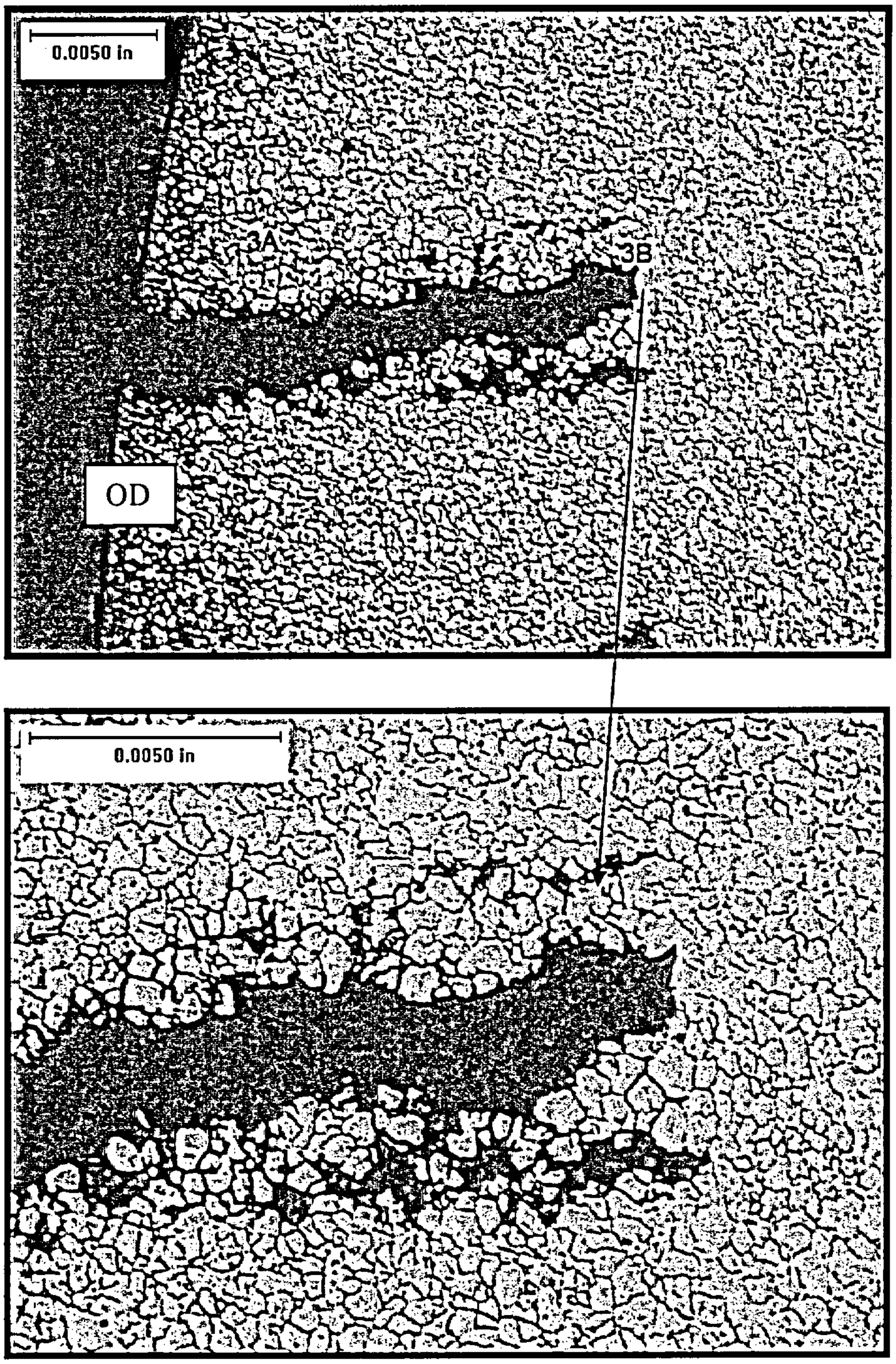

Figure 7-15

R11C41HL- Piece 4B (H03 Plate) – Specimen 4B2B2 – Position 3

Etched Micrographs Showing Observed ODSCC

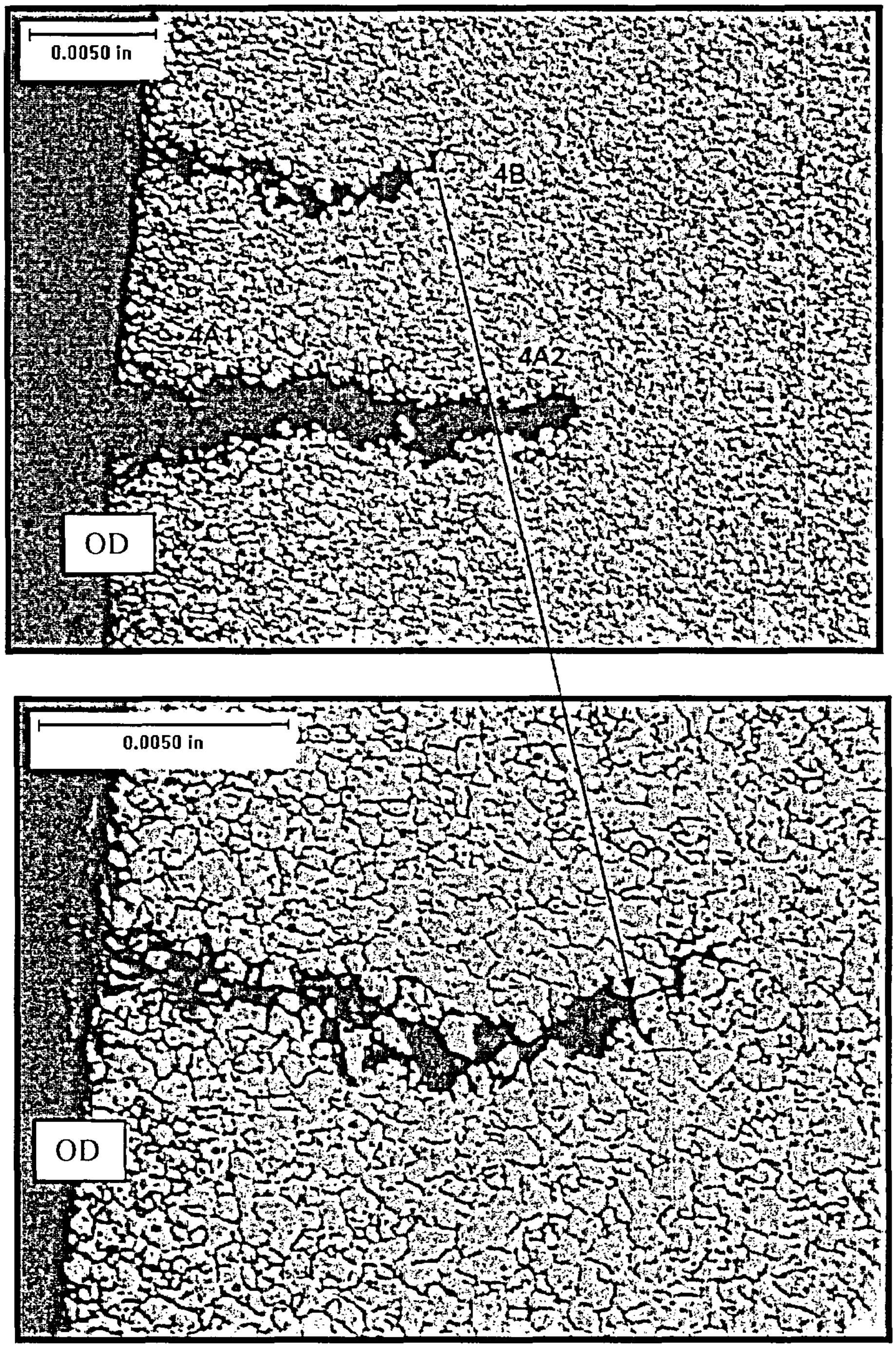

Figure 7-16

R11C41HL- Piece 4B (H03 Plate) – Specimen 4B2B2 – Position 4

Etched Micrographs Showing Observed ODSCC

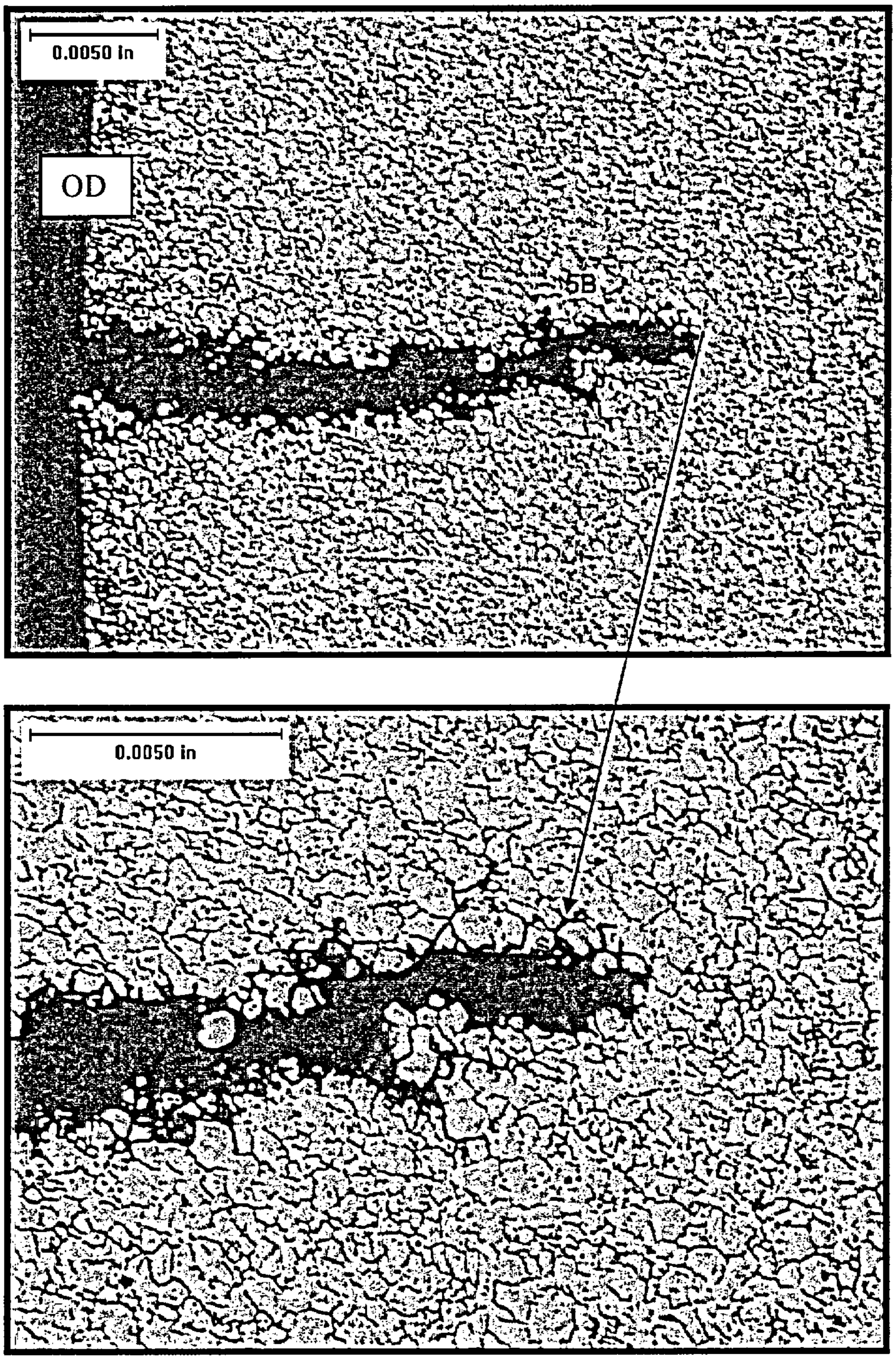

Figure 7-17

R11C41HL- Piece 4B (Ho3 Plate) – Specimen 4B2B2 – Position 5

Etched Micrographs Showing Observed ODSCC

SECTION 8
TUBING MATERIAL CHARACTERIZATIONS

8.1 Introduction

The material characterization tests were performed to determine the tensile, bulk chemistry, microstructural, modified Huey test, microhardness, and residual stress characteristics of the as-removed tube materials. The following sections detail the procedures and the results of each test performed.

8.2 Tensile Tests

Procedure

The tensile properties (i.e., yield strength, ultimate strength, percent elongation) for R10C39 Piece 4C and for R11C41 Piece 5B were determined by a room temperature tensile test of a full cross section tubular specimen approximately 10 inches in length. The full cross section tubular specimens were fitted with snug-fitting stainless steel plugs (mandrels) machined in accordance with ASTM Standard Method E8 to provide a minimum 2.000-inch gage length as prescribed by ASME SB-163. The crosshead speed was maintained at 0.1 inch/minute until fracture.

Results

Table 8-1 provides the results of the room temperature tensile tests. Figures 8-1 and 8-2 show the stress-strain curves for the two tubes. The results are consistent for Alloy 600 steam generator tubing in the mill annealed, straightened, and polished condition. The yield and ultimate strength values measured for the Watts Bar pulled tubes are higher than the values listed in the Certified Materials Test Report (CTMR). This observation is consistent with other pulled tube data which normally shows an increase in tensile properties.

During the preparation of the tensile test specimens, as well as the burst specimens, wall thickness measurements were taken to verify uniform wall thickness. OD and ID measurements were taken every 45° on both ends of each specimen. Table 8-2 summarizes the wall thickness measurements obtained on the tensile test specimens, while similar measurements for the burst specimens are provided in Table 8-3. These tables show that the maximum variation for any set of measurements was 0.002 inch and is less than the 0.003 inch variation normally measured for this vintage tubing.

8.3 Microstructure

Procedure

The microstructure of the pulled tubing was examined to determine the grain size and the general distribution of the carbide precipitation. Transverse metallographic mounts were prepared from Piece 4D1 (R10C39 HL) and Piece 4A3 (R11C41 HL) and were evaluated for grain size and carbide distribution. The specimens were etched in a 5% Nital solution and examined by optical microscopy for grain size rating per the ASTM procedures. The samples were also examined for carbide precipitation by Scanning Electron Microscopy following polishing and etching in a 2% bromine-methanol solution.

Results

The grain size for R10C39 HL is shown in Figure 8-3, while the grain size for R11C41 HL is shown in Figure 8-4. The ASTM grain size for R10C39 HL is 10.9 and the ASTM grain size for R11C41 HL is 10.6. These grain sizes are typical of mill annealed Alloy 600 tubing produced for Model D4 steam generators.

Representative SEM micrographs showing the carbide distribution in the R10C39 HL and R10C41 HL tubes are presented in Figures 8-5 and 8-6. The carbide distribution seen for both tubes is typical of mill annealed Alloy 600 tubing of this vintage. The carbide precipitates are predominantly intragranular with regions exhibiting carbide "banding ". Minimal intergranular carbide precipitation is seen.

8.4 Bulk Chemistry

Procedure

The chemical composition of the base metal of both tubes was determined by quantitative chemical analysis. The radioactivity of each section was reduced by several cycles of immersion in a room temperature solution of 35% HNO_3 + 4% HF (by volume), plus surface abrasion with silicon carbide wheels. Quantitative analysis was performed using a combination of inductively coupled plasma, graphite furnace atomic absorption, inert gas fusion, and combustion methods.

Results

The results of the chemical analyses for R10C39 HL and R11C41 HL are provided in Table 8-4. Included also are the CMTR values for the respective heats. The CMTR values represent the mill analysis for the heat. The slight differences noted between the CMTR and pulled tube chemical analyses are within the expected variability based on industry experience.

8.5 Modified Huey Tests

Procedure

It has been Westinghouse practice in the manufacture of Alloy 600 heat transfer tubing – both mill annealed and thermally treated – to ensure that the material was not sensitized. Westinghouse, along with the industry in general, adopted a modified Huey test (ASTM A262 Practice C) as the principal tool for the evaluation of grain boundary chromium depletion in Alloy 600. The test was modified to a single 48-hr exposure in boiling 25% nitric acid. This modification was necessary to enhance the sensitivity of the test for detecting chromium depletion. In view of this historical practice, it has been Westinghouse experience that SG heat transfer tubing in Westinghouse PWRs is not sensitized, and therefore not prone to in-service degradation in faulted secondary environments due to this condition. This experience notwithstanding, in order to complete the assessment of the Watts Bar Unit 1 tubing materials, the sensitization level of R10C39 HL and R11C41 HL tubing was determined using a modified Huey test (48 hours in 25% nitric acid). Two ½ inch rings were cut from each pulled tube and subjected to the test.

Results

The results of the test are presented in Table 8-5. The results are consistent for Alloy 600 steam generator tubing in the mill annealed, straightened, and polished condition. The average weight loss observed for R10C39 HL ring specimens was 33.9 $mg/dm^2/day$, while the ring specimens for R11C41 HL exhibited an average weight loss of 37.2 $mg/dm^2/day$. Grain boundary chromium depletion is considered present if the weight loss is greater than 300 $mg/dm^2/day$.

8.6 Microhardness

Procedure

Microhardness tests are used to provide information such as general hardness, verification of specific heat treatment, random hardness variations, and hardness gradients caused by localized cold work. Microhardness measurements were performed across the tube wall for both R10C39 HL and R11C41 HL. Vickers hardness measurements were performed in accordance with Westinghouse Procedure MR 8111, Revision 1. Vickers hardness is determined by dividing the applied kg-force load by the surface area of the indentation in square millimeters, computed from the mean of the measured diagonals of the indentation. A 500-g load was used for through-wall (OD surface to ID surface) measurements.

Results

The results of the microhardness tests are presented in Table 8-6. No localized hardness variations were noted and the results are consistent with tubing of this vintage.

8.7 Residual Stress

8.7.1 Split Ring Technique

Introduction

The hoop stress was measured by a split tube method per Westinghouse Procedure MCT-003, Revision 1. The procedure was used to measure the net-section residual hoop stress for the pulled tubes. The resulting calculated residual stress assumes a linear distribution of residual stress through the tube wall and is an approximate average value of the stresses over the whole specimen surface. When the tube is split, a change in strain is observed on the OD surface and is inversely related to the residual strain in the tubing. Multiplying the observed strain by the elastic modulus (E) provides a value for the average residual stress.

Procedure

One specimen from each tube was tested for residual hoop stress. The specimens were: R10C39 HL - Piece 5D and R11C41 HL – Piece 3C3. The length of the specimens was at least three times the tube diameter. The residual stress was determined from change-in-diameter measurements.

The OD of the tubing was measured prior to and following the cut. The tube section was slit axially along one side of the tube and the hoop stress was calculated from the diameter changes of the tube. The residual stresses were calculated from the average of the four readings for the wall thickness values and the measured diameters with the following equation:

$$\sigma_R = \left[\frac{E}{1-\nu^2}\right] W \left[\frac{1}{D_o} - \frac{1}{D_f}\right]$$

where: σ_R = residual stress

E = elastic modulus

ν = Poisson's Ratio

W = average wall thickness

D_o = average OD before splitting

D_f = average OD after splitting

Results

The experimental data are presented in Table 8-7. The calculated residual hoop stress was 13.8 ksi in R10C39 HL and 14.5 ksi in R11C41 HL. These values are within the range of residual stress levels expected for mill annealed, straightened, and polished Alloy 600 tubing produced by Westinghouse for Model D steam generators.

Table 8-1
Tensile Properties

Specimen Dimensions			Test Values			Tensile Properties		
Gage OD, in.	Gage ID, in.	Gage Area, in^2	Load @ 0.2% Offset, lbs	Load @ Ultimate, lbs	Displacement, in.	0.2% Yield Strength, ksi	Ultimate Strength, ksi	Elongation, %
Row 10 Column 39 Hot Leg - Piece 4C								
0.75175	0.66475	0.096789	6385	11119	3.31	66.1	114.9	35.6
CMTR Values – Heat NX 4616								
-	-	-	-	-	-	53.0	103.75	-
Row 11 Column 41 Hot Leg – Piece 5B								
0.754	0.66425	0.099972	6924	11346	3.22	69.1	113.5	39.3
CMTR Values – Heat NX 4505								
-	-	-	-	-	-	54.0	101.25	-

Table 8-2
Tensile Specimen Dimensional Data

Specimen	Measurement Location		Diameter, Inch ID	Diameter, Inch OD	Wall Thickness, Inch
R10C39 Piece 4C	Top	0° to 180°	0.664	0.750	0.043
		90° to 270°	0.665	0.754	0.0445
	Bottom	0° to 180°	0.665	0.750	0.0425
		90° to 270°	0.665	0.753	0.044
R11C41 Piece 5B	Top	0° to 180°	0.663	0.754	0.0455
		90° to 270°	0.665	0.754	0.0445
	Bottom	0° to 180°	0.665	0.754	0.0445
		90° to 270°	0.664	0.754	0.045

Table 8-3

Wall Thickness Variations

Specimen	Approximate Elevation Above TTS (Inches)	Wall Thickness Measurements	Wall Thickness (Inches) at Selected Circumferential Position							
			0	45	90	135	180	225	270	315
R10C39 - 3B [1st TSP (H02)]	53.75	Top	0.047	0.046	0.046	0.047	0.048	0.047	0.047	0.047
	43.75	Bottom	0.046	0.0455	0.046	0.046	0.0455	0.0455	0.046	0.046
R10C39 - 4B [2nd TSP (H03)]	77.625	Top	0.045	0.044	0.044	0.044	0.045	0.045	0.044	0.045
	67.625	Bottom	0.046	0.046	0.046	0.046	0.045	0.045	0.045	0.046
R10C39 - 3C (Freespan)	63.75	Top	0.046	0.046	0.046	0.047	0.047	0.046	0.047	0.046
	53.75	Bottom	0.045	0.046	0.047	0.046	0.047	0.047	0.046	0.045
R11C41 - 2B (TTS)	26.18	Top	0.046	0.047	0.046	0.046	0.047	0.047	0.047	0.047
	n/a	Bottom	n/a	n/a	n/a	n/a	n/a	n/a	n/a	n/a
R11C41 - 3B [1st TSP(H02)]	54.125	Top	0.046	0.046	0.046	0.046	0.045	0.045	0.046	0.045
	44.125	Bottom	0.045	0.045	0.045	0.0455	0.0445	0.044	0.045	0.045
R11C41 - 4B [2nd TSP(H03)]	78	Top	0.046	0.0455	0.046	0.0455	0.046	0.046	0.0455	0.046
	68	Bottom	0.046	0.0465	0.0465	0.046	0.046	0.0455	0.0455	0.046
R11C41 - 5A (Freespan)	99.375	Top	0.045	0.046	0.045	0.044	0.046	0.045	0.046	0.045
	89.375	Bottom	0.047	0.0465	0.047	0.046	0.047	0.046	0.046	0.047

Table 8-4

Chemical Composition of Comanche Peak Unit 1 Tubes

Element	R10C39 HL – Heat NX 4616		R11C41 HL – Heat NX 4505	
	Analysis	CMTR	Analysis	CMTR
C	0.05	0.04	0.044	0.03
Ni	75.02	75.20	75.07	75.75
Fe	7.52	8.64	7.55	8.65
Cr	15.70	15.26	15.64	14.78
Mn	0.32	0.34	0.32	0.29
Mo	0.10	-	0.10	-
Ti	0.26	0.18	0.26	0.21
Nb	0.07	-	0.07	-
Al	0.25	0.14	0.25	0.24
Si	0.27	0.17	0.27	0.16
Pb	0.00026	-	0.00020	-
S	<0.001	0.007	<0.001	0.007
Cu	0.30	0.32	0.29	0.31
P	-	-	-	-
Co	0.06	0.05	0.06	0.05
Mg	0.02	-	0.02	-
N	0.0050	-	0.0052	-
V	0.03	-	0.03	-
B	-	-	-	-

Table 8-5
Modified Huey Results

Specimen Identity	HNO_3 % (wt.)	Material Condition	Corrosion rate ($mg/dm^2/day$)
R10C39 HL Piece 5A	25	Alloy 600 MA – As pulled	36.4
R10C39 HL Piece 5B	25	Alloy 600 MA – As pulled	31.4
R11C41 HL Piece 3C1	25	Alloy 600 MA – As pulled	35.5
R11C41 HL Piece 3C2	25	Alloy 600 MA – As pulled	38.9

Table 8-6
Results of Vickers Microhardness Measurements
(500 gram Through-wall Measurements)

Specimen	Distance from OD, in.	Hardness
R10C38 Piece 4D1 @ 180°	0.006	218
	0.014	215
	0.022	204
	0.030	215
	0.038	221
R11C41 Piece 4A3 @180°	0.005	209
	0.013	206
	0.021	215
	0.029	212
	0.036	215

Table 8-7

Net-Section Residual Stress – Pulled Watts Bar Unit 1 Tubes

Split Ring Technique

Tube	Piece	Average Tube Wall Thickness W (in.)	Average OD Before Splitting D_o (in)	Average OD After Splitting D_f (in)	Residual Hoop Stress (ksi)
R10C39 HL	5D	0.0448	0.7518	0.7569	13.8
R11C41 HL	3C3	0.0454	0.7537	0.7590	14.5

Figure 8-1

Stress-Strain Curve for R10C39 HL – Piece 4C

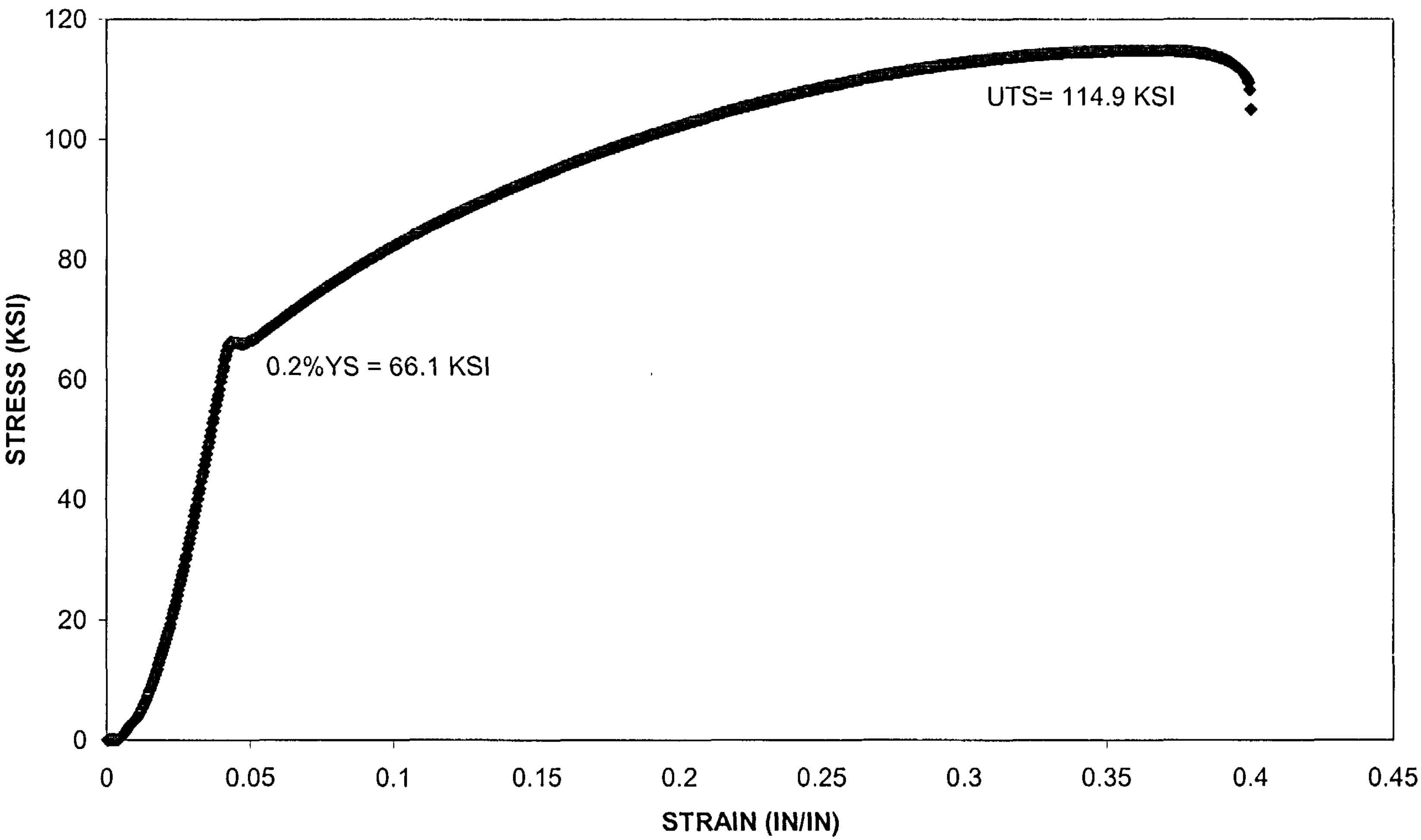

Figure 8-2

Stress-Strain Curve for R11C41 HL, Piece 5B

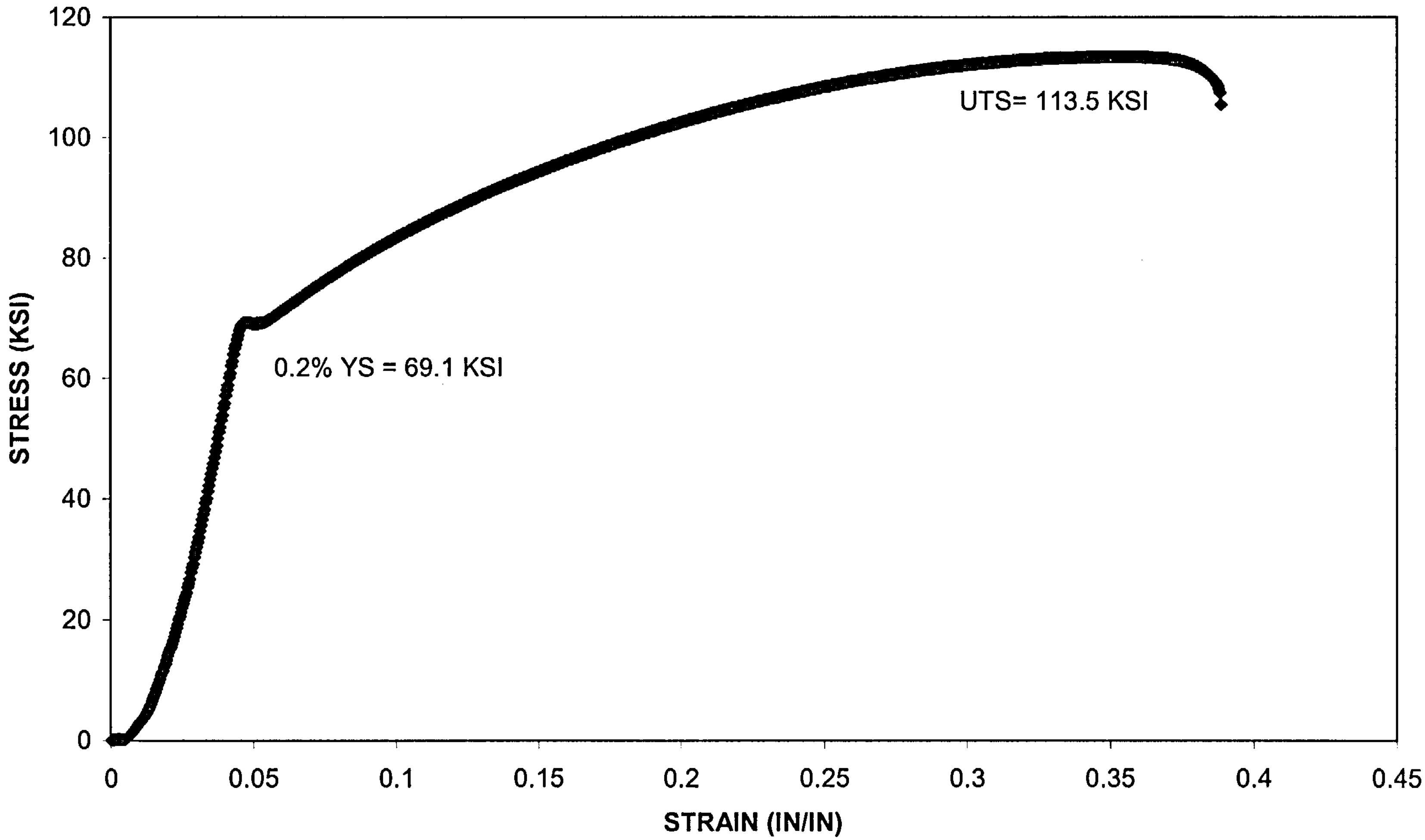

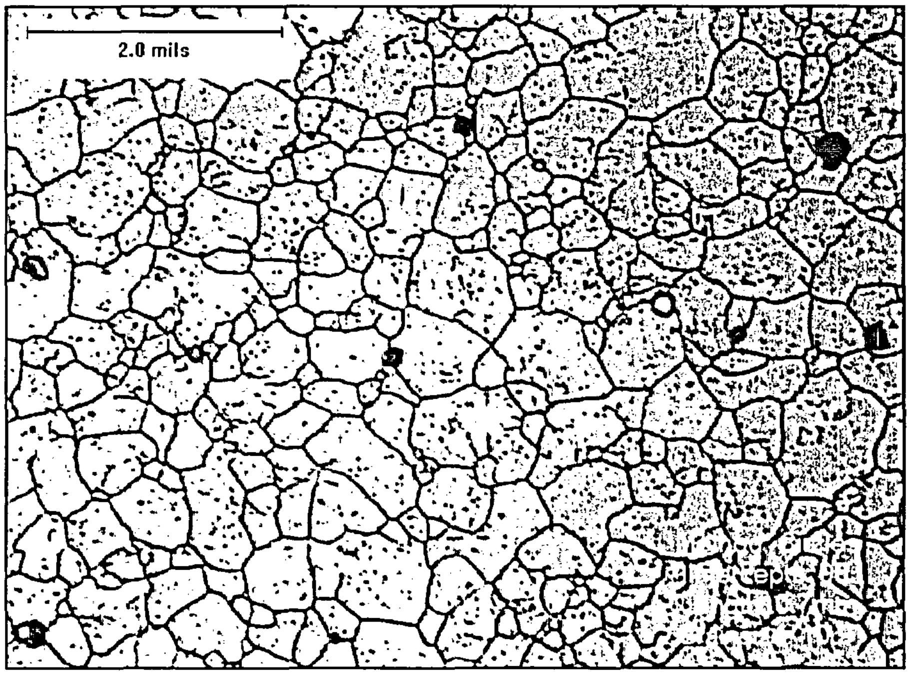

Figure 8-3
Grain Size for R10C39 HL – Piece 4D1 – Mount #2618

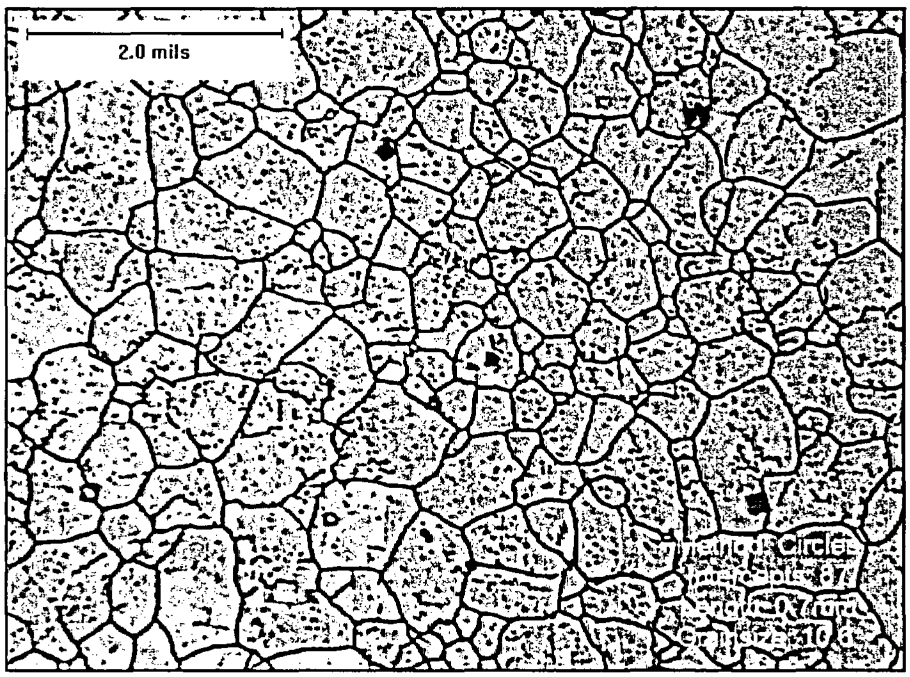

Figure 8-4
Grain Size – R11C41 HL – Piece 4A3 – Mount #2617

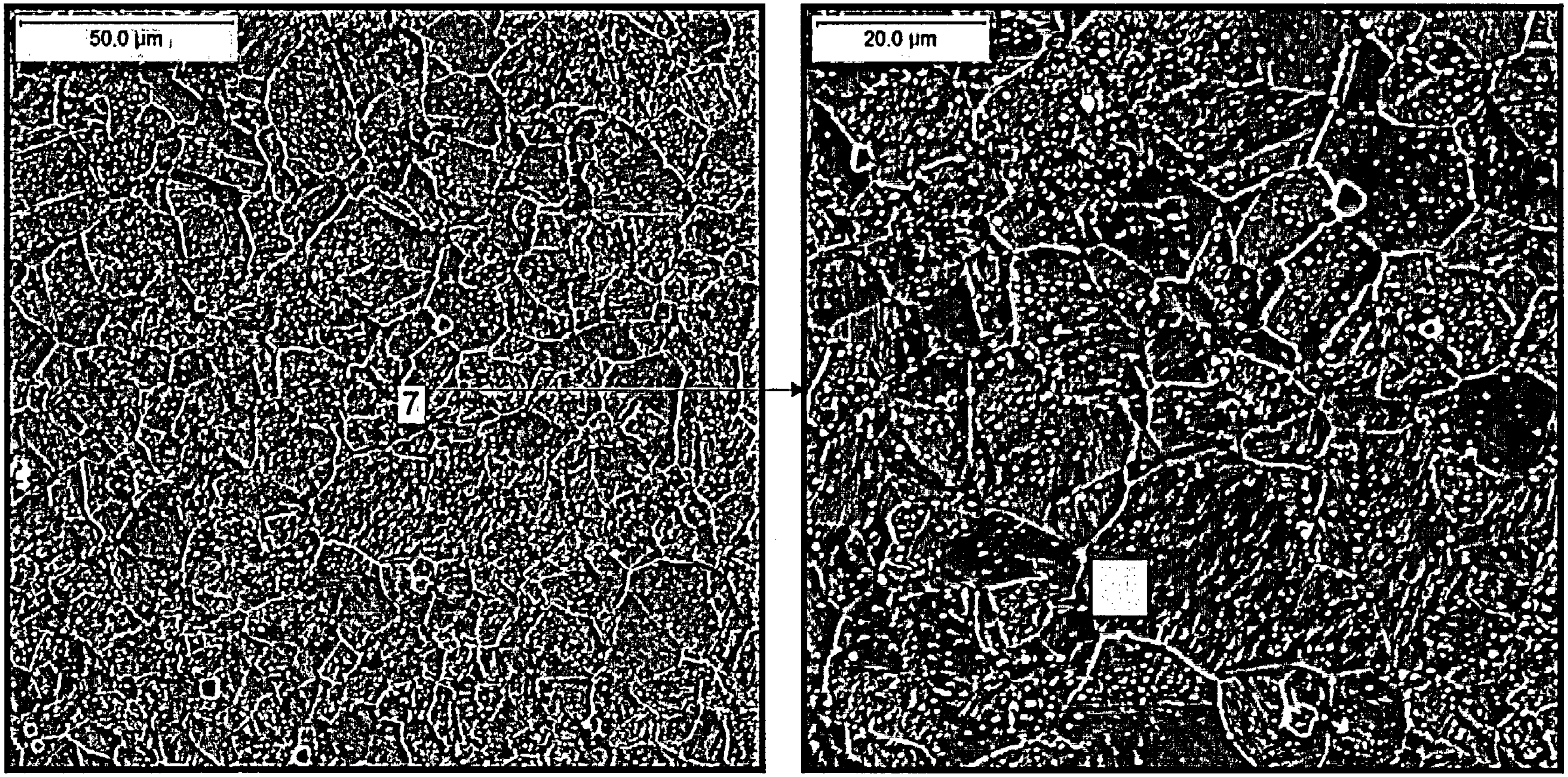

Figure 8-5

R10C39 HL – Piece 4D1

Scanning Electron Micrographs Showing Carbide Distribution – 2% Bromine-Methanol Etch

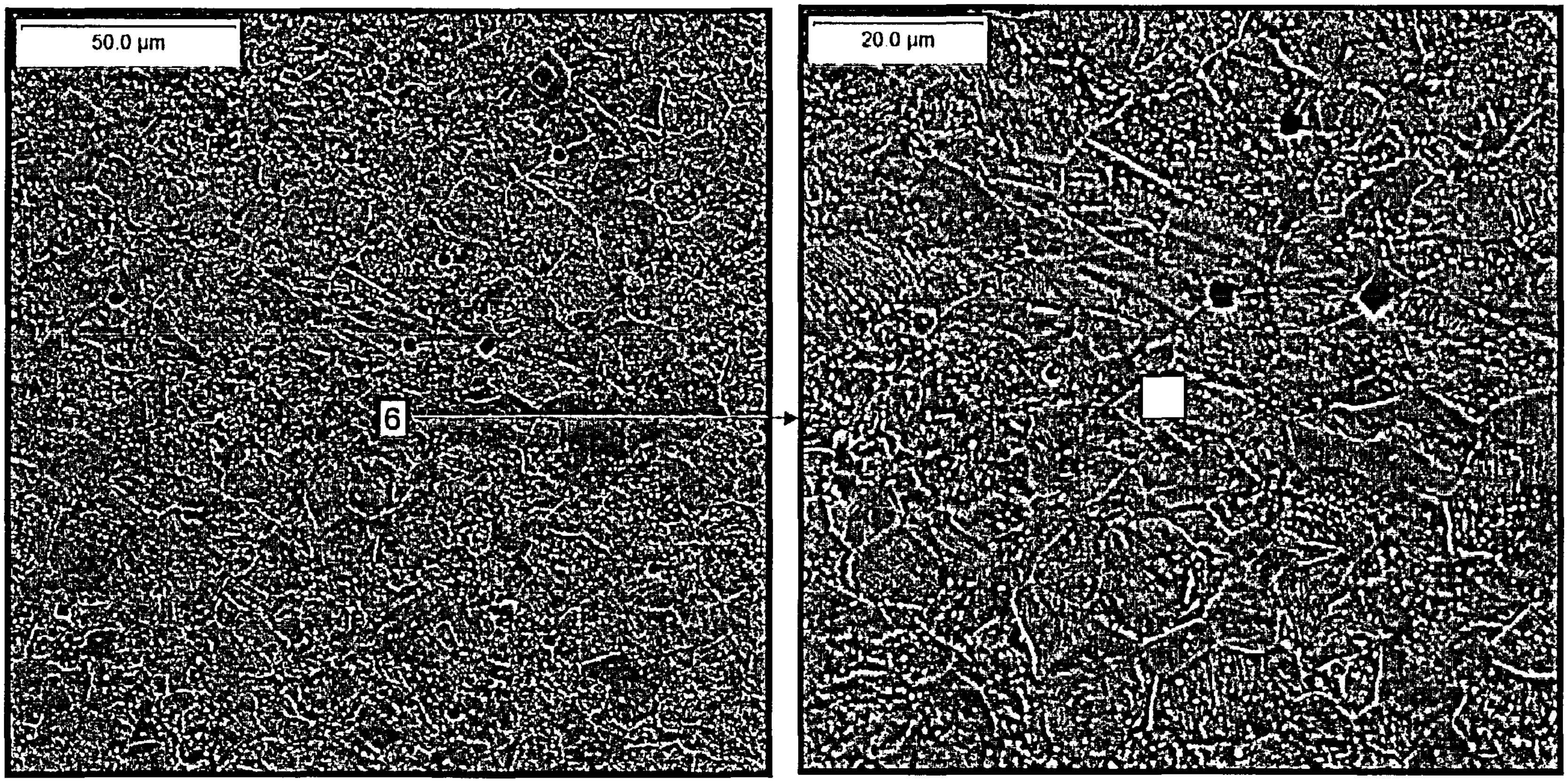

Figure 8-6

R11C41 HL – Piece 4A3

Scanning Electron Micrographs Showing Carbide Distribution – 2% Bromine-Methanol Etch

SECTION 9

SUMMARY AND CONCLUSIONS

9.1 Summary

The non-destructive and destructive examinations of Watts Bar Unit 1 steam generator tubes R10C39 and R11C41 confirmed the presence of OD-initiated axial degradation within the H02 and H03 tube support plate crevices. OD-initiated circumferential cracking was also confirmed at the top of the tubesheet for the R11C41 tube. The observed cracking was limited to the support plate crevices and the crevice at the top of the tubesheet. All four support plate regions had axial intergranular ODSCC with minimal evidence of IGA or cellular corrosion. The cracks were discrete with little evidence of branching.

Based on destructive examination, the maximum depth of the axial IGSCC for tube R10C39 HL was 100% through-wall at the H02 TSP intersection and approximately 40% through-wall at the H03 TSP intersection. For R11C41 HL, the maximum depth was 100% through-wall at the H03 TSP intersection and approximately 50% through-wall at the H02 intersection. The maximum depth of the circumferential crack seen at the top of tubesheet for R11C41HL was approximately 60%. The fracture face of the circumferential indication at the TTS indicated multiple short cracks separated by ductile ligaments. The morphology of all cracking was intergranular and OD-initiated. A summary of the eddy current and destructive examination results are presented in Table 9-1. Good agreement between the destructive examination results and the eddy current results are seen.

EDS results of OD surface deposits and fracture faces did not identify any chemical species that would appear to have directly contributed to the intergranular cracking. This finding is not uncommon in that the results of chemical and other microanalytical analyses do not establish a unique condition or species responsible for the degradation. EDS spectra results on both the ductile and IGSCC surfaces were dominated by chromium, nickel, and iron. Minor concentrations of calcium, aluminum, titanium, and silicon were also detected on these surfaces. Minor evidence of copper was detected on OD surfaces adjacent to the IGSCC fracture face. Copper can be associated with an oxidizing environment, however, the oxidation state of the copper could not be assessed from the EDS results.

The characteristics and properties of the pulled tubes were determined by a number of standard metallurgical tests. No unusual results were seen. Chemical analyses were generally consistent with the compositions reported in the Certified Materials Test Report (CMTR). The yield and ultimate strength values obtained on the pulled tube sections were higher than the values reported on the CMTR's. This observation is consistent with other tube pull data which normally shows an increase in tensile properties. The ASTM grain size for both tubes was approximately 10 to 11, which is typical of most early Westinghouse-supplied steam generator tubing. The carbide precipitation was predominantly intragranular with minimal evidence of intergranular carbides. Results of the modified Huey tests indicated the pulled tube material to be non-sensitized, i.e., grain boundary chromium depletion was not detected.

The results of the split-ring residual stress tests indicated residual net-section tensile hoop stresses from 13.8 to 14.5 ksi. These values are typical for mill annealed, straightened, and polished Alloy 600 tubing employed by Westinghouse for Model D3 application.

9.2 Conclusions

All burst test results were in excess of the most limiting requirement of three times the normal operating pressure differential. All tests performed on tubes R10C39 HL and R11C41 HL and the results obtained, satisfy the ODSCC voltage-based Alternate Repair Criteria. The burst and leak results were consistent with the existing ODSCC ARC database and the data obtained was appropriate for use in determining the parameters of correlations for analysis of the Watts Bar tube indications. The measured burst results fall within the scatter band of the EPRI reference database. The burst values obtained fall within the 95% confidence band for 90% of the population about the regression line (5% in each tail). There was no strong indication of a statistical anomaly although the R10C39 HL – Piece 3B burst pressure at the H02 TSP intersection was less than expected and approximately on the lower tolerance band.

Table 9-1
Comparison of Eddy Current and Destructive Examination Results for Crack Depth and Length

Tube Section	+ Pt Crack Depth and Length				Destructive Examination		
	Lab Review of Field Eddy Current Data		Laboratory Eddy Current Data				
	Max Depth	Length	Max Depth	Length	Max Depth	Avg. Depth	Length
R10C39 HL H02	76%	0.71"	90% 46%	0.71 -	100%	66.5%	0.60"
R10C39 HL H03	NDD	-	NDD	-	39.6%	20.6%	0.21"
R11C41 HL TTS	64%	103°	56% 74%	291°	61%	42.3%	360°
R11C41 HL H02	NDD	-	NDD	-	53.7%	27.9%	0.11"
R11C41 HL H03	76%	0.65"	88%	0.67"	100%	47.8%	0.63"

Section 10

Appendix A

Update of ODSCC Database for ¾" Diameter Tubes

Westinghouse

Comparison of Watts Bar 1 Data with Existing ARC Correlations

1.0 Comparison of Additional Data with Existing ARC Correlations

This document reports on the evaluations performed using the results of leak rate and burst testing of the tube sections which were removed from Watts Bar Unit 1 in 2003 (SG 2, R10C39 and R11C41). The destructive examination of the tubes was performed by the Science and Technology Department of the Westinghouse Electric Company in Churchill, Pennsylvania. A draft of the examination results was provided by Reference 1. The results from the leak tests of the indications were obtained from Reference 2 and the results from the destructive examinations, i.e., burst and tensile test data, were obtained from Reference 3. Fabrication tensile properties were obtained via Reference 4, which transmitted copies of the fabrication record pages for the affected tubes. The Watts Bar 1 pulled tube data germane to the alternate repair criteria (ARC) correlations, the material properties, leak rate and burst pressure characteristics, and the ODSCC indications bobbin amplitudes for ARC applications, are listed in Table 1. The reported leak test values result from adjusting the test data to reflect the pressure and temperature conditions of interest relative to the conditions that existed at the time the actual measurement was taken. The tests were performed at elevated temperatures near those corresponding to SLB conditions. The differential pressures also closely match the SLB condition, but the absolute pressures are elevated, i.e., the secondary pressure may be on the order of 300 psig. The results from the burst and leak tests were compared to the database of similar test results for 3/4" outside diameter steam generator tubes. In addition, the effect of including the new test data in the reference database on the correlations used for the evaluation of outside diameter stress corrosion cracking (ODSCC) indications at tube support plate (TSP) elevations was evaluated. In summary, the test data are consistent with the database relative to the burst pressures, and the probability of leak as a function of the bobbin amplitude. One of the indications exhibited significant leakage relative to that expected at postulated steam line break (SLB) conditions, leading to a meaningful effect on the ODSCC leak rate correlations as well as nontrivial effect on the probability of leak (POL) correlation. The comparisons and evaluations are discussed in the following sections.

The reference database for comparison consisted of the data reported in Reference 5, the most recent addendum to the original ODSCC ARC report of Reference 6. Addendum 5 contains a complete listing of the current database, inclusive of prior addenda. It is noted that there were no leak rate data for 3/4" diameter tubes added to the database by Addenda 3 and 4; leak rate data from two plants were added to the database as documented in Addendum 5. The examination of the tube sections removed from Watts Bar 1 adds two data points to each of the regression analyses, burst pressure, probability of leak, and leak rate as a function of bobbin amplitude.

2.0 Suitability for Inclusion in the Database

The report information on the destructive examinations of the tube sections was reviewed relative to the EPRI guidelines for inclusion/exclusion of tube specimen data in the ARC database. This review revealed no morphology or other information that would lead to a conclusion that the data should not be included in the database. Therefore, the resulting correlations should be considered applicable to the use of ARC for indications in 3/4" diameter tubes in Westinghouse SGs. As previously noted, the results from the leak tests were adjusted for use in the database. The leak rate values reported in Table 1 reflect the results of the adjustments to match the conditions used for the rest of the database. Results from the tensile tests of the tube material are also included in the table. The combined yield plus ultimate strength values are 25 to 30 ksi larger than the values reported in the fabrication records for the respective heats of material used to fabricate the tubes[1].

3.0 Burst Pressure versus Bobbin Amplitude

The result from burst tests, performed on both tube specimens which exhibited a non-zero bobbin amplitude at a TSP elevation location, were considered for evaluation. The measured burst pressures of the Watts Bar 1 tube specimens are depicted on Figure 1 and Figure 2 relative to the burst pressure correlation developed using the Reference 5 database. Figure 1 illustrates the results relative to a 90% tolerance band expected for future test results. The following observations are apparent from an examination of that figure:

1. A visual examination of the data relative to the EPRI database indicates that the measured burst pressures fall within the scatter band of the reference data.
2. The data points for both of the indications fall within the 95% confidence band for 90% of the population about the regression line (5% in each tail). There is no strong indication of a statistical anomaly although the R10C39 burst pressure is less than expected and approximately on the lower tolerance line.

The net result is that the visual examination of the plot of the data indicates that there is no significant departure from the reference database. Based on the placement of the new data it may be judged that there would be no significant effect on the analysis of the residuals of

the regression; either on the scatter plot of the residuals as a function of the predicted burst pressures or on the normal probability plot of the residuals.

---

[1] Fabrication data are expected to be from tests of tube specimens and should reflect any cold work from straightening the tubes. A rationale for the increase in the ultimate tensile strength has not been developed.

Since the Watts Bar 1 burst pressure data were not indicated to be from a separate population from the reference data, the regression analysis of the burst pressure on the common logarithm of the bobbin amplitude was repeated with the additional data included. A comparison of the regression results obtained by including these data in the regression analysis is provided in Table 2. Regression predictions obtained by including these data in the regression analysis are also shown on Figure 2. A summary of the changes is as follows:

1. Intercept — The intercept of the burst pressure, P_B, as a linear function of the common logarithm of the bobbin amplitude regression line is decreased by 0.3%, or about 20 psi. This has the effect of decreasing the predicted burst pressure as a function of the bobbin amplitude for small amplitudes. Although there is a tendency to decrease the value of the structural limit slightly, an examination of the figure reveals that the practical effects of the change are negligible.
2. Slope — The absolute slope of the regression line is increased by 0.4%, i.e., the slope is steeper with the additional data. This has the effect of decreasing the burst pressure as a function of bobbin amplitude for large indications. As with the change in the intercept, the tendency is to decrease the value of the structural limit, but the practical effect of the slope change is negligible.
3. Standard Error — There is an increase in the standard error of the residuals of 1.1%. The effect of this change is reflected in a slightly larger deviation of the 95% prediction line from the regression line, leading to a tendency to decrease the calculated value of the structural limit and minor changes in the probability of burst for a given voltage level. The tendency to decrease the structural limit.

The net effect of the changes on the 2560 psi differential pressure SLB structural limit (found as $1.4 \cdot \Delta P$), using 95%/95% lower tolerance limit material properties, is to decrease it by 0.16V (to 4.69V). The corresponding change on the 2405 psi structural limit is a 0.19V reduction (to 5.64V). The decrease of the intercept and slope and the increase in the standard error leads to small increases in the expected probability of burst. Given the relatively small change in the structural limit, the change in the probability of burst would also be expected to be small. Predicted values of the probability of burst of a single indication as a function of the bobbin amplitude are illustrated on Figure 3. The probability of burst is increased slightly over the full range of the data used for the correlation and beyond the effective range of interest.

4.0 Probability of Leak

The Watts Bar 1 data were examined relative to the reference correlation for the POL as a function of the common logarithm of the bobbin amplitude. Figure 4 illustrates the Watts Bar 1 data relative to the reference correlation. The lower amplitude indication had a calculated POL of 16% and it leaked. The POL for the higher amplitude indication was calculated to be 70% it also leaked. There is no implication of irregular results, i.e., outlying behavior is not indicated. The fact that the lower voltage indication leaked is not totally unexpected although the odds against leakage were 5:1. Two other tube indications in the ARC database exhibited leakage at lower voltage levels.

In order to assess the quantitative effect of the new data on the correlation curve, the database was expanded to include the two Watts Bar 1 data points and a *Generalized Linear Model* regression of the POL on the common logarithm of the bobbin amplitude was repeated. A comparison of the regression parameters with those for the reference database is shown in Table 3. These results indicate:

1. Intercept — A 7.5% reduction in the absolute value of the *logistic* intercept parameter. Since the intercept is negative, this increases the intercept slightly. This is not unexpected given the fact that the lower voltage indication leaked.

2. Slope — A 4.2% decrease in the *logistic* slope parameter.

3. Variance/Covariance — The values of the elements of the covariance matrix of the parameters changed from 14 to 21%. Examination of Figure 4 indicates that there is an increase in the POL over the entire range of interest for the application of the ARC. The POL increased by a factor of two at an amplitude of 0.1V (from 1.7 to $3.5 \cdot 10^{-6}$) and by a factor of 1.4 at 1V (from $8 \cdot 10^{-3}$ to $1.1 \cdot 10^{-2}$). However, the POL is of secondary importance in determining the total estimated leak rate and the effect on predicted 95th percentile values would be expected to be small.

4. Mean Square Error — The mean square error (deviance divided by number of degrees of freedom) increased by 808%. The deviance increased, however this is expected when data is added to the database because the deviance is akin to the error sum of squares. The Pearson standard deviation decreased slightly from 0.967 to 0.874. The ideal value for this indicator is unity, however, change is judged to be not significant.

The ratio of the probabilities of leak as a function of bobbin amplitude is shown on Figure 5 As previously noted, when the total leak rate is determined using the leak rate to bobbin volts correlation, the result is usually quite insensitive to the form of the POL function. So, the effect of the changes in the parameter values and variances would be expected to be small or immaterial relative to the calculation of the 95% confidence bound of the total leak rate from a SG.

5.0 Leak Rate vs. Bobbin Amplitude

The laboratory leak rate values are listed in Table 1 for the tested specimens. The leak rate tests were performed at elevated temperature conditions and the results adjusted slightly to postulated accident conditions using the methodology described in Appendix B of Reference 6. The effect of the test results on the correlation parameters of the log-leak rate to log bobbin voltage are listed in Table 4 for a differential pressures of 2560 and 2405 psi respectively. The changes due to the inclusion of the additional data are as follows (described for two values of the differential pressure associated with a postulated steam line break event):

1. Intercepts — The intercepts of the regression equations decreased in absolute value by 7.2 and 4.6% for postulated SLB event differential pressures of 2560 and 2405 psi respectively.

2. Slopes — The slopes of the regression equations decreased by 3.6 and 2.6% for differential pressures of 2560 and 2405 psi respectively.

3. Standard Error Values — The standard deviations of the log leak rate prediction errors as a function of the log bobbin amplitude were essentially unchanged, decreasing by 0.5 and 1.2% respectively.

4. *p* Value — The one-sided *p* value for the correlation at a differential pressure of 2560 psi decreased from $2.1 \cdot 10^{-11}$ to $8.1 \cdot 10^{-12}$, while the change for a ΔP of 2405 psi was from $9.6 \cdot 10^{-12}$ to $2.1 \cdot 10^{-12}$. In other words, the one-sided 95% confidence interval for the population slope for the correlation of log leak rate to log bobbin amplitude does not include zero for either differential pressure of interest.

Figure 6 illustrates the results from the tests of the leaking specimens relative to the database for a differential pressure of 2560 psi. Figure 7 provides a similar illustration for a differential pressure of 2405 psi. The magnitude of the leakage from both indications is not remarkable relative to the rest of the database. Both figures illustrate the effect of the added data points on their respective fitted regression lines (the median of the log-normal distribution) and on the expected leak rate (the mean of the log-normal distribution). The net effect of adding the results is a slight increase in the predicted leak rates for bobbin amplitudes up to about 10V, regardless of the differential pressure of consideration, with a slight decrease thereafter.

A scatter plot of the residuals of the regression analysis for a SLB differential pressure of 2405 psi is provided on Figure 8. A normal plot of the residuals is provided on Figure 9. Both of the charts are confirmatory of assumptions made in performing the regression analysis, i.e., the residual log leak rates are independent of the predicted log leak rates, and the residuals log leak rates approximate a normal distribution. Finally, an illustration of the combined effect of the added data on the POL and leak rate is provided by the ratio information presented on Figure 10. The relative increase in the leak rates is greatest for small indications with small leak rates.

6.0 Consideration of EdF Data

A commitment was made by the industry prior to the preparation of Reference 3 that future updates of the ODSCC ARC database would include the results of considerations made to determine if statistical findings regarding the French data remained valid with the inclusion of new data. There are no considerations to be made relative to the Watts Bar tube data because the EdF data are for 7/8" nominal diameter SG tubes.

7.0 General Conclusions

The review of the effect of the Watts Bar 1 data indicates that the burst pressure and the probability of leak correlations to the common logarithm of the bobbin amplitude are slightly changed by the inclusion of the test data. Therefore, it is likely that the conclusions relative to EOC probability of burst would not be significantly affected by the addition of the Watts Bar 1 data. This was illustrated on Figure 3.

The effect of the data on the 95th percentile of the total leak rate when only the POL is considered could be meaningful. However, when taken in conjunction with the minor changes in the leak rate as a function of bobbin amplitude regression, the effect of the test data on the 95th percentile of the total leak rate is expected to be not significant.

8.0 References

1. Electronic Mail, "Watts Bar Watts Bar Tube Examination Effort," A. Vaia (Westinghouse) to R. Keating, Westinghouse Electric Company, Madison, PA, December 5, 2003.
2. Letter (Draft), "Summary of Watts Bar Unit 1 Steam Generator Tubes R10C39 and R11C41 Examination Results," A. Vaia (Westinghouse) to R. Keating, Westinghouse Electric Company, Madison, PA, December 5, 2003.
3. Electronic Mail, "Burst R11C41 piece 4B – Watts Bar," A. Vaia (Westinghouse) to R. Keating, Westinghouse Electric Company, Madison, PA, December 10, 2003.
4. Electronic Mail, "Re: Watts Bar Pulled Tubes," E. Camp, Tennessee Valley Authority, Chattanooga, TN, December 8, 2003.
5. 1007660, *Steam Generator Tubing Outside Diameter Stress Corrosion Cracking at Tube Support Plates Database for Alternate Repair Limits, NP 7480-L, Addendum 5, 2002 Database*, EPRI, Palo Alto, November, 2002.
6. NP-7480-L, *Steam Generator Tubing Outside Diameter Stress Corrosion Cracking at Tube Support Plates - Database for Alternate Repair Limits, Volume 2: 3/4 Inch Diameter Tubing*, EPRI, Palo Alto, CA: August, 1996.
7. CN-SGDA-03-XX, "ODSCC ARC Database Update for 3/4" Diameter Tubes," Westinghouse Electric Company, Nuclear Services Division, Madison, PA, USA, June, 2003.

Table 1: Analysis Properties of the SG 2 Watts Bar 1 Pulled Tube Sections for Inclusion in the ODSCC ARC Database

Tube Section	Bobbin Amplitude (Volts) [1.]	Yield + Ultimate (ksi) [2.]	Burst Pressure (ksi)	Probability of Leak at SLB	Leak Rate at 2405 psi (lph) [3.]	Leak Rate at 2560 psi (lph) [3.]
R10C39-2H	4.51	181.0	4.931	1	3.80	9.62
R10C39-3H	NDD	181.0	12.058	N/A	N/A	N/A
R10C39-FS	NDD	181.0	12.991	N/A	N/A	N/A
R11C41-2H	NDD	182.6	12.649	N/A	N/A	N/A
R11C41-3H	2.45	182.6	9.998	1	0.38	0.79
R11C41-FS	NDD	182.6	13.235	N/A	N/A	N/A

Notes:

1. Locations with an amplitude of NDD are included for information only.
2. The value of S_y+S_u is rounded to one decimal place for use in the regression analyses. The mill test reported (CMTR) values were from 152 to 166 ksi and 150 to 163 ksi respectively.
3. Leak rates were measured at conditions closely approximating postulated accident values and adjusted to exact accident conditions using the procedure described in Appendix B of Reference 6.

Table 2: Effect of Watts Bar 1 Data on the 3/4" Tube
Burst Pressure vs. Bobbin Amplitude Correlation

$$P_B = a_0 + a_1 \log(Volts)$$

Parameter	Addendum 5 Database	Addendum 5+ Database	New / Old Ratio
Intercept, a_0	7.4605	7.4402	0.997
Slope, a_1	-2.9572	-2.9682	1.004
r^2	80.7%	80.2%	0.994
Std. Dev., σ_{Error}	0.9009	0.9106	1.011
Mean Log(V)	0.3994	0.4018	
SS of Log(V)	37.2648	37.3292	
N (data pairs)	98	100	
Structural Limit (2560 psi) (1)	4.85	4.69	0.967
Structural Limit (2405 psi) (1)	5.83	5.64	0.967
p Value for a_1 (2)	$2.3 \cdot 10^{-36}$	$1.6 \cdot 10^{-36}$	
Reference σ_f	68.78 ksi (3)		

Notes: The number of significant figures reported simply corresponds to the output from the calculation code and does not represent true engineering significance.

(1) Values reported correspond to applying a safety factor of 1.4 on the differential pressure associated with a postulated SLB event.

(2) Numerical values are reported only to compare the calculated result to a criterion value of 0.05. For such small values the relative change is statistically meaningless.

(3) This is the flow stress value to which all data was normalized prior to performing the regression analysis.

Table 3: Effect of Watts Bar 1 Data on the Probability of Leak Correlation

$$\Pr(Leak) = \frac{1}{1 + e^{-[b_1 + b_2 \log(Volts)]}}$$

Parameter	Addendum 5 Database	Addendum 5+ Database	New / Old Ratio
Intercept, β_1	-4.8270	-4.4637	0.925
Slope, β_2	8.4488	8.0947	0.958
V_{11} (1)	1.1623	0.9392	0.808
V_{12}	-1.7094	-1.4115	0.826
V_{22}	2.8755	2.4739	0.860
DoF(2)	123	125	
Deviance	45.9	49.93	1.088
Pearson SD	0.967	0.874	0.904
MSE	0.373	0.399	1.071

Notes: (1) Parameters V_{ij} are elements of the covariance matrix of the coefficients, β_i, of the regression equation.

(2) Degrees of freedom.

Table 4: Effect of Watts Bar 1 Data on the 3/4" Tubes
Leak Rate vs. Bobbin Amplitude Correlation (2560 & 2405 psi)

$$Q = 10^{[b_3 + b_4 \log(Volts)]}$$

Parameter	Addendum 5 Database Value	Addendum 5+ Database	Effect Ratio
SLB ΔP = 2560 psi			
Intercept, b_3	-1.6384	-1.5208	0.928
Slope, b_4	2.9409	2.8347	0.964
Index of Deter., r^2	61.6%	61.5%	0.999
Std. Error, σ_{Error} (b_5)	0.6064	0.6033	0.995
Mean of Log(Q)	1.0702	1.0450	
Std. Dev. of Log(Q)	0.9679	0.9623	
p Value for b_4	$2.05 \cdot 10^{-11}$	$8.09 \cdot 10^{-12}$	0.396
SLB ΔP = 2405 psi			
Intercept, b_3	-1.8708	-1.7849	0.954
Slope, b_4	2.9767	2.8990	0.974
Index of Deter., r^2	62.8%	63.6%	1.012
Std. Error, σ_{Error} (b_5)	0.5979	0.5904	0.988
Mean of Log(Q)	0.8707	0.8391	
Std. Dev. of Log(Q)	0.9700	0.9681	
p Value for b_4	$9.6 \cdot 10^{-12}$	$2.1 \cdot 10^{-12}$	0.222
Common Data			
Data Pair, N	48	50	
Mean of Log(V)	0.9210	0.9051	
SS of Log(V)	3.1348	3.4733	

Note: The number of significant figures reported simply corresponds to the output from the calculation code and does not represent true engineering significance.

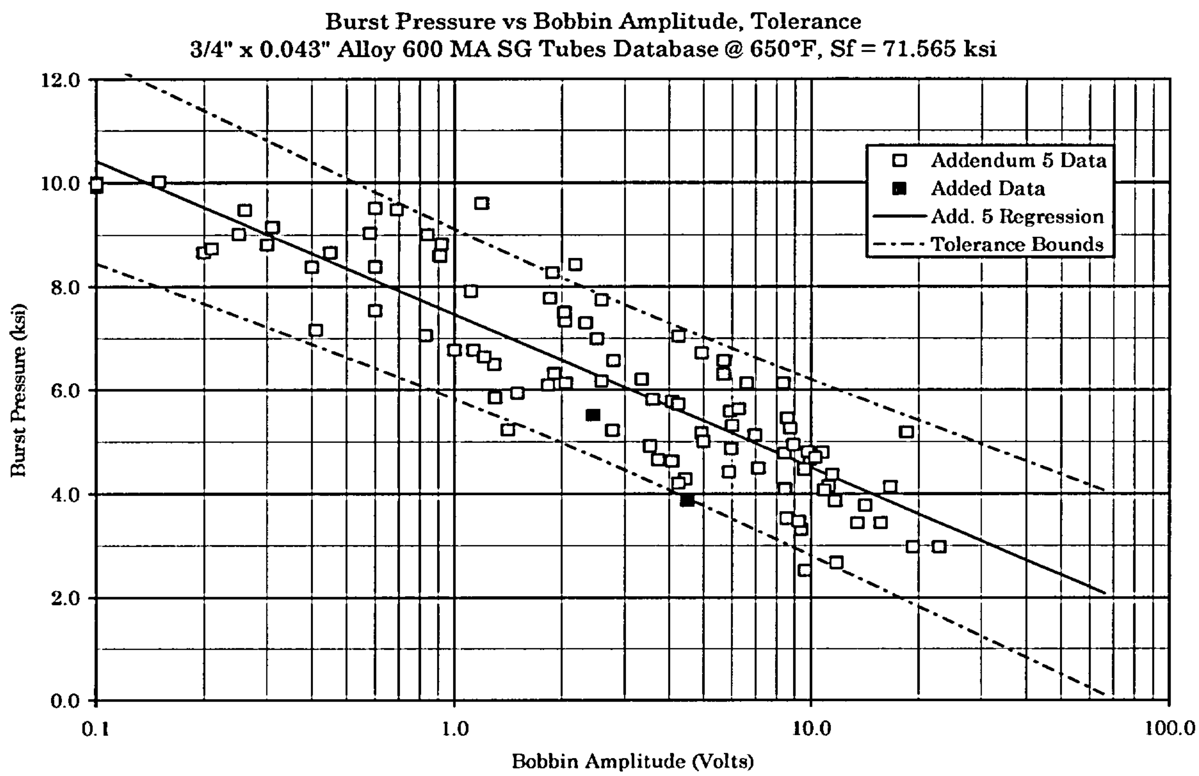

Figure 1: Comparison of additional test data to database tolerance bounds.

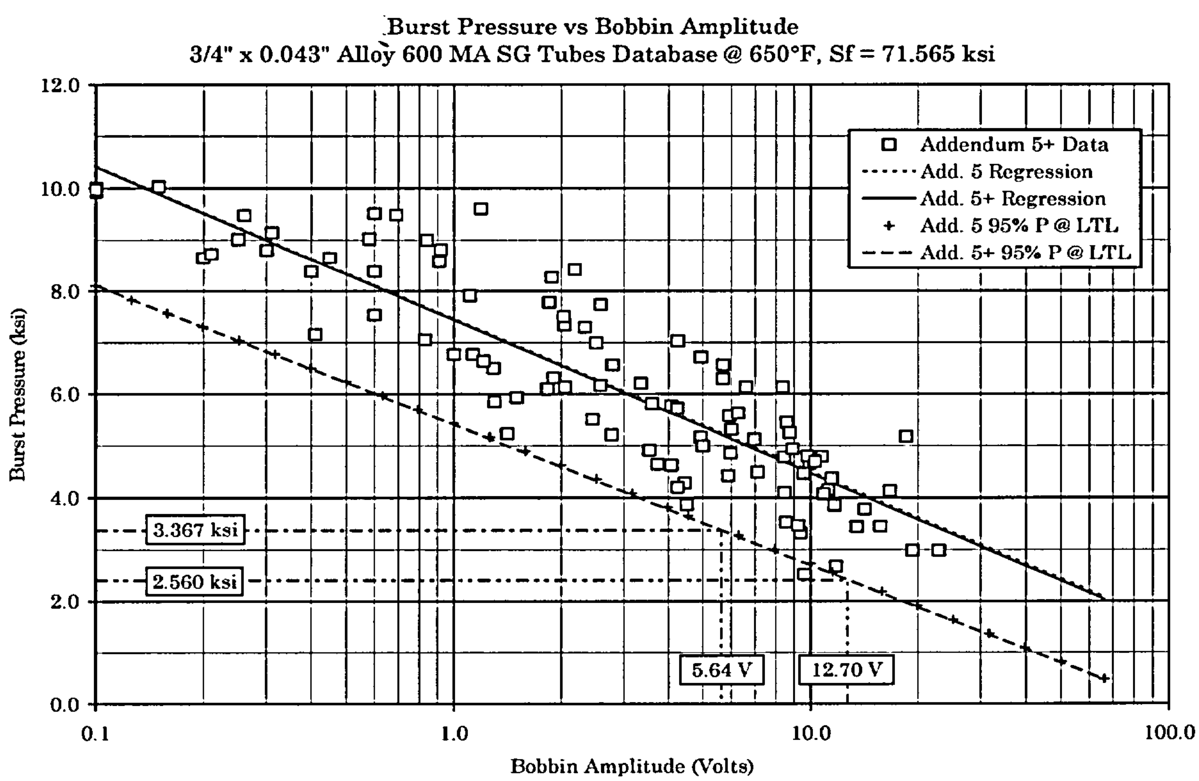

Figure 2: Affect of additional data on the burst pressure correlation.

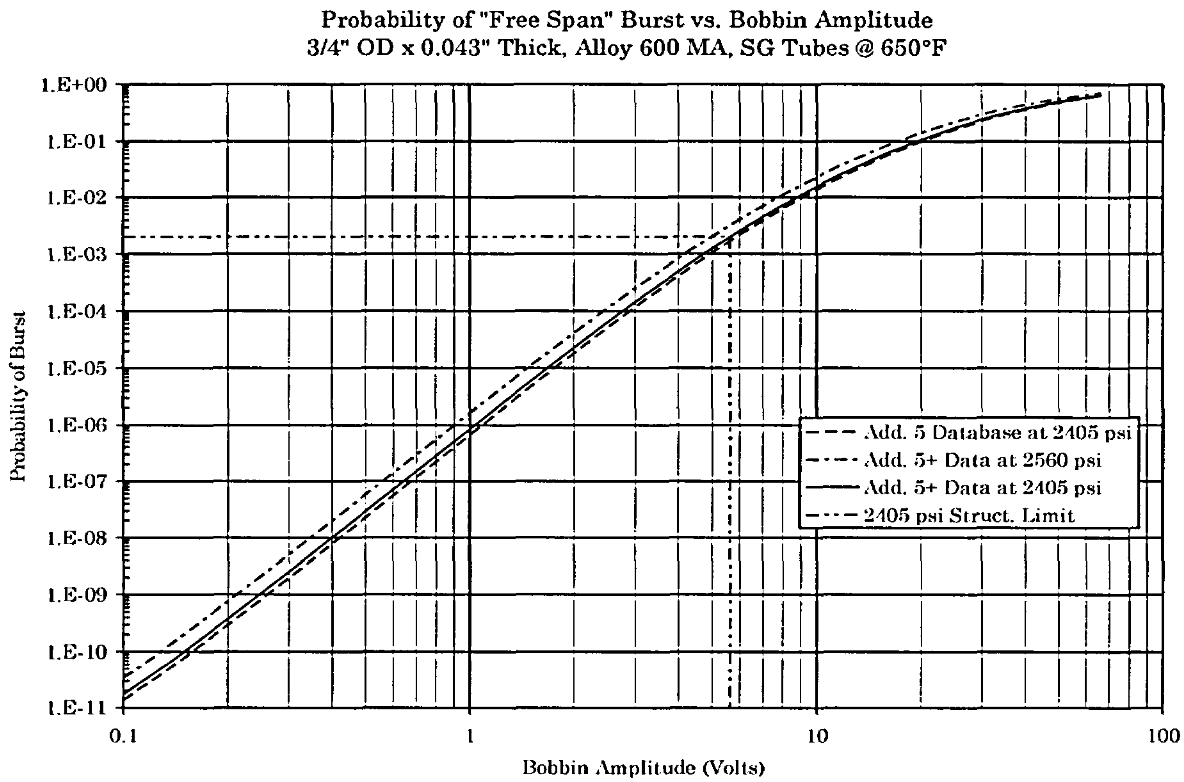

Figure 3: Probability of burst with additional data

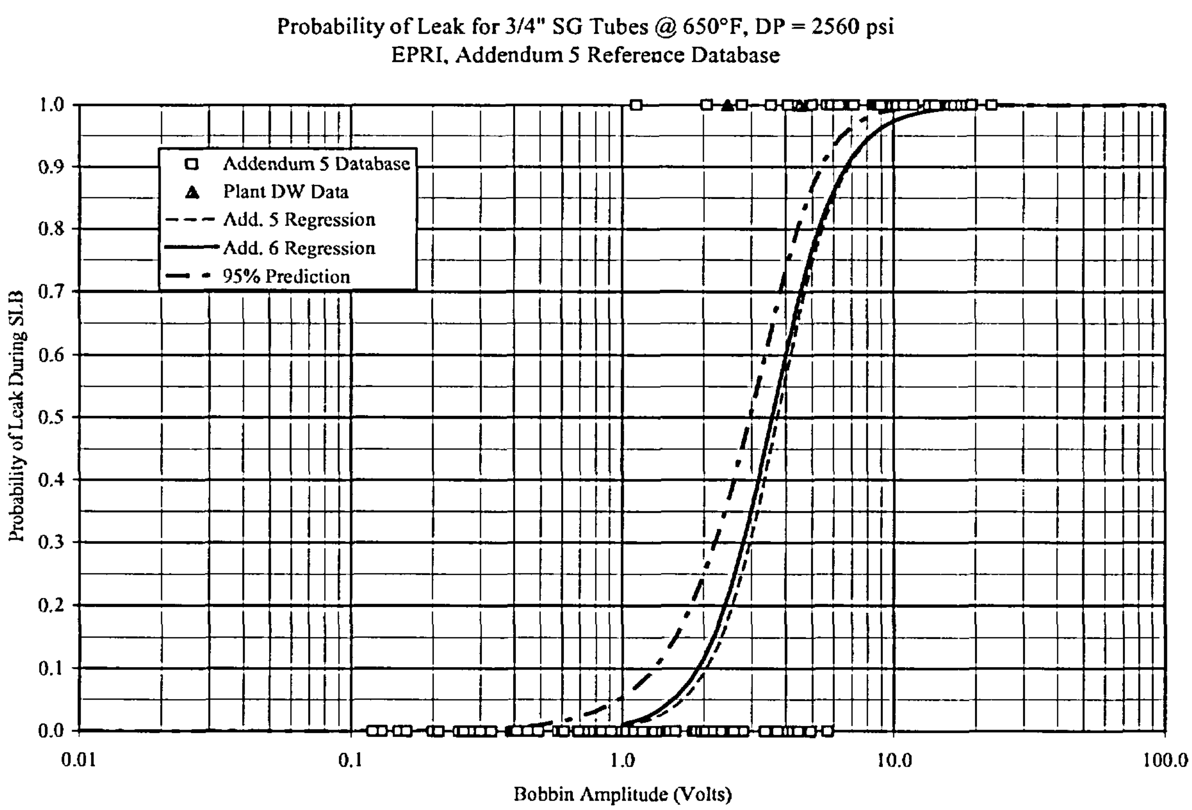

Figure 4: Probability of leak correlation with additional data

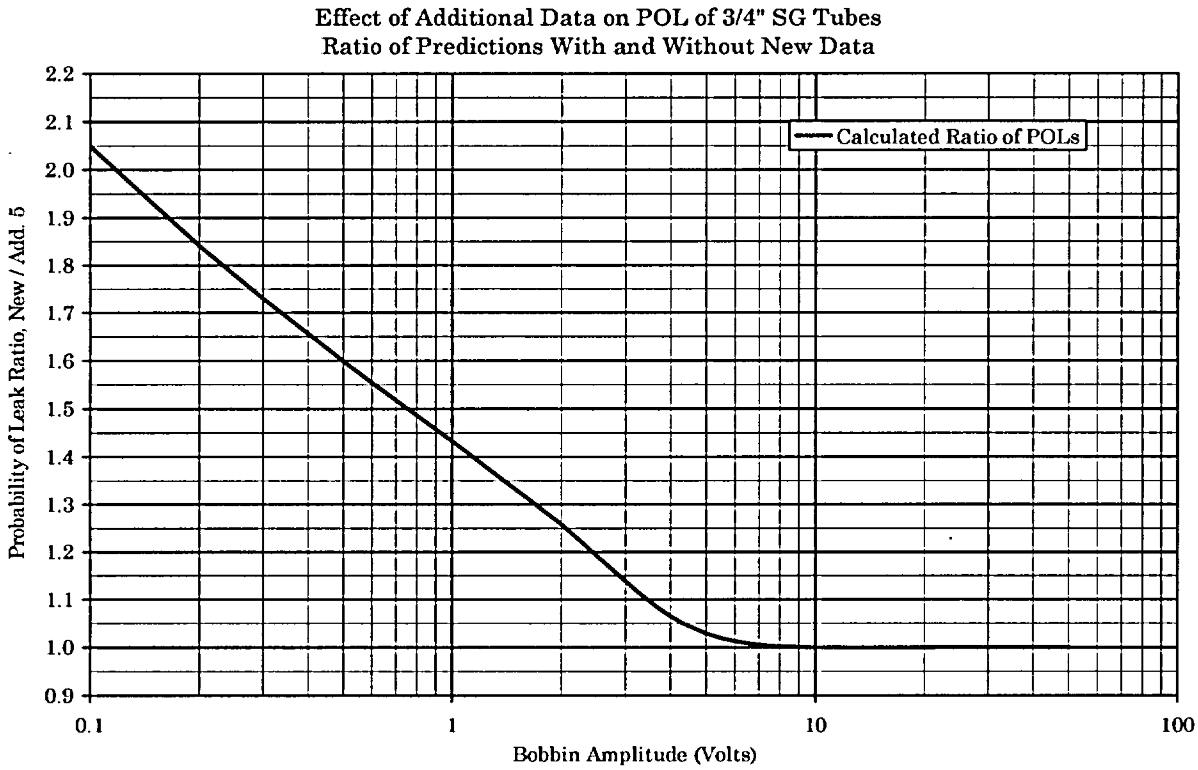

Figure 5: Ratio of after to before POL as a function of bobbin amplitude.

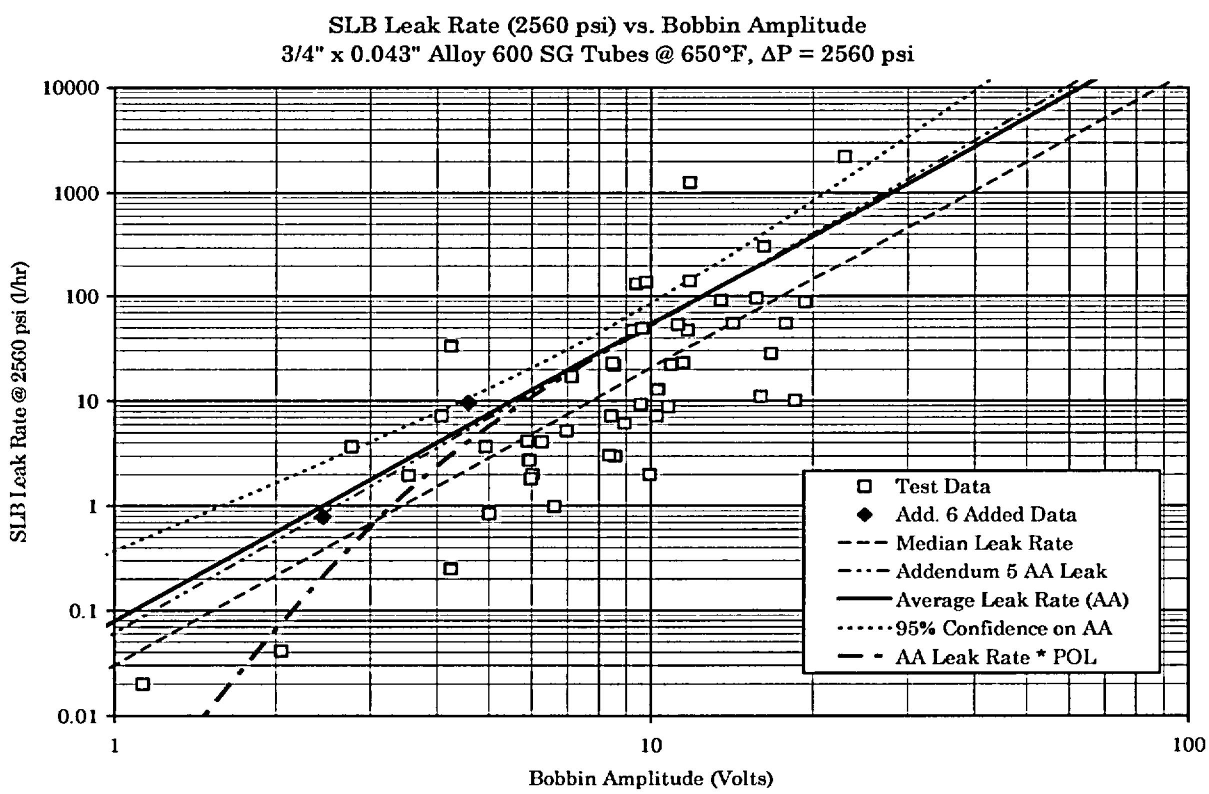

Figure 6: Affect of additional data on the leak rate at 2560 psid

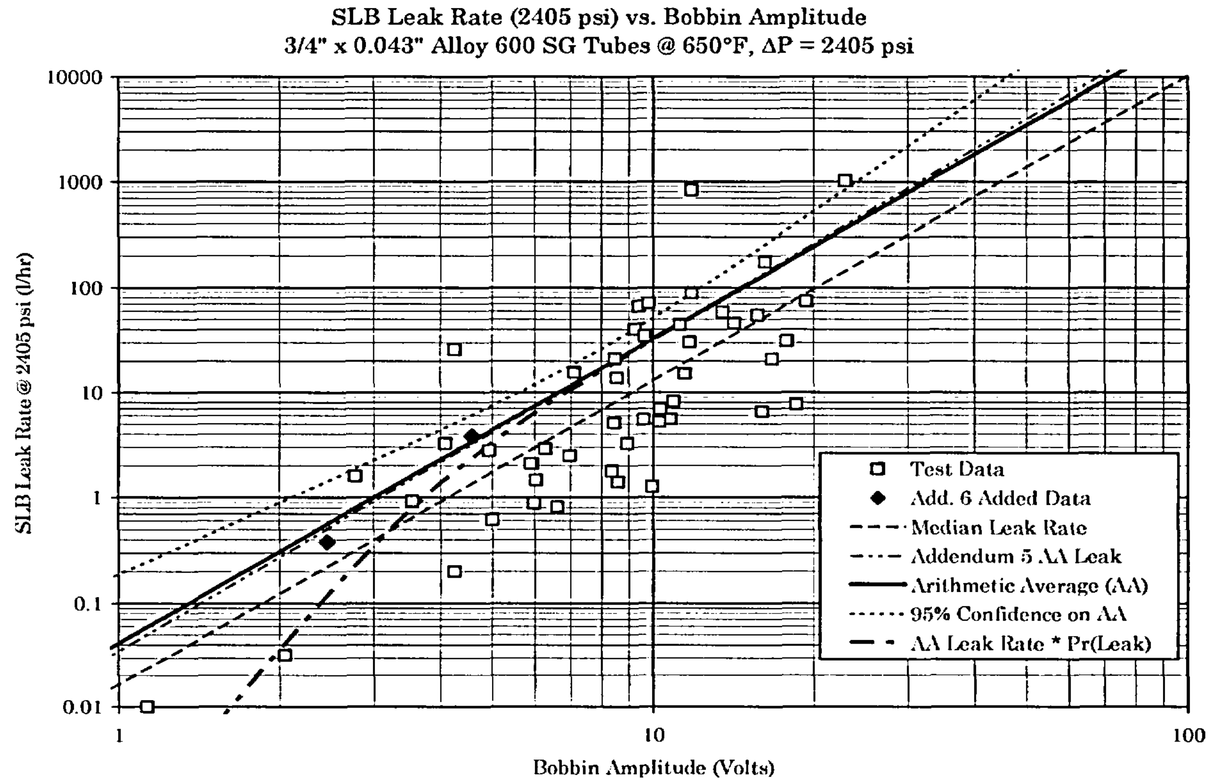

Figure 7: Affect of the additional data on the leak rate at 2405 psid

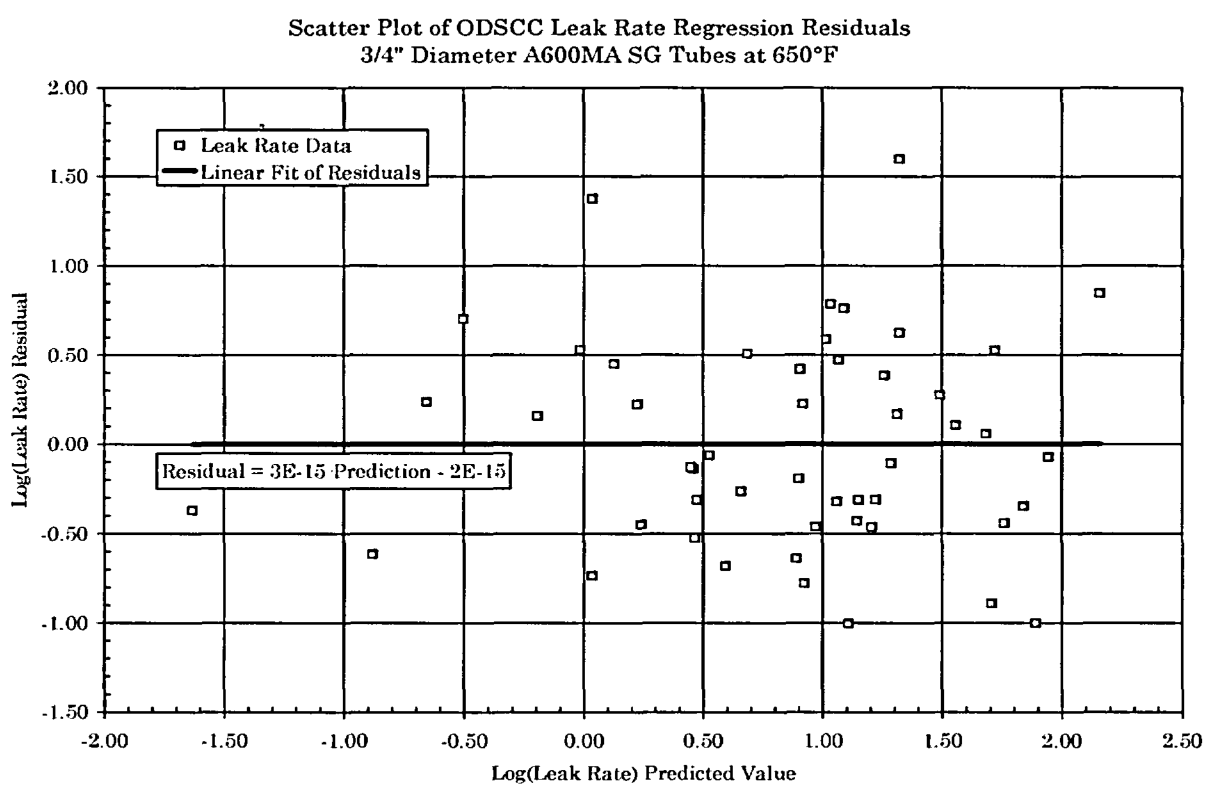

Figure 8: Residual scatter plot for SLB ΔP of 2405 psi.

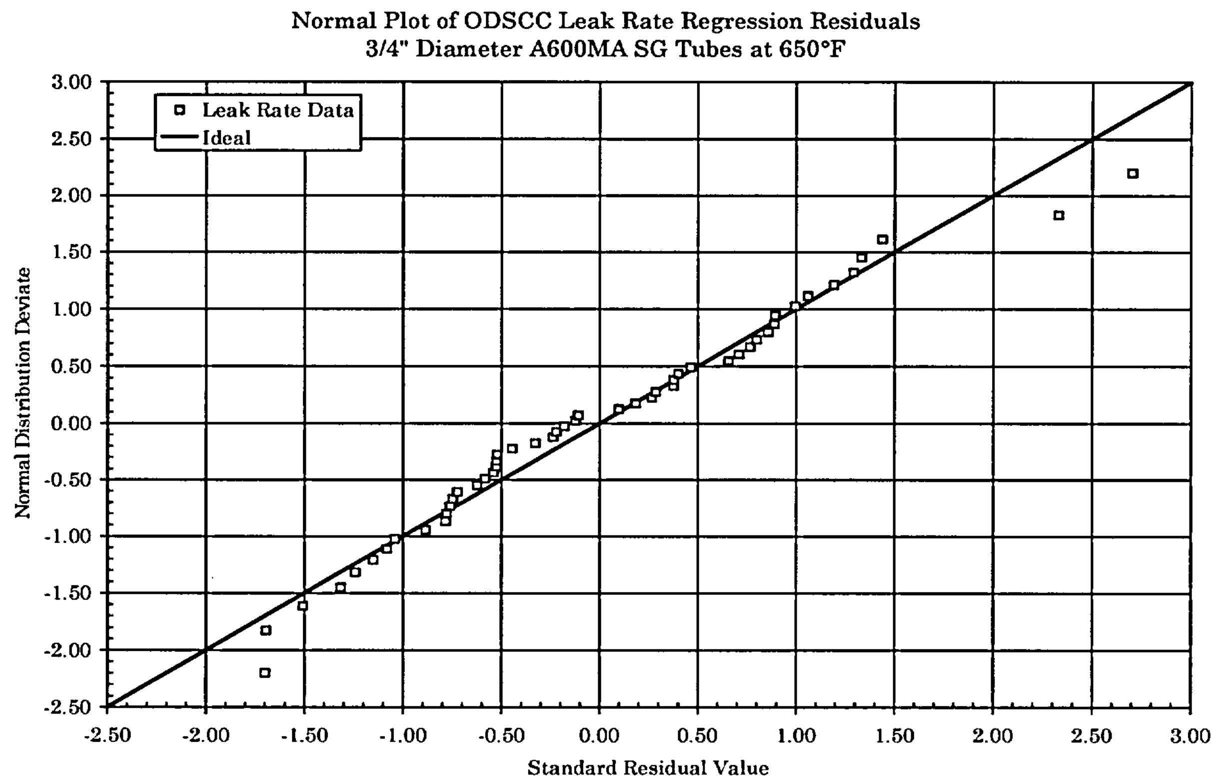

Figure 9: Residual normal plot for SLB ΔP of 2405 psi.

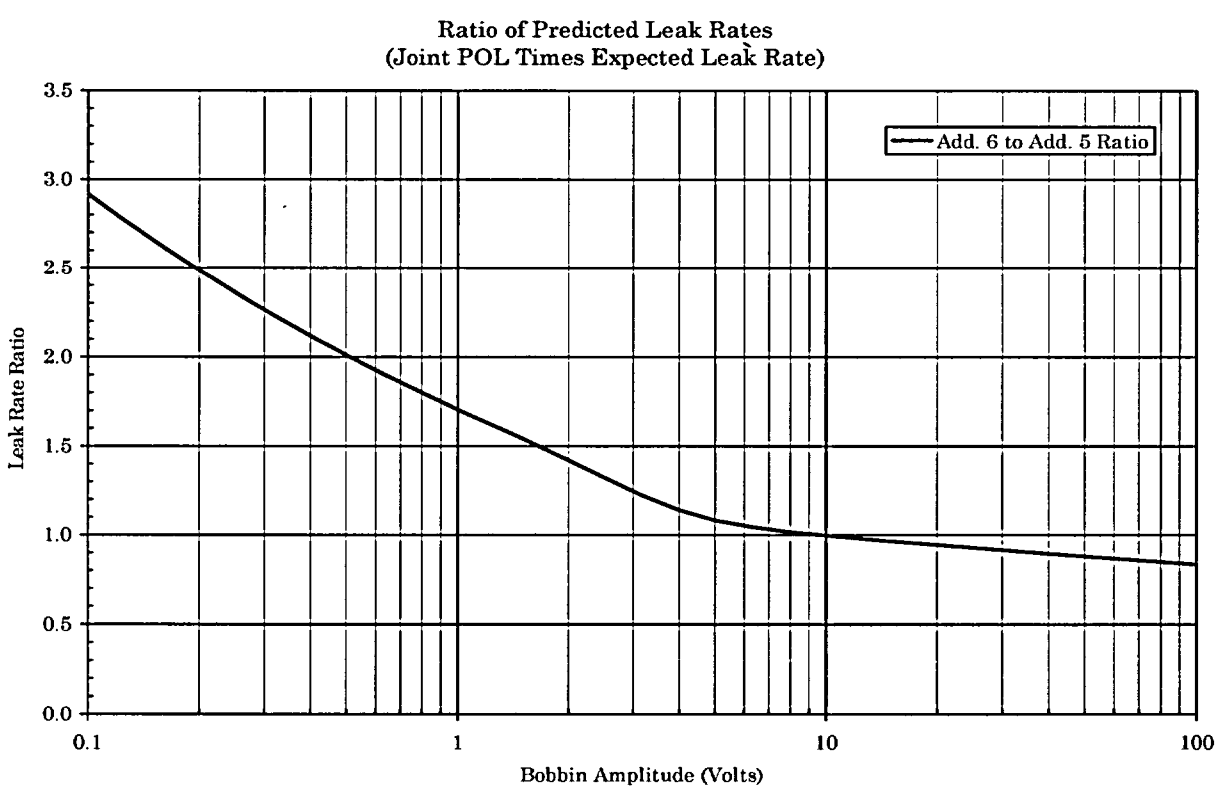

Figure 10: Ratio of expected leak rate as a function of amplitude.